DOCTORAATSPROEFSCHRIFT

2014 l Faculteit Wetenschappen

Biosensors for the characterization of DNA molecules based on electronic-, thermal-, and photonic sensing principles

Proefschrift voorgelegd tot het behalen van de graad van doctor in de wetenschappen, fysica, te verdedigen door:

Mohammed Sharif Murib

Promoter: Prof. Dr. Patrick Wagner

Copromoters: Prof. Dr. Luc Michiels

Prof. Dr. –Ing. Michael J. Schöning

Jury

Chair:	Prof. Dr. K. Coninx Hasselt University
Promotor:	Prof. Dr. P. Wagner Hasselt University, IMO-IMOMEC
Co-promotors:	Prof. Dr. -Ing. M.J. Schöning Aachen University of Applied Sciences, INB
	Prof. Dr. L. Michiels Hasselt University, BIOMED
Members of the Jury:	Prof. Dr. Ir. P. Bienstman Gent University, INTEC
	Prof. Dr. W. De Ceuninck Hasselt University, IMO
	Prof. Dr. J. Lammertyn K. U. Leuven, MeBIOS
	Prof. Dr. A. Serpengüzel Koç University, KUMRL
	Dr. B. van Grinsven Hasselt University, IMO

Acknowledgements

This thesis has benefited from the advice, guidance and assistance of many. First, I want to express my deepest gratitude to my advisor, Prof. Dr. Patrick Wagner for his guidance, advice, criticism, encouragements and insight throughout the research. Without his unwavering support, I could not have completed this work.

I would like to thank Prof. Dr. Karin Coninx, Prof. Dr. Ir. Peter Bienstman, Prof. Dr. Ward De Ceuninck, Prof. Dr. Jeroen Lammertyn, Prof. Dr. Ali Serpengüzel, Prof. Dr.-Ing. Michael J. Schöning, Prof. Dr. Luc Michiels, and Dr. Bart van Grinsven for their acceptance to be in the jury committee of my PhD degree theses. They took part in my thesis committee and made valuable feedback and suggestions.

I am especially indebted to my Prof. Dr. Ali Serpengüzel who has dedicated considerable time and thought for academic support, supervision, and motivation during my research with endless tolerance and patience.
A deep thank for Boumédièn Benmoussa and Naphat Paesuwan for their help, support and brotherhood.
Many thanks for Weng Siang Yeap for his help, support, and deep discussions.

I would like to thank Guy Reggers for the TGA measurements, Huguette Penxten for the FT-IR measurements, Kathia L. Jiménez Monroy for the AFM measurements, Matthias van Gompel for providing the sapphire chips and Bart Ruttens for the XRD measurements, Jan Mertens, Johnny Baccus, and Lieven Dewinter for their scientific support and advice to improve measurement setups, Christel and Hilde for their guidance in the chemistry lab.
Many thanks for Lea, Relinde, Lisette, and Ellen for their help in the official documents.

A deep thank for Bart, Lars, Rob, Marloes, Jan, Kasper, and Karolien, Karolien, Patricia, Kathia, Evelien, Mathias, Andreas, Nathalie, Kaushik, Sathya, Tim, Thijs, Bert, Stijn, Jeroen, Dieter for their friendship.

Many thanks for Stoffel, Wiebke, Jaso, and Weng Siang for their friendship, supply of diamond on silicon substrates, and hydrogenating loads of diamond substrates every week.

I teach in order to learn. Many thanks for the students Andrea, Benno, Tran Anh, Elka, Kai, Frederick, Gideon, Yannick, and Wim that I had the opportunity to guide in my PhD thesis work.

I would like to acknowledge the support of this research by the Life-Science Initiative Limburg and the Research Foundation Flanders (FWO) Projects G.0829.09, Synthetic diamond films as platform materials for novel DNA sensors based on electronic detection techniques and G.0B62.13N, Exploration of heat conductivity effects for applications in bio- and chemosensors, and Methusalem project NANO (Antwerp-Hasselt).

Finally, this research would have been impossible without the support of my family and to whom I dedicate this thesis. I also owe my biggest gratitude to my Mom, my Father, my sisters and to my brother (RIP). Their unconditional love and continuous belief in me amplified my determination and quest for knowledge. The sincere wishes of other family members, friends and colleagues were equally important. Even if I did not mention all the names, I am so grateful to all and will always be.

Table of Contents

Abstract

Deoxyribonucleic acid (DNA) recognition is an important tool in DNA biosensors. DNA biosensors are being developed with a rapid pace with the aim to achieve an inexpensive and rapid testing tool for genetic and infectious disease and to detect DNA damage and interactions. The study of single nucleotide polymorphisms (SNPs) and the analysis of gene sequences play a fundamental role in rapid detection of genetic mutations. It also opens up new opportunities for reliable diagnosis even before any symptoms of a disease appear. The aim of this thesis was to optimize and develop biosensors for the characterization of DNA molecules based on electronic-, thermal-, and photonic sensing principles.

In Chapter 1, a general description to DNA and DNA sensors was introduced. A brief explanation about the fundamentals of DNA as described by James D. Watson and Francis Crick was given. The concept and consequences of mutations in DNA sequences were explained briefly. The composition of a DNA sensor, the different sensing techniques used to sense DNA standards, and the sensor preparation with DNA were described briefly. Probe DNA, consisting of a 36-mer fragment was covalently immobilized on nanocrystalline chemical vapour deposition (CVD) diamond electrodes and hybridized with a 29-mer target DNA.

In Chapter 2, label-free real-time electronic monitoring of DNA denaturation upon exposure to NaOH solution at different flow rates and molarities, using electrochemical impedance spectroscopy as readout technology, was reported. The impedance response was separated into a denaturation time constant and a medium exchange time constant by means of a double exponential fit. It was observed that the denaturation time is dependent on the flow rate as well as on the molarity of the NaOH solution used. Surprisingly, it was observed that at low molarities (0.05 M) the DNA does not fully denature at low flow rates. Only after flushing the flow cell a second time with 0.05 M NaOH, complete denaturation was achieved. Confocal images were obtained and plotted in 3D graphs to confirm the results.

In Chapter 3, we showed that synthetic sapphire (Al_2O_3), an established implant material, can also serve as a platform material for biosensors comparable to nanocrystalline diamond. Sapphire chips, beads, and powder were first modified with (3-Aminopropyl) triethoxysilane (APTES), followed by succinic anhydride (SA), and, finally, single-stranded deoxyribonucleic acid (ss-DNA) probe was coupled using the zero-length cross-linker 1-ethyl-3-[3-dimethylaminopropyl]-carbodiimide (EDC) to the functionalized layer. The presence of ATPES-succinic anhydride layer on sapphire powder was confirmed by thermogravimetric analyis (TGA) and Fourier-transform infrared spectroscopy (FT-IR). The areal DNA density was quantified in X-ray photoelectron spectroscopy (XPS). Fluorescence microscopy was performed to demonstrate the successful coupling of fluorescently tagged target DNA to the pre-immobilized probe DNA. Synthetic sapphire is especially suitable for the heat-transfer method (HTM) due to its high thermal conductivity and chemical inertness. This measuring method analyzes the heat-transfer resistance at the solid-liquid interface when a target DNA molecule interacts with a ssDNA probe-functionalized surface. The heat transfer method was performed for the characterization of DNA on synthetic sapphire chips.

Within Chapter 4, a comparative theoretical study of an optical biosensor concept based on elastic light scattering from microspheres and the corresponding shift of whispering gallery modes (WGMs), after an add-on layer to the sphere, was performed. The study included sapphire, glass and diamond microspheres. The theoretical calculation of the expected resonant wavelength shifts were based on the generalized Lorenz–Mie theory (GLMT). The transverse electric (TE) and the transverse magnetic (TM) elastic light scattering intensity of electromagnetic waves at 600 and 1400 nm are numerically calculated for DNA and unspecific binding of proteins to the microsphere surface. The effect of changing the optical properties was studied for diamond (refractive index 2.34), glass (refractive index 1.50), and sapphire (refractive index 1.75) microspheres with a 50 μm radius. The mode spacing, the linewidth of WGMs, and the shift of resonant wavelength due to the change in radius and refractive index, were analyzed by numerical simulations. Preliminary results of unspecific binding of biomolecules showed that the calculated shift in WGMs can be used for biomolecules detection.

Therefore, an optical setup for DNA optical biosensor based on sapphire spherical microcavity was built as described in Chapter 5. Transmitted and elastic scattering intensity at 1510 nm were analyzed from a sapphire microsphere (radius 500 μm, refractive index 1.77) on an optical fiber half coupler for the first time. The 0.43 nm angular mode spacing of the resonances correlated well with the optical size of the sapphire sphere. The spectral linewidths of the resonances were on the order of 0.01 nm, which corresponded to quality factors on the order of 10^5. As a proof for principle, polydopamine (PDA) layer has been used as a functionalizing agent on sapphire microspherical resonators in view of the implementation of biosensors. The various PDA layer thicknesses on the sapphire microsphere were characterized as a function of the resonances wavelength shift. It was shown that the polymeric functionalization does not affect the high quality factor ($Q \approx 10^4$) of the sapphire microspheres. This functionalizing process of the microresonator constitutes a promising step towards the achievement of an ultrasensitive biosensor.

Then, the sapphire sphere was modified with DNA and an optical biosensor is demonstrated for the first time using an insulating implant material as illustrated in Chapter 6. Probe DNA, consisting of a 36-mer fragment was covalently immobilized on sapphire microsphere and hybridized with a 29-mer target DNA. Whispering gallery modes (WGMs) were monitored before the sapphire being functionalized with DNA and after it was functionalized with single stranded DNA (ssDNA) and double stranded DNA (dsDNA). The shift in resonances due to the surface modification with DNA was measured and correlated well with the estimated add-on DNA layer. It was shown that ssDNA are more uniformly oriented on the sapphire surface than the dsDNA. In addition, it was shown that functionalization of the sapphire spherical surface with DNA does not affect the high quality factor ($Q \approx 10^4$) of the sapphire microspheres. Future work may focus on optimization of this method further and to perform measurements on mismatched dsDNA and in liquid medium.

All in all, we have taken the first step towards utilizing a structural, electrically insulating implant material as a heat-transfer based and optical microcavity based biosensor platform paving the way for future in vivo biosensing devices. Our efforts are expressed in details in the concluding Chapter 7.

Nederlandse Samenvatting

De karakterisering van desoxyribonucleïnezuren (DNA) is een belangrijk doel van DNA-gebaseerde biosensoren. Vandaag kent de technologie van DNA-sensoren een snelle vooruitgang en men legt zich vooral toe op de ontwikkeling van efficiënte en goedkope testmethoden voor de opsporing van genetische afwijkingen, DNA beschadiging en infectieziektes. Binnen het onderzoek naar genetische mutaties spelen de sequentieanalyses en de opsporing van puntmutaties (SNP's: single nucleotide polymorphisms) een vooraanstaande rol. Deze aspecten hebben een hoge meerwaarde in de medische diagnostiek omdat ze als risico-indicatoren gelden voor bepaalde aandoeningen alvorens de patiënt daadwerkelijk ziektesymptomen vertoont. Het doel van deze thesis is de ontwikkeling en optimalisatie van nieuwe methoden voor de karakterisering van DNA fragmenten volgens elektronische-, thermische- en optische meetprincipes.

In hoofdstuk 1 wordt een algemene beschrijving van DNA moleculen en DNA sensoren gegeven. Hierbij wordt nader ingegaan op de koppeling tussen de bazenparen zoals beschreven door James D. Watson en Francis Crick en op de mogelijke gevolgen van mutaties in de DNA sequenties. Voorts worden de basisconcepten van DNA-sensoren beschreven, hun verschillende technische werkingsprincipes en de nodige voorbereidingen voor de implementatie van een DNA-sensor. In het bijzonder gaat het hierbij om de covalente aanhechting van probe-DNA (enkelstreng fragmenten met 36 basen) aan nanokristallijne diamantelektroden (bereid met chemische dampfazendepositie CVD) en de hybridisatie target DNA-fragmenten van 20 basen lang.

Hoofdstuk 2 beschrijft het elektronische monitoren van DNA-denaturatie in echttijd met behulp van elektrochemische impedantiespectroscopie waarbij de denaturatie wordt opgewekt door blootstelling aan NaOH oplossingen met verschillende concentraties en stromingsdebieten. De impedimetrische response wordt uitgesplitst in een intrinsieke tijdsconstante voor de denaturatie zelf en in een tijdconstante voor de mediumwissel op basis van een dubbel-exponentiële fitfunctie. Hierbij wordt aangetoond dat de tijdsconstante voor denaturatie zowel van het vloeistofdebiet als van de molariteit van de NaOH-oplossing afhangt. Hierbij blijkt dat lage concentraties (0.05 M NaOH) in combinatie met lage stro-

mingsdebieten slechts tot onvolledige denaturatie leiden en een tweede blootstelling vereist is voor volledige denaturatie. Dit wordt bevestigd door confocale fluorescentiemicroscopie die de resultaten als 3D-grafieken weergeeft.

In hoofdstuk 3 tonen we aan dat synthetisch saffier (Al_2O_3), een bekend implantaatmateriaal, eveneens als platformmateriaal voor biosensoren gebruikt kan worden met eigenschappen vergelijkbaar aan die van diamant. Saffier-chips, parels en poeders werden eerst met (3-Aminopropyl) triethoxysilane (APTES) en succinic anhydride (SA) gemodificeerd alvorens enkelstrengige probe-DNA m.b.v. de EDC-koppeling aan de gemodificeerde oppervlakken te hechten. De aanwezigheid van de APTES-succinic anhydride laag op saffierpoeder wordt bevestigd door thermogravimetrische analyse (TGA) en Fourier-transformatie infrarood spectroscopie (FT-IR). Voorts wordt de oppervlakdensiteit van DNA kwantitief bepaald met x-stralen fotoemissie-spectroscopie (XPS). De koppeling van fluorescerend gelabelde target-DNA aan de geïmmobiliseerde probe-DNA wordt met fluorescentiemicroscopie in beeld gebracht. Dankzij zijn hoge thermische geleidbaarheid en chemische stabiliteit is synthetisch saffier bijzonder geschikt als platformmateriaal voor een sensor-uitlezing volgens de 'heat-transfer method HTM': Deze methode analyseert de warmtegeleidingsweerstand van het grensvlak tussen vaste- en vloeibare stoffen en reageert zeer gevoelig op de aanwezigheid van al dan niet gehybridiseerde DNA fragmenten op de saffier-chip. We tonen aan dat dit meetprincipe inderdaad in staat om de aanwezigheid van puntmutaties in DNA-fragmenten aan te tonen.

Het vierde hoofdstuk beschrijft een theoretische studie op een optisch biosensor concept dat op elastische lichtverstrooiing aan microsferen en een verschuiving van de 'whispering gallery modes' (WGMs) berust ten gevolge van (biologische) deklagen. Deze vergelijkende studie werd uitgevoerd voor microsferen van saffier, glas en diamant en de theoretische berekening van de verwachte verschuiving van de resonantiegolflengtes was gebaseerd op de gegeneraliseerde Lorenz–Mie theorie (GLMT). De transversaal-elektrische (TE) en de transversaal-magnetische (TM) strooi-intensiteit werden numeriek berekend in het golflengtegebied van 600 tot 1400 nm en dit zowel voor DNA als voor onspecifiek gebonden proteïnen op de microsferen. De verandering van de optische eigenschappen hangt af van de brekingsindex van het materiaal in kwestie waarbij de

diameter van de sferen zelf constant werd gehouden. Numerieke simulaties werden uitgevoerd voor de spatiëring en de lijnbreedte van de WGMs en voor de verschuiving van de resonantiegolflengtes door de dikte en de brekingsindices van de biologische deklagen. De resultaten geven aan dat reeds de verschuiving door onspecifieke adsorptie van biomoleculen voldoende groot is om met dit meetprincipe biomoleculen te kunnen detecteren.

In het vijfde hoofdstuk wordt een optische setup beschreven voor een DNA-sensor volgens het voorgestelde werkingsprincipe waarbij er met een microsfeer van saffier (straal 500 μm, brekingsindex 1.77) werd gewerkt. De getransmitteerde en elastisch gestrooide intensiteiten werden opgemeten bij een golflengte van 1510 nm waarbij het licht d.m.v. een vezeloptische half coupler aan de saffier-microsfeer werd gekoppeld. De spatiëring van 0.43 nm tussen opeenvolgende resonantiemodes kwam zeer goed overeen met de optische grootte van de microsfeer zelf. De spectrale lijnbreedtes van de resonanties waren in de orde van 0.01 nm, we kunnen dus over een kwaliteitsfactor in de orde van 10^5 spreken. Als een eerste test voor de beoogde biosensor werden lagen van polydopamine (PDA, een biochemisch linker-molecule) afgezet op de sferische saffierresonatoren en de verschuiving van de resonantiegolflengtes opgemeten in functie van de PDA-laagdikte. De functionalisatie van de saffiersferen met het polymeer had geen uitgesproken nadelige invloed op de kwaliteitsfactor ($Q \approx 10^4$). Hiermee was dan ook de basis gelegd om een ultragevoelige, fotonische biosensor te kunnen implementeren.

Tenslotte beschrijft hoofdstuk 6 de functionalisatie van de saffiersferen met DNA in combinatie met de fotonische uitlezingstechniek voorgesteld in het vorige hoofdstuk. Er werd voor de zelfde types van DNA fragmenten gekozen als in het geval van de elektronische- en de thermische sensorconcepten. De resonanties van de whispering gallery modes werden bepaald met blanko saffiersferen, na aankoppeling van de enkelstrengige DNA-probes, en na de hybridisatie met complementaire target-fragmenten. De verschuiving van de resonantie door deze modificaties met DNA werden geanalyseerd en kwamen zeer goed overeen met de geschatte dikte van de additionele DNA laag. Bovendien werd aangetoond dat enkelstrengige DNA op een meer uniforme manier op de saffiersferen uitgelijnd is dan dubbelstrengige DNA. Tevens bleek dat de

kwaliteitsfactor van de microsferen door de functionalisatie niet nadelig wordt beïnvloed. Toekomstig werk zal zich toespitsen op een verdere optimalisatie in de richting van de opsporing van puntmutaties en het uitvoeren van dergelijke metingen rechtstreeks in vloeibare middens.

In de som werd dus voor het eerst aangetoond dat ook saffier, een elektrisch isolerend implantaatmateriaal, geschikt is om als sensorplatform voor de karakterisering van DNA te dienen. Dit werd mogelijk gemaakt dankzij twee niet-elektrische sensorprincipes, namelijk op een thermische manier met de warmtegeleidingsmethode en op een fotonische manier m.b.v. optische micro-caviteiten. Dit kan mogelijk de basis vormen voor toekomstige generaties van implanteerbare biosensoren.

Chapter 1

Introduction

This first chapter opens with the fundamentals of DNA as described by James D. Watson and Francis Crick [1]. It explains the concept and consequences of mutations in DNA sequences. It then describes the composition of a DNA sensor, followed by a brief description of the different sensing techniques used to sense DNA standards and the sensor preparation with DNA.

1.1 Deoxyribonucleic acid (DNA)

Deoxyribonucleic acid (DNA) contains the genetic information fundamental to all known living organisms [1]. Chromosomes are the place where the DNA is stored in the cell nucleus [1]. DNA consists of three groups of molecules: deoxyribose sugar (Figure 1.1 a), organic bases and inorganic phosphate. The inorganic phosphate is derived from phosphoric acid (Figure 1.1 b).

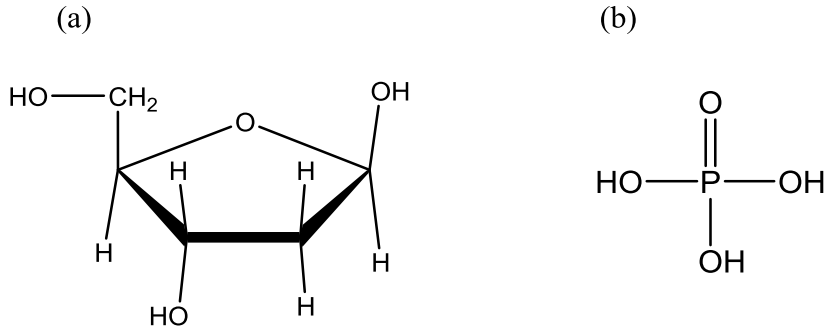

Figure 1.1 Chemical structure of (a) the Deoxyribose sugar and (b) the phosphate group in DNA.

DNA principally consists of 4 bases, which are adenine (A), guanine (G), cytosine (C), and thymine (T). C and T are derived from pyrimidine (Figure 1.2a, 1.2b) whereas A and G are derived from purine (Figure 1.2c, 1.2d).

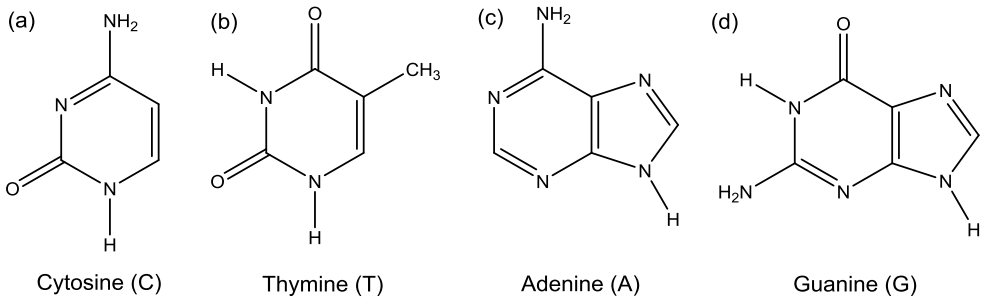

Figure 1.2 Chemical structure of the four bases in DNA. (a) Cytosine, (b) Thymine, (c) Adenine, and (d) Guanine.

When one of the bases is joined to the deoxyribose sugar molecule, we get a compound known as deoxyribonucleoside. The bond linking the base to the sugar is known as glycoside bond. The addition of a phosphate group to the sugar residue of the nucleoside molecule then produces a deoxyribonucleotide (Figure 1.3). The combination of deoxyribonucleotide molecules through sugar-phosphate bonds forms a deoxyribonucleic acid (DNA).

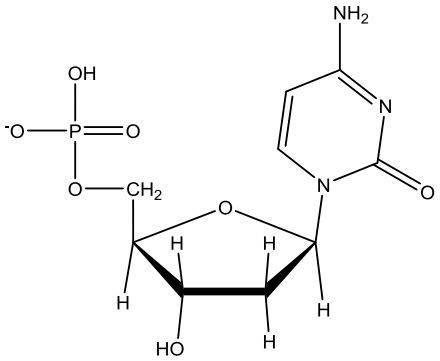

Figure 1.3 Chemical structure of the deoxyribonucleotide with the cytosine base.

In 1953, Watson and Crick deduced the double helix structure of the DNA using X-ray crystallography. This double helix structure comprises two strands of sugar-phosphate backbone [2, 3]. The DNA sequence on each strand of a double helix is complementary to the other. For a given strand, A is paired across from T on the opposite strand by two hydrogen bonds, and C is paired across from G by three hydrogen bonds, and *vice versa* [3]. Each such pairing is referred to as a base pair (bp). This pairing process is known as hybridization (Figure 1.4).

The breaking of the double strand (ds) DNA into two single strands (ss) is known as denaturation or melting. DNA in the nuclei of living cells becomes single-stranded (ss) during replication, transcription, and repair. Disruption of the native structure may also result from modifications of the bases or sugar backbone induced by chemicals, light or radiation. In living cells such changes are reversed by specialised enzymatic systems responsible for preventing loss of genetic information [4]. Denaturation can be induced in isolated DNA or in fixed cells by exposure to elevated temperatures [5], alkaline solutions or acids [6, 7], and low ionic concentration buffer [8].

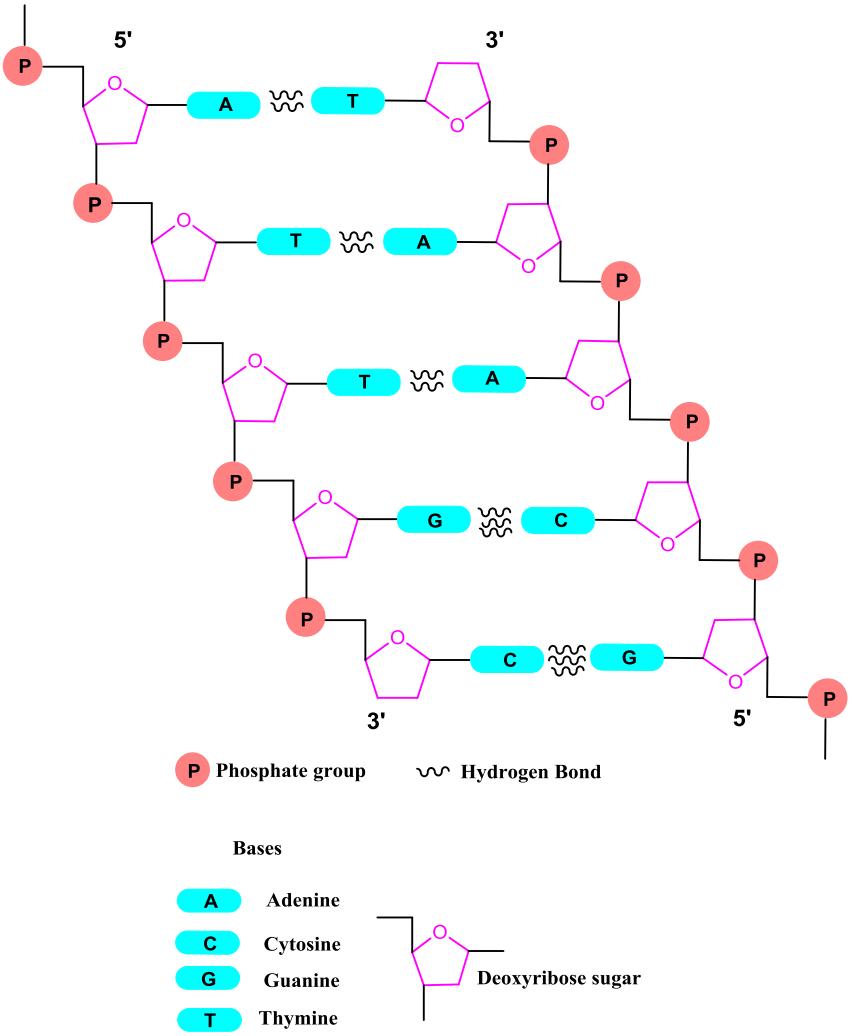

Figure 1.4: Detail of the interaction between complementary nucleotides.

1.2 Single Nucleotide Polymorphisms (SNPs)

A SNP is defined as a single-base difference in DNA among individuals [9]. SNPs are useful for finding genes that contribute to disease. The challenge is to relate these genetic differences to disease risk and response to therapies [10]. Mutation mechanisms result either in transitions: purine-purine (A⇔G) or pyrimidine-pyrimidine (C⇔T) exchanges, or transversions: purine-pyrimidine or pyrimidine-purine (A⇔C, A⇔T, G⇔C, G⇔T) exchanges [11]. SNPs are used for identification and forensics [12-14], mapping and genome-wide association

studies of complex diseases [15, 16], estimating predisposition to disease [17, 18], predict specific genetic traits [19, 20], and classifying patients in clinical trials [21].

Figure 1.5: Base sequences of a probe DNA and the corresponding full match and mismatch with 1 SNP at position 7 and position 20. A SNP is a single-letter change in DNA, part of the natural genetic variation within a population.

1.3 DNA sensor

A biosensor is an analytical device incorporating a deliberate and intimate combination of a specific biological element that creates a recognition event and a physical element that transduces the recognition event [22]. As demonstrated in Figure 1.5, a DNA sensor is composed of 3 elements: (i) modified solid surface (transducer), (ii) single-stranded DNA that is immobilized onto the solid surface (probe) and (iii) a complementary single-stranded DNA (target) hybridized to the probe DNA [23]. The transducer of the DNA sensor serves to transfer the signal from the output domain of the biological recognition system to the (usually electrical) signal. DNA sensors can be electrical [24, 25], thermal [26] or optical [27].

An electrochemical DNA sensor relies solely on the measurement of currents and/or voltages to detect the binding of DNA molecules to the transducer surface. The transducer can be a conducting or semiconducting electrode [22, 28, 29]. The underlying principle for an electrical DNA sensor is that when a target DNA molecule interacts with a ssDNA probe-functionalized surface, changes in the electrical properties of the surface (e.g. dielectric constant and resistance) can result solely from the presence of the target DNA molecule [30]. In recent years there has been a major development of DNA electrochemical

biosensors such as field-effect transistors (FET) [31, 32] and impedimetric sensors [24]. These field effect sensors rely on the interaction of external charges of the negatively charged DNA molecules with carriers in a nearby semiconductor and thus exhibit enhanced sensitivity at low ionic strength where counter ion shielding is reduced [30]. A DNA-FET is obtained by immobilizing well-defined sequences of ssDNA onto a field-effect transducer, which can convert the specific recognition process between the two complementary DNA single strands into a measurable signal [33]. A Field-effect sensor measures the equivalent gate-voltage difference before and after attachment of the DNA molecules to the surface, ΔV_{GS}, in a potentiometric way. It may also measure the effective impedance change of the FET gate input due to the attachment of the DNA layer to the gate surface [31]. Impedimetric sensors monitor the electrical impedance, conductance [24] and capacitance [34] of a solid surface-liquid interface in alternating (AC) potential steady state [24]. When a solid surface is modified with DNA, the overall resistance, conductance or capacitance changes and these are monitored by the impedimetric sensors.

A thermal DNA sensor relates the temperature difference between the liquid and the transducer surface to the input power provided by the heating element. The underlying principle for a thermal DNA sensor is that when a target DNA molecule interacts with a ssDNA probe-functionalized surface, changes in the heat transfer resistance at the solid-liquid interface are monitored [26].

Optical DNA sensors detect the changes in the optical properties (index of refraction, size) of the sensing transducer, resulting from surface reactions between target DNA molecules and the ssDNA probe-functionalized surface [27]. Surface-enhanced Raman spectroscopy (SERS) [35] and total internal reflection fluorescence (TIRF) microscopy [36, 37] were also used as DNA sensors.

SERS is a Raman Spectroscopic (RS) technique based on the Raman effect, which is the inelastic scattering of photons by molecules. In SERS, the target molecule is brought into close proximity to a metallic surface (typically Ag, Au or Cu) with nanoscopically defined features or in solution next to a nanoparticle with a diameter much smaller than the wavelength of the excitation light. When light is incident on the surface or particle, a surface plasmon mode is excited which locally enhances the electromagnetic energy in the vicinity of the target

molecule, significantly enhancing the intensity of the inelastically scattered light [38].

TIRF employs the phenomena of total internal refection and evanescent waves to selectively excite fluorophore labeled DNA located at the surface and in close proximity (100-200 nm) to the surface of a glass, silica, or plastic slide. However, the labeling of the DNA also behaves as an amplifier for an otherwise undetectable single-molecule signal, and requires a prior knowledge of the target molecule that must be modified to be compatible with the label, which restricts an experiment's scope [39].

As a result, the demand for label-free biosensors has increased, and different technologies have been developed such as fiberoptic waveguides [40, 41] and (ring and spherical) microcavity resonators [39, 42]. In such devices, light is coupled through these devices and an evanescent field extends beyond the device surface [43].

The analytes deposited onto the surfaces of the fiber-optic waveguides are in the path of the evanescent field, and, as a result, they change the effective refractive index of the guided mode [43]. Fiber-optic waveguide sensors are size-effective. For example, in order to achieve a high signal and low detection limit, the waveguide must be of the order of a few centimeters long, since the sensing signal is accumulated along the waveguide [43].

Optical microcavities such as ring resonators or spherical resonators are promising optical label free detection setups [39, 42]. Recently, a silicon on insulator (SOI) microring resonator for sensitive label free biosensing was fabricated [44]. In addition, microring surface functionalization and a detection limit of 0.37 fg avidin mass (3260 molecules) were established [45, 46]. In an optical microcavity, the target molecules are sampled hundreds of times due to the recirculation of light within the microcavity by total internal reflection (TIR) [39]. The target molecule induces a change on the optical microcavity properties such as the size and refractive index, and as a result, a change in the whispering gallery mode (WGM) resonant wavelength is encountered [47].

1.4 DNA Sensor preparation

CVD nanocrystalline boron doped diamond and synthetic sapphire chips are used in this thesis for DNA sensing using impedance spectroscopy and the heat transfer method. Sapphire microspheres of 1 mm diameter were also used in this thesis for optical sensing setup optimization and DNA optical sensing. Diamond and sapphire show outstanding chemical inertness, wear resistance, and biocompatibility [23, 48]. They also have a good thermal conductivity [49, 50] and low thermal expansion [50]. Hence, they appear to be favorable for use in optical biosensors operating at a broader temperature regime.

Probe DNA, consisting of a 36-mer fragment was covalently immobilized on NCD and sapphire electrodes and then hybridized with 29-mer target DNA.

First, the diamond surface was hydrogenated [51]. After hydrogenation, unsaturated fatty acid (10-undecenoic acid; Merck) was reacted with the diamond surface during 20 hours under 254 nm ultraviolet (UV) (265 $mWcm^{-2}$) illumination. This photoreaction results in a carboxyl-terminated surface. Subsequent covalent coupling of amino-modified dsDNA to the carboxyl-terminated surface was carried out using the zero-length cross-linker 1-ethyl-3-[3-dimethylaminopropyl]-carbodiimide (EDC) [52, 53].

The covalent functionalization of sapphire with probe DNA was done along the silane route [54]. Silanization of the sapphire sample was carried out by liquid phase deposition of a solution of silane (3-Aminopropyl)triethoxysilane (APTES, 99%) [54]. This creates an amine-modified sapphire surface [55]. Here, two different modification routes were utilized. The first route was converting the amine-modified sapphire surface into carboxyl-modified sapphire surface using succinic anhydride (SA) and finally, amino-modified dsDNA was EDC coupled to the carboxyl-modified surface [54]. The second route was covalent coupling of carboxyl-terminated dsDNA to the amine-modified sapphire surface using EDC.

The sapphire microspheres for optical sensing setup optimization were functionalized with PDA. Trizma hydrochloride (reagent grade, minimum 99%) and dopamine hydrochloride (98.5%) were purchased from Sigma and used as received. Immersion times were varied (2 h, 5 h, 10 h and 20 h) to create

polydopamine films with different thicknesses [56]. The Sapphire microsphere for optical DNA sensing were functionalized as described for the sapphire chip.

1.5 Objectives

The aim of this project is to develop biosensors for the characterization of DNA molecules based on electronic-, thermal-, and photonic sensing principles.

In Chapter 2, CVD nanocrystalline diamond (NCD) was functionalized with dsDNA. The denaturation process was monitored by using a homemade electrochemical impedance setup [24]. The effect of different flow rates and concentrations of sodium hydroxide (NaOH) was studied. The optimization of these parameters provides a valuable asset in the field of mutation analysis.

In Chapter 3, sapphire chips, beads, and powder were first modified with (3-Aminopropyl) triethoxysilane (APTES), followed by succinic anhydride (SA), and, finally, single-stranded deoxyribonucleic acid (ss-DNA) probe was EDC coupled to the functionalized layer. The heat transfer method [26] was performed for the characterization of the thermal denaturation of the target DNA on the functionalized synthetic sapphire chips.

In Chapter 4, a comparative theoretical study of an optical biosensor concept based on elastic light scattering from sapphire, glass, and diamond microspheres is performed. The corresponding shift of whispering gallery modes (WGMs), after an add-on layer to these spheres, is analysed. All the analyses were performed based on the Generalized Lorenz-Mie Theorem (GLMT) [57].

In Chapter 5, a set of proof-of-principle experiments were performed using a sapphire sphere with an add-on layer of polydopamine (PDA). The shift of the whispering gallery modes (WGMs) due to different thicknesses of PDA on the sapphire microsphere was monitored. Moreover, the high quality factor of WGM resonances was found to be preserved before and after surface modification.

In Chapter 6, the WGM resonances shift due to the sapphire microsphere surface modification with ssDNA, dsDNA, and chemical denaturation of dsDNA was monitored. These results proved the possibility of using sapphire microsphere as a label free DNA optical biosensor.

1.6 References

1. J. D. Watson, and F. H. C. Crick, "Molecular structure of nucleic acids - A structure for deoxyribose nucleic acid (Reprinted from Nature vol 171, pg. 737, 1953)," Clinical Orthopaedics and Related Research, 3-5 (2007).

2. G. M. Blackburn, and J. M. Gait, "Nucleic acids in chemistry and biology," (Oxford University Press, 1996).

3. W. Saenger, "Principles of Nucleic Acid Structure," (Springer - Verlag, 1984).

4. R. P. Sinha, and D. P. Hader, "UV-induced DNA damage and repair: a review," Photochemical & Photobiological Sciences **1**, 225-236 (2002).

5. A. V. Zelenin, "Acridine orange as a probe for molecular and cell biology," in Luminescent Probes for Biological Activity (Academic Press, 1993).

6. Z. Darzynkiewicz, "Acid-induced denaturation of DNA in-situ as a probe of chromatin structure," Methods in cell biology **41**, 527-541 (1994).

7. J. Dobrucki, and Z. Darzynkiewicz, "Chromatin condensation and sensitivity of DNA in situ to denaturation during cell cycle and apoptosis - a confocal microscopy study," Micron **32**, 645-652 (2001).

8. E. Özkumur, S. Ahn, A. Yalçın, C. A. Lopez, E. Çevik, R. J. Irani, C. DeLisi, M. Chiari, and M. S. Ünlü, "Label-free microarray imaging for direct detection of DNA hybridization and single-nucleotide mismatches," Biosensors & Bioelectronics **25**, 1789-1795 (2010).

9. L. X. Shen, J. P. Basilion, and V. P. Stanton, "Single-nucleotide polymorphisms can cause different structural folds of mRNA," Proceedings of the National Academy of Sciences of the United States of America **96**, 7871-7876 (1999).

10. E. S. Lander, "The new genomics: Global views of biology," Science **274**, 536-539 (1996).

11. A. Vignal, D. Milan, M. SanCristobal, and A. Eggen, "A review on SNP and other types of molecular markers and their use in animal genetics," Genetics Selection Evolution **34**, 275-305 (2002).

12. C. Borsting, H. S. Mogensen, and N. Morling, "Forensic genetic SNP typing of low-template DNA and highly degraded DNA from crime case samples," Forensic Science International-Genetics **7**, 345-352 (2013).

13. G. Chemale, G. G. Paneto, M. A. M. Menezes, J. M. de Freitas, G. S. Jacques, R. M. B. Cicarelli, and P. R. Fagundes, "Development and validation of a D-loop mtDNA SNP assay for the screening of specimens in forensic casework," Forensic Science International-Genetics **7**, 353-358 (2013).

14. C. Phillips, L. Fernandez-Formoso, M. Gelabert-Besada, M. Garcia-Magarinos, C. Santos, M. Fondevila, A. Carracedo, and M. V. Lareu, "Development of a novel forensic STR multiplex for ancestry analysis and extended identity testing," Electrophoresis **34**, 1151-1162 (2013).

15. K. Y. Urayama, A. P. Chokkalingam, C. Metayer, H. Hansen, S. May, P. Ramsay, J. L. Wiemels, J. K. Wiencke, E. Trachtenberg, P. Thompson, Y. Ishida, P. Brennan, K. W. Jolly, A. M. Termuhlen, M. Taylor, L. F. Barcellos, and P. A. Buffler, "SNP association mapping across the extended major histocompatibility complex and risk of B-cell precursor acute lymphoblastic leukemia in children," Plos One **8** (2013).

16. J. C. Almlof, P. Lundmark, A. Lundmark, B. Ge, S. Maouche, H. H. H. Goring, U. Liljedahl, C. Enstrom, J. Brocheton, C. Proust, T. Godefroy, J. G. Sambrook, J. Jolley, A. Crisp-Hihn, N. Foad, H. Lloyd-Jones, J. Stephens, R. Gwilliam, C. M. Rice, C. Hengstenberg, N. J. Samani, J. Erdmann, H. Schunkert, T. Pastinen, P. Deloukas, A. H. Goodall, W. H. Ouwehand, F. Cambien, A. C. Syvanen, and C. Consortium, "Powerful identification of cis-regulatory SNPs in human primary monocytes using allele-specific gene expression," Plos One **7** (2012).

17. G. V. Glinsky, "Disease phenocode analysis identifies SNP-guided microRNA maps (MirMaps) associated with human "master" disease genes," Cell Cycle **7**, 3680-3694 (2008).

18. M. Gaustadnes, T. F. Orntoft, J. L. Jensen, and N. Torring, "Validation of the use of DNA pools and primer extension in association studies of sporadic colorectal cancer for selection of candidate SNPs," Human Mutation **27**, 187-194 (2006).

19. S. Renaut, A. W. Nolte, S. M. Rogers, N. Derome, and L. Bernatchez, "SNP signatures of selection on standing genetic variation and their association with adaptive phenotypes along gradients of ecological speciation in lake whitefish species pairs (Coregonus spp.)," Molecular Ecology **20**, 545-559 (2011).

20. N. Y. Long, D. Gianola, G. J. M. Rosa, K. A. Weigel, A. Kranis, and O. Gonzalez-Recio, "Radial basis function regression methods for predicting quantitative traits using SNP markers," Genetics Research **92**, 209-225 (2010).

21. K. Kiyotani, T. Mushiroda, C. K. Imamura, N. Hosono, T. Tsunoda, M. Kubo, Y. Tanigawara, D. A. Flockhart, Z. Desta, T. C. Skaar, F. Aki, K. Hirata, Y. Takatsuka, M. Okazaki, S. Ohsumi, T. Yamakawa, M. Sasa, Y. Nakamura, and H. Zembutsu, "Significant effect of polymorphisms in CYP2D6 and ABCC2 on clinical outcomes of adjuvant tamoxifen therapy for breast cancer patients," Journal of Clinical Oncology **28**, 1287-1293 (2010).

22. D. R. Thevenot, K. Toth, R. A. Durst, and G. S. Wilson, "Electrochemical biosensors: recommended definitions and classification," Biosensors & Bioelectronics **16**, 121-131 (2001).

23. S. Wenmackers, V. Vermeeren, M. vandeVen, M. Ameloot, N. Bijnens, K. Haenen, L. Michiels, and P. Wagner, "Diamond-based DNA sensors: surface functionalization and read-out strategies," Physica Status Solidi A Applications and Materials Science **206**, 391-408 (2009).

24. B. van Grinsven, N. Vanden Bon, L. Grieten, M. Murib, S. D. Janssens, K. Haenen, E. Schneider, S. Ingebrandt, M. J. Schöning, V. Vermeeren, M. Ameloot, L. Michiels, R. Thoelen, W. De Ceuninck, and P. Wagner, "Rapid assessment of the stability of DNA duplexes by impedimetric real-time monitoring of chemically induced denaturation," Lab on a Chip **11**, 1656-1663 (2011).

25. M. S. Murib, B. van Grinsven, L. Grieten, S. D. Janssens, V. Vermeeren, K. Eersels, J. Broeders, M. Ameloot, L. Michiels, W. De Ceuninck, K. Haenen, M. J. Schöning, and P. Wagner, "Electronic monitoring of chemical DNA denaturation on nanocrystalline diamond electrodes with different molarities and flow rates," Physica Status Solidi A Applications and Materials Science **210**, 911-917 (2013).

26. B. van Grinsven, N. Vanden Bon, H. Strauven, L. Grieten, M. Murib, K. L. J. Monroy, S. D. Janssens, K. Haenen, M. J. Schöning, V. Vermeeren, M. Ameloot, L. Michiels, R. Thoelen, W. De Ceuninck, and P. Wagner, "Heat-transfer resistance at solid-liquid interfaces: A tool for the detection of single-nucleotide polymorphisms in DNA," Acs Nano **6**, 2712-2721 (2012).

27. F. Vollmer, S. Arnold, D. Braun, I. Teraoka, and A. Libchaber, "Multiplexed DNA quantification by spectroscopic shift of two microsphere cavities," Biophysical Journal **85**, 1974-1979 (2003).

28. T. G. Drummond, M. G. Hill, and J. K. Barton, "Electrochemical DNA sensors," Nature Biotechnology **21**, 1192-1199 (2003).

29. E. Bakker, "Electrochemical sensors," Analytical Chemistry **76**, 3285-3298 (2004).

30. J. S. Daniels, and N. Pourmand, "Label-free impedance biosensors: Opportunities and challenges," Electroanalysis **19**, 1239-1257 (2007).

31. S. Ingebrandt, Y. Han, F. Nakamura, A. Poghossian, M. J. Schöning, and A. Offenhäusser, "Label-free detection of single nucleotide polymorphisms utilizing the differential transfer function of field-effect transistors," Biosensors & Bioelectronics **22**, 2834-2840 (2007).

32. S. Sorgenfrei, C. Y. Chiu, R. L. Gonzalez, Y. J. Yu, P. Kim, C. Nuckolls, and K. L. Shepard, "Label-free single-molecule detection of DNA-hybridization kinetics with a carbon nanotube field-effect transistor," Nature Nanotechnology **6**, 125-131 (2011).

33. A. Poghossian, A. Cherstvy, S. Ingebrandt, A. Offenhäusser, and M. J. Schöning, "Possibilities and limitations of label-free detection of DNA hybridization with field-effect-based devices," Sensors and Actuators B Chemical **111**, 470-480 (2005).

34. A. Poghossian, M. H. Abouzar, M. Sakkari, T. Kassab, Y. Han, S. Ingebrandt, A. Offenhäusser, and M. J. Schöning, "Field-effect sensors for monitoring the layer-by-layer adsorption of charged macromolecules," Sensors and Actuators B Chemical **118**, 163-170 (2006).

35. F. Gao, J. Lei, and H. Ju, "Label-free surface-enhanced raman spectroscopy for sensitive DNA detection by DNA-mediated silver nanoparticle growth," Analytical Chemistry **85**, 11788-11793 (2013).

36. H. P. Lehr, A. Brandenburg, and G. Sulz, "Modeling and experimental verification of the performance of TIRF-sensing systems for oligonucleotide microarrays based on bulk and integrated optical planar waveguides," Sensors and Actuators B Chemical **92**, 303-314 (2003).

37. K. Kroger, A. Jung, S. Reder, and G. Gauglitz, "Versatile biosensor surface based on peptide nucleic acid with label free and total internal reflection fluorescence detection for quantification of endocrine disruptors," Analytica Chimica Acta **469**, 37-48 (2002).

38. Y. S. Huh, A. J. Chung, and D. Erickson, "Surface enhanced Raman spectroscopy and its application to molecular and cellular analysis," Microfluidics and Nanofluidics **6**, 285-297 (2009).

39. A. M. Armani, R. P. Kulkarni, S. E. Fraser, R. C. Flagan, and K. J. Vahala, "Label-free, single-molecule detection with optical microcavities," Science **317**, 783-787 (2007).

40. V. M. N. Passaro, F. Dell'Olio, B. Casamassima, and F. De Leonardis, "Guided-wave optical biosensors," Sensors **7**, 508-536 (2007).

41. J. P. Golden, G. P. Anderson, S. Y. Rabbany, and F. S. Ligler, "An evanescent-wave biosensor .II. fluorescent signal acquisition from tapered fiber optic probes," IEEE Transactions on Biomedical Engineering **41**, 585-591 (1994).

42. M. Baaske, and F. Vollmer, "Optical resonator biosensors: Molecular diagnostic and nanoparticle detection on an integrated platform," Chemphyschem **13**, 427-436 (2012).

43. J. D. Suter, I. M. White, H. Y. Zhu, H. D. Shi, C. W. Caldwell, and X. D. Fan, "Label-free quantitative DNA detection using the liquid core optical ring resonator," Biosensors & Bioelectronics **23**, 1003-1009 (2008).

44. K. De Vos, I. Bartolozzi, E. Schacht, P. Bienstman, and R. Baets, "Silicon-on-insulator microring resonator for sensitive and label-free biosensing," Optics Express **15**, 7610-7615 (2007).

45. K. De Vos, J. Girones, S. Popelka, E. Schacht, R. Baets, and P. Bienstman, "SOI optical microring resonator with poly(ethylene glycol) polymer brush for label-free biosensor applications," Biosensors & Bioelectronics **24**, 2528-2533 (2009).

46. R. Kirchner, M. K. Kaiser, B. Adolphi, R. Landgraf, and W. J. Fischer, "Chemical functional polymers for direct UV assisted nanoimprinting of polymeric photonic microring resonators," Physica Status Solidi A Applications and Materials Science **208**, 1308-1314 (2011).

47. F. Vollmer and S. Arnold, "Whispering-gallery-mode biosensing: label-free detection down to single molecules," Nature Methods **5**, 591-596 (2008).

48. A. G. Mamalis, J. J. Ramsden, A. I. Grabchenko, L. A. Lytvynov, V. A. Filipenko, and S. N. Lavrynenko, "A novel concept for the manufacture of individual sapphire-metallic hip joint endoprostheses," Journal of Biological Physics and Chemistry **6**, 113-117 (2006).

49. G. Q. Zhou, Y. J. Dong, J. Xu, H. J. Li, J. L. Si, X. B. Qian, and X. Q. Li, "Ø 140 mm sapphire crystal growth by temperature gradient techniques and its color centers," Materials Letters **60**, 901-904 (2006).

50. M. Keith, "The Crystran Handbook of Infra-Red and Ultra-Violet Optical Materials," (Crystran Ltd., 2008).

51. V. Mortet, J. D'Haen, J. Potmesil, R. Kravets, I. Drbohlav, V. Vorlicek, J. Rosa, and M. Vanecek, "Thin nanodiamond membranes and their micro structural, optical and photoelectrical properties," Diamond and Related Materials **14**, 393-397 (2005).

52. P. Christiaens, V. Vermeeren, S. Wenmackers, M. Daenen, K. Haenen, M. Nesládek, M. vandeVen, M. Ameloot, L. Michiels, and P. Wagner, "EDC-mediated DNA attachment to nanocrystalline CVD diamond films," Biosensors & Bioelectronics **22**, 170-177 (2006).

53. W. S. Yang, O. Auciello, J. E. Butler, W. Cai, J. A. Carlisle, J. Gerbi, D. M. Gruen, T. Knickerbocker, T. L. Lasseter, J. N. Russell, L. M. Smith, and R. J. Hamers, "DNA-modified nanocrystalline diamond thin-films as stable, biologically active substrates," Nature Materials **1**, 253-257 (2002).

54. E. T. Vandenberg, L. Bertilsson, B. Liedberg, K. Uvdal, R. Erlandsson, H. lwing, and I. Lundstrom, "structure of 3-aminopropyl triethoxy silane on silicon-oxide," Journal of Colloid and Interface Science **147**, 103-118 (1991).

55. K. van der Maaden, K. Sliedregt, A. Kros, W. Jiskoot, and J. Bouwstra, "Fluorescent nanoparticle adhesion assay: A novel method for surface pK(a) determination of self-assembled monolayers on silicon surfaces," Langmuir **28**, 3403-3411 (2012).

56. H. Lee, S. M. Dellatore, W. M. Miller, and P. B. Messersmith, "Mussel-inspired surface chemistry for multifunctional coatings," Science **318**, 426-430 (2007).

57. B. R. Johnson, "Theory of morphology-dependent resonances - shape resonances and width formulas," Journal of the Optical Society of America A Optics Image Science and Vision **10**, 343-352 (1993).

Chapter 2

Electronic monitoring of chemical DNA denaturation on nanocrystalline diamond electrodes with different molarities and flow rates

Published in *Phys. Status Solidi A*, **210**, 911 – 917 (2013)

M. S. Murib[1], B. van Grinsven[1], L. Grieten[1], S. D. Janssens[1], V. Vermeeren[2], K. Eersels[1], J. Broeders[1], M. Ameloot[2], L. Michiels[2], W. De Ceuninck[1,3], K. Haenen[1,3], M. J. Schöning[4], and P. Wagner[1,3]

1. Institute for Materials Research, Hasselt University, Wetenschapspark 1, B-3590 Diepenbeek, Belgium
2. Biomedical Research Institute, Agoralaan, Hasselt University, B-3590 Diepenbeek, Belgium
3. IMEC vzw, Division IMOMEC, Wetenschapspark 1, B-3590 Diepenbeek, Belgium
4. Institute for Nano- and Biotechnologies, Aachen University of Applied Sciences, Heinrich-Mußmann-Straße 1, 52428 Jülich, Germany

2.1 Abstract

Probe DNA, consisting of a 36-mer fragment was covalently immobilized on nanocrystalline chemical vapour deposition (CVD) diamond electrodes and hybridized with a 29-mer target DNA. In this paper, we report on the label-free real-time electronic monitoring of DNA denaturation upon exposure to NaOH at different flow rates and molarities, using electrochemical impedance spectroscopy as readout technology. The impedance response was separated into a denaturation time constant and a medium exchange time constant by means of a double exponential fit. It was observed that the denaturation time is dependent on the flow rate as well as on the molarity of the NaOH. Surprisingly, it was observed that at low molarities (0.05 M) the DNA does not fully denature at low flow rates. Only after flushing the flow cell a second time with 0.05 M NaOH, complete denaturation was achieved. Confocal images were obtained and plotted in 3D graphs to confirm the results. This paper provides a systematic overview of measured denaturation times for different flow rates and at different molarities of NaOH. Optimization of these parameters can be a valuable asset in the field of mutation analysis.

Keywords: CVD diamond, denaturation time constant, deoxyribonucleic acid, electrochemical impedance spectroscopy, mutation analysis

2.2 Introduction

Diamond has proven to be an excellent platform for biomedical research due to its outstanding material properties such as chemical inertness, thermal conductivity and electronic properties [1]. In addition, intrinsic diamond displays a high chemical and electrochemical stability and has a wide band gap (5.5 eV) [2 – 4]. Diamond is an insulator and can be made semiconductive by chemical doping [5]. In recent years there has been a major development of DNA electrochemical biosensors such as field-effect sensors [6 – 8] and sensors monitoring electrical surface properties such as conductance, resistance [9] and capacitance [10]. In addition, diamond proved to be a good transducer for protein sensing [11 – 13]. In previous work it was established that the monitoring of chemically induced denaturation at room temperature is an interesting approach to measure DNA duplex stability as an alternative to thermal denaturation at elevated temperatures [14, 15]. Elaborating on these results we now report on the electronic monitoring of DNA denaturation by NaOH, induced at different flow rates (0.1 – 0.4 mL min^{-1}) with variable molarities (0.05 - 0.4 M), using electrochemical impedance spectroscopy as readout technology. The aim of this paper is to find optimal DNA denaturation conditions, ensuring complete denaturation within the shortest time span possible, while leaving the possibility for electrochemical detection. These optimal conditions can be implemented in single nucleotide polymorphism (SNP) detection studies based on electrochemical detection of DNA denaturation [14].

2.3 Experimental

2.3.1 Synthesis of nanocrystalline diamond (NCD)

A 2-inch doped (1 – 2 Ω cm) p-type crystalline silicon wafer (100) was seeded with ultra-dispersed detonation diamond powder in an ultrasonic bath. NCD films with thicknesses of ~ 100 nm and grain sizes of 50 nm were grown on this silicon substrate, using microwave plasma-enhanced chemical vapour deposition (MPECVD) in an ASTEX reactor equipped with a 2.45 GHz microwave generator. This is achieved by using a standard mixture of 15 sccm methane gas (CH_4) and 485 sccm hydrogen gas (H_2) to deposit the NCD thin films onto the silicon wafer. The growth was performed under a pressure of 33 Torr, and temperature of

710 °C, the microwave power was set to 3500 W. The growth rate was ~ 600 nm h^{-1}. In addition, the chemical vapour deposition (CVD) deposition was done with an admixture of trimethyl borane ($B(CH_3)_3$) to the CH_4 gas with a concentration ratio of 200 ppm B/C to dope the NCD with boron and achieve a good electrical conductivity in the range of 1 Ω cm [16].

2.3.2 Sample preparation

Probe DNA, consisting of a 36-mer fragment was covalently immobilized on NCD electrodes and hybridized with 29-mer target DNA. First, the diamond surface was hydrogenated. The hydrogenation was done at 700 °C during 30 s at 3500 W, 12 kPa and 1000 sccm hydrogen gas (H_2) [17]. After hydrogenation the samples were placed inside a glovebox under nitrogen atmosphere. The hydrogenated NCD was covered with a thin film of unsaturated fatty acid (10-undecenoic acid) and was exposed to UV radiation (254 nm, 265 mW cm^{-2}) for 20 h under nitrogen atmosphere. The double bonds of the unsaturated fatty acid chains were broken down and a covalent bond with the hydrogen-terminated diamond was established. This process was mediated by photoemission from the surface as proposed for the photochemical grafting of alkenes to silicon surfaces [3, 4]. The fatty acid layer was about 2 nm thick [18]. The unbound fatty acid chains were washed off using acetic acid and ultrapure water at 120 °C. In this way, a carboxyl (COOH) terminated NCD surface was obtained. Zero-length 1-ethyl-3-3-dimethylaminopropyl-carbodiimide (EDC) was used for the covalent coupling of the 50 side of an aminomodified 36-mer ssDNA fragment to the carboxyl-terminated surface in 2-[N-morpholino]-ethannesulphonic acid (MES) buffer at 4 °C. In a following step, 6mL FAM-488-modified DNA was mixed with 14 μL 1 × PCR buffer and added to the ssDNA-modified NCD sample. The sample was then incubated at 35 °C for 2 h. Non-specifically bound DNA was removed using a double washing step. In a first step, the sample was washed with 2 × saline sodium citrate (SSC) + 0.5% sodium dodecyl sulphate (SDS) for 30 min. Secondly, the sample was washed twice with 0.2 × SSC at 30 °C for 5 min. Finally, the sample was rinsed with phosphate buffered saline (PBS) of pH 7.2 and stored in PBS at 4 °C [2]. By using low salt concentrations in comparison to the concentration in the hybridization buffer and by washing at

temperatures lower than hybridization temperature we avoided premature denaturation.

2.3.3 Experimental setup

Electrochemical impedance measurements were performed using a homemade miniaturized impedance spectroscopy unit [19]. The impedance spectroscopy unit measures the impedance in a frequency range of 100 Hz to 100 kHz, built up logarithmically with 10 equidistant frequencies per decade and a scanning speed of 5.3 s per sweep. The amplitude of the AC voltage was fixed to 10 mV with an offset of 0 mV [19]. A transparent Perspex flow cell with an inner volume of 110 μL was used to exchange media. In this cell, the DNA-modified NCD sample acts as a working electrode, and a gold wire (diameter 500 μm) acts as a counter electrode. The working electrode was pressed onto a copper lid using silver paste. The copper lid serves as back electrode as well as heat sink. Dilutions of PBS and NaOH buffer used in all experiments were made from 10 × PBS pH 7.4 and 2 M NaOH stock solutions in ultrapure water. The exchange of media was conducted through two identical programmable syringe pumps (ProSense, model NE-500, The Netherlands) enabling flow rates of 0.73 μL h^{-1} to 1699 mL h^{-1}. All measurements were done at room temperature ~ 19.2 °C. Conductivity measurements on the different solutions were performed using a conductivity meter (Mettler Toledo, Zaventem, Belgium).

2.3.4 Fluorescence imaging

Fluorescence images were taken on a Zeiss LSM 510 META Axiovert 200M laser scanning confocal fluorescence microscope. To excite the FAM-488 fluorescence dye, a 488 nm argon-ion laser was used with a maximum intensity at the sample surface of 30 μW, in order to avoid bleaching during the image acquisition. The peak emission has a longer wavelength of 518 nm due to vibrational relaxation of the FAM molecule after photon absorption. All images were collected with a 10 × /0.3 Plan Neofluar air objective with a working distance of 5.6 mm. The image size was 225 by 225 μm^2. The pinhole size was 150 μm and the laser intensity was set at 10%. The detector gain, being a measure for the photomultiplier voltage in arbitrary units, was set to 950. The fluorescent intensity was analysed using ImageJ software.

2.4 Experimental Results

2.4.1 Impedimetric characterization

Figure 2.1 shows the Nyquist plots for a DNA-modified diamond sample in different states in PBS buffer solution. The NCD was modified first with ssDNA and measured with the impedance spectroscopy unit. The real (Y_{real}) and imaginary ($Y_{imaginary}$) admittance were found to be 0.00249 and 0.0012 Ω^{-1}, respectively. After hybridization with target DNA the impedance was measured again, resulting in 0.00242 and 0.00121 Ω^{-1} for Y_{real} and $Y_{imaginary}$. Then, the DNA was denatured by introducing 0.1 M NaOH into the flow cell and a third Nyquist plot is constructed. As a result, Y_{real} increased to 0.00256 Ω^{-1} and $Y_{imaginary}$ decreased to 0.0011 Ω^{-1}. After denaturation the impedance was not completely reversed towards its initial state. The lack of this complete reversibility is yet unclear but might be due to the induced changes in the molecular layer by NaOH [20]. The admittance was drawn instead of the impedance in order to get a higher resolution spectrum.

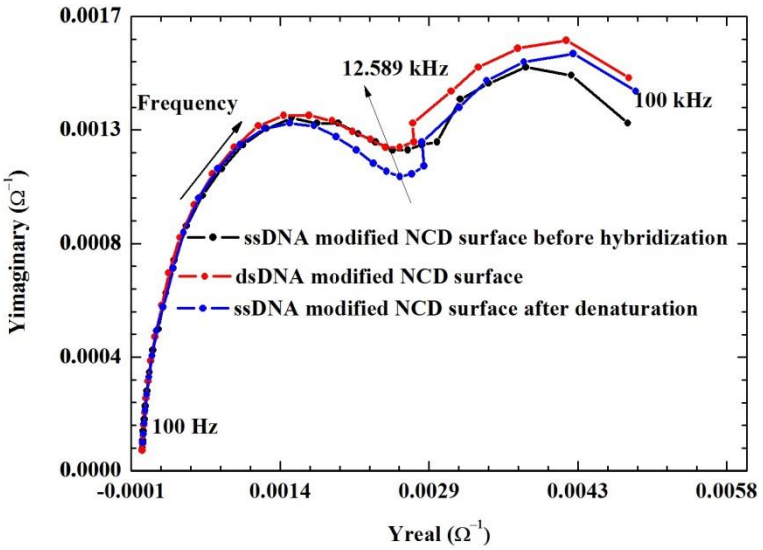

Figure 2.1: Nyquist plots for NCD, modified with ssDNA, then hybridized with its target and after denaturation.

The full frequency spectrum of the impedimetrical data (100 Hz to 100 kHz) can be simulated with a 5-element circuit consisting of a resistor, representing the bulk solution inside the flow cell, in series with two complex resistors, representing the molecular layer and space-charge region, respectively. This circuit is shown in Figure 2.2. In the low frequency part, R_2 and R_3 will dominate most of the impedimetric signal with only a minor contribution of the capacitive elements inside the circuit. In the mid-frequency range, the capacitive elements play a more prominent role leading to a more pronounced imaginary part of the Nyquist plot in these frequencies. At 1 MHz, the impedance is dominated by the solution resistance R_1 [20].

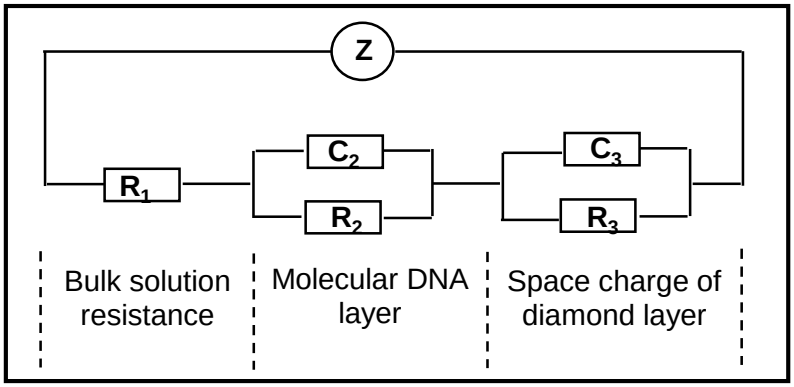

Figure 2.2: Circuit model used to analyse Nyquist plots.

2.4.2 Real-time monitoring of denaturation

Hybridization induced a significant change in the impedance of the interface in the frequency range between ~ 10 kHz and 1 MHz [20]. Therefore, the data was monitored at 12.589 kHz, ensuring a high effect size and a high signal-to-noise ratio and is not conflicting with the frequency of the power net (always a multiple of 50 Hz).

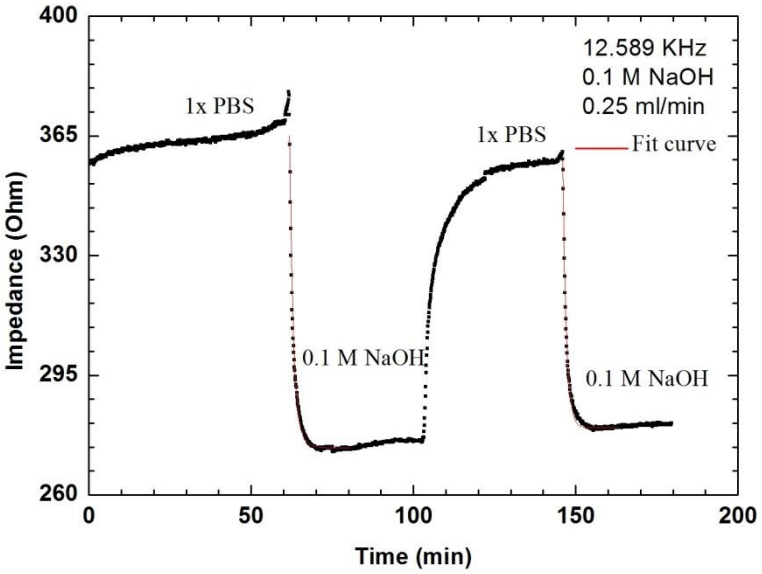

Figure 2.3: Real-time denaturation of dsDNA at 0.25 mLmin^{-1} medium exchange flow rate and using 0.1M NaOH. The red curves indicate the exponential fits. Results are monitored at 12.589 kHz.

Figure 2.3 shows the real-time denaturation of dsDNA immobilized onto boron doped NCD. First, 1 × PBS was administered into the flow cell. After stabilization of the impedance, 0.1 M NaOH was injected into the cell, causing the dsDNA to denature. As a result the impedance started to decrease exponentially due to the denaturation effect and due to the fact that 0.1 M NaOH is more conductive than PBS [19]. However, a small overshoot was encountered as a result of the perturbation of the fluid in the cell caused by pumping medium into the flow cell. After stabilization of the signal, 3 mL of PBS solution was pumped at a speed of 0.25 mL min^{-1} into the cell replacing any NaOH present in the cell, causing the impedance to increase again to a lower level than the initial PBS level. To determine the time constant of medium exchange, NaOH is administered a second time, causing a second decrease in impedance solely due to exchanging PBS with NaOH. The time constants of denaturation (τ_1), and medium exchange (τ_2) were mathematically calculated using the following fit functions [6, 14, 21]:

Fit function 1:

$$Z(t) = Z(t = \infty) + A_1 . exp\left\{-\frac{t}{\tau_1}\right\} + A_2 . exp\left\{-\frac{t}{\tau_2}\right\},$$

Fit function 2:

$$Z(t) = Z(t = \infty) + A_2 . exp\left\{-\frac{t-t_2}{\tau_2}\right\}.$$

The double-exponential fit function 1 for superimposed, independent decay processes is known e.g. from the decomposition of biomass (tomato leaves) and the mass loss of tomato DNA as a function of time [21] and the protein adsorption to solution-gate field-effect transistors [6]. The parameter A_1 represents the denaturation-related decay amplitude and τ_1 the associated time constant; the amplitude A_2 refers to the impedance drop by the medium exchange and τ_1 is the corresponding time constant. The fit function 2 describes solely the influence of the medium exchange from 1 × PBS to 0.1 M NaOH after the denaturation has taken place and is therefore representative for the medium exchange as such. The values for τ_1 and τ_2, calculated in this way were 2.3 ± 0.2 min (95% confidence limit) and 1.1 ± 0.01 min, respectively. These values correlate well with values described by van Grinsven *et al.* [14]. To determine the effect of slow and fast medium exchange on the denaturation time constant of dsDNA, measurements were performed at four different flow rates (0.1, 0.25, 0.5 and 1 mL min^{-1}). The data were analysed as described above.

Figure 2.4 shows the normalized impedance decay at these four flow rates. It can be observed that the increase in flow rate caused the dsDNA to denature faster. The time constant for denaturation τ_1 decreased from 3.5 ± 0.01 min to 2.3 ± 0.2 min, 0.8 ± 0.2 min and 0.6 ± 0.1 min, respectively. Next, the change in denaturation time constant as a function of NaOH concentration change was analysed at a constant flow rate of 0.1 mL min^{-1} by using three different NaOH concentrations (0.1, 0.2 and 0.4 M) as shown in Figure 2.5. The increase in NaOH concentration caused the dsDNA to denature faster. It was calculated that the time constant for denaturation τ_1 decreased from 3.5 ± 0.01 min to 1.8 ± 0.3 min and 0.9 ± 0.05 min, respectively, at increasing concentrations of NaOH.

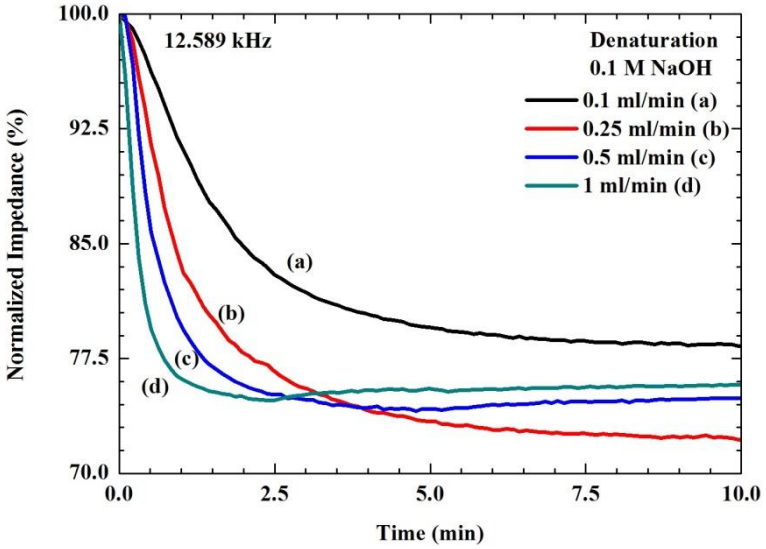

Figure 2.4: Normalized exponential decay at different medium exchange flow rates using 0.1 M NaOH as a denaturing agent.

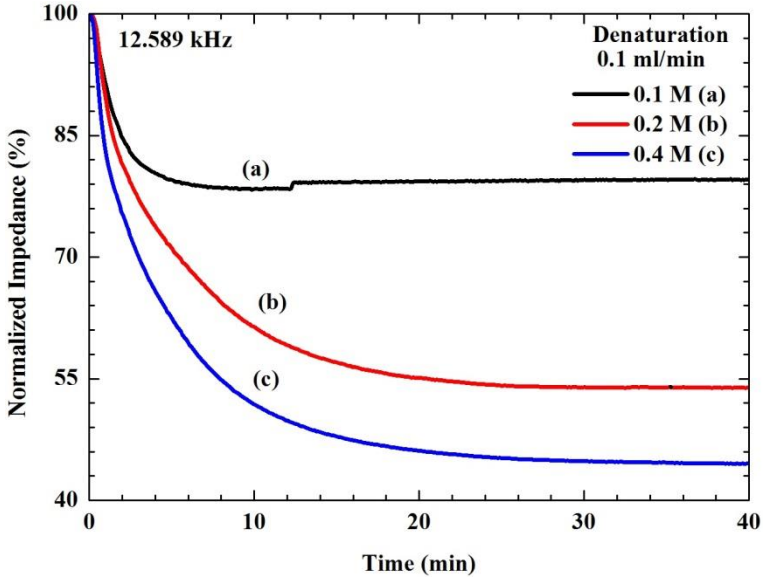

Figure 2.5: Normalized exponential decay at a fixed flow rate of 0.1 mL min^{-1}, using different molarities of NaOH (0.1, 0.2 and 0.4 M).

Fluorescence images were taken after every hybridization and denaturation step to support the experiments. The results are summarized in Figure 2.6. The average fluorescence intensity after three hybridization cycles is 63 arbitrary

units (a.u.). The average fluorescent intensity after denaturation is 14 a.u., proving complete denaturation of the dsDNA.

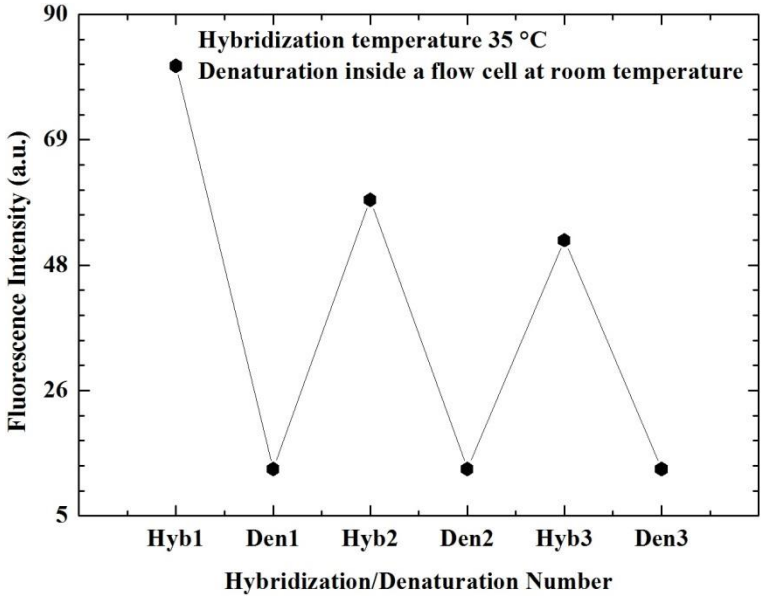

Figure 2.6: Fluorescence intensity graph after successive hybridization and denaturation steps.

In addition, denaturation was also performed using 0.05 M NaOH at a constant flow rate of 1 mL min^{-1}. The results are shown in Figure 2.7. It could be observed that the impedance showed an exponential growth rather than a decay when denaturing the DNA using 0.05 M NaOH. This can be explained by the fact that 0.05 M NaOH holds a lower salt concentration than 1 × PBS, resulting in a lower conductivity. These results were confirmed by measuring the conductivity of the different solutions using a conductivity meter (Mettler Toledo, Zaventem, Belgium). Conductivity measurements are summarized in Table 2.1.

Time constants were calculated in a similar manner as described above. This behaviour was analysed at the four flow rates described earlier. The denaturation at 0.5 mL min^{-1} speed showed a similar behaviour. The respective time constants for denaturation τ_1 at 1 and 0.5 mL min^{-1} were 1.2 ± 0.1 min and 1.7 ± 0.3 min, respectively. Decreasing the flow rate to 0.25 and 0.1 mL min^{-1} resulted in a drift in impedance at the first and second NaOH plateau.

Table 2.1: Conductivity measurements performed on the solutions used during electrochemical monitoring of denaturation.

Solution	Conductivity ($mScm^{-1}$)
1 x PBS	13.3
0.05 M NaOH	11.2
0.1 M NaOH	22.3
0.2 M NaOH	42.1
0.4 M NaOH	79.2

To understand this behaviour in more detail, confocal images were taken at these plateaus as well as at the first PBS plateau (indicated as a, b and c in Figure 2.7) when measuring at these low flow rates.

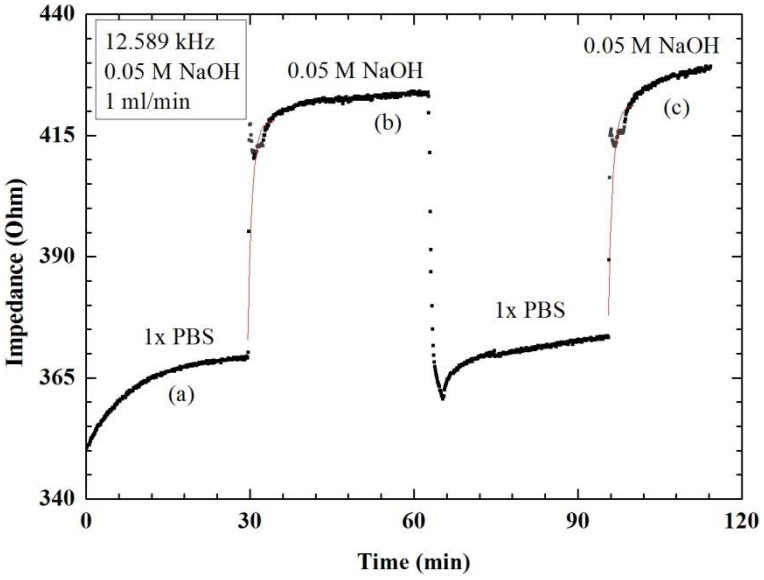

Figure 2.7: Real-time denaturation of dsDNA at 1 mL min^{-1} medium exchange flow rate and using 0.05 M NaOH. Results are monitored at 12.589 kHz.

The resulting fluorescence profiles were plotted in 3D graphs using the 'interactive 3D surface plot' plugin in ImageJ as shown in Figure 2.8. Hybridization of target DNA was achieved as can be concluded from Figure 2.8a. After the first addition of NaOH, not all DNA was denatured as proven by the

image in Figure 2.8b, showing that part of the DNA is still present on the sample. To give a more complete overview of the sample coverage, a bigger area was scanned. This provides an explanation for the continuous drift in impedance at these low flow rates. After a second addition of NaOH to the flow cell, the DNA was denatured more completely, as can be obtained from Figure 2.8c. The little remaining DNA on the surface explains why a small drift is still observed after the second addition of 0.05 M NaOH at these low flow rates. The interactive 3D surface plot settings were for Figure 2.8a: grid size 128, smoothing 3.0, max 32% and min 27% and for the Figures 2.8b and 2.8c: grid size 128, smoothing 3.0, max 40% and min 8%.

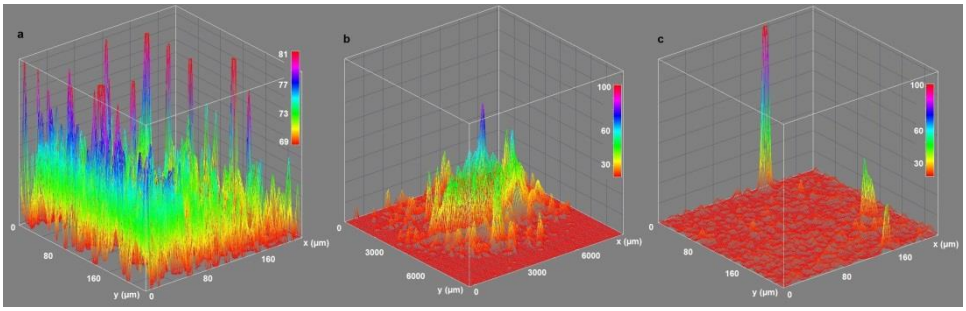

Figure 2.8: Fluorescence 3D graphs after 0.05 M NaOH introduction into the flow cell. Panels a, b and c correspond with points a, b and c in Figure 2.7. (a) Surface plot of NCD modified with dsDNA (225 × 225 μm^2). (b) Surface plot of the same sample after the first addition of 0.05 M NaOH at a flow rate of 0.1 mL min^{-1} (9000 × 9000 μm^2). (c) Surface plot of the same sample after a second addition of NaOH of the same molarity at the same flow rate (225 × 225 μm^2).

2.5 Discussion

This paper provides an overview of the effect of varying flow rates and NaOH concentration on the denaturation time constant τ_1 and the medium-exchange constant τ_2. Measurements were performed at four different flow rates and four different NaOH concentrations. Table 2.2 summarizes the denaturation and medium exchange time constants for 0.05, 0.1, 0.2 and 0.4 M NaOH as a function of flow rate. It can be concluded from these results that τ_1 decreases with increasing flow rate for all molarities of NaOH. Furthermore, τ_1 decreases at increasing concentration of NaOH at constant flow rate. In addition the denaturation time values at 0.1 M NaOH and 0.25 mL min^{-1} flow rate correlate

well with denaturation time constant values reported by van Grinsven *et al.* [14]. However, when using 0.05 M NaOH a flow rate of at least of 0.5 mL min^{-1} is required to fully denature the DNA during the first addition of NaOH. This can be attributed to the fact that there is less shear force in the cell at low flow rates, and as a result only chemical denaturation is taking place with no frictional force to enhance the denaturation. At high concentrations of NaOH the DNA can be denatured by chemical denaturation alone, whereas at 0.05 M NaOH the concentration is too low to fully denature the DNA and thus requiring additional frictional shear force.

Table 2.2: Denaturation and medium-exchange time constants (τ_1 and τ_2) at differential flow rates and different NaOH concentrations.

	Medium-exchange flow rate (mL min^{-1})	τ_1 (min)	Denaturation R^2	τ_2 (min)	Medium exchange R^2
0.05 M NaOH	0.10	/	/	/	/
	0.25	/	/	/	/
	0.50	1.7 ± 0.3	0.968	1.2 ± 0.1	0.946
	1.00	1.2 ± 0.1	0.948	0.8 ± 0.1	0.977
0.1 M NaOH	0.10	3.5 ± 0.01	0.996	1.6 ± 0.02	0.996
	0.25	2.3 ± 0.2	0.993	1.1 ± 0.01	0.993
	0.50	0.8 ± 0.2	0.986	0.7 ± 0.02	0.993
	1.00	0.6 ± 0.1	0.989	0.3 ± 0.01	0.995
0.2 M NaOH	0.10	1.8 ± 0.3	0.979	3.9 ± 0.1	0.962
	0.25	1.3 ± 0.3	0.988	2.4 ± 0.1	0.980
	0.50	0.6 ± 0.2	0.974	1.1 ± 0.1	0.971
	1.00	0.3 ± 0.1	0.990	0.6 ± 0.02	0.990
0.4 M NaOH	0.10	0.9 ± 0.1	0.932	2.5 ± 0.1	0.912
	0.25	0.5 ± 0.1	0.932	1.6 ± 0.04	0.944
	0.50	0.3 ± 0.1	0.967	1.5 ± 0.03	0.921
	1.00	0.2 ± 0.04	0.975	0.9 ± 0.02	0.907

2.6 Conclusions

The results provided in this paper prove that the denaturation times provided by van Grinsven *et al.* [14] can be decreased by increasing the flow rate or the concentration of NaOH. Measurements performed using low concentrations of NaOH show that high flow rates are necessary to denature the DNA. The

mechanical force exerted by the fluid motion contributes to the denaturation of the dsDNA and the removal of the denatured strands. Therefore, the NaOH concentration should be at least 0.1 M to ensure full denaturation of the dsDNA at flow rates below 0.5 mL min^{-1}. Optimal conditions for industrial applications, requiring high throughput can be found in the high molarity and high flow rate range where denaturation occurs faster. However, if the application requires more detail, lower flow rates at a NaOH concentration of 0.1 M should be used.

2.7 Acknowledgements

Financial support by the Life-Science Initiative of the Province of Limburg and the Research Foundation Flanders FWO (Project G.0829.09: 'Synthetic diamond films as platform material for novel DNA sensors with electronic detection principles') is greatly appreciated.

2.8 References

1. S. Wenmackers, V. Vermeeren, M. vandeVen, M. Ameloot, N. Bijnens, K. Haenen, L. Michiels, and P. Wagner, "Diamond-based DNA sensors: surface functionalization and read-out strategies," Physica Status Solidi a-Applications and Materials Science **206**, 391-408 (2009).

2. V. Vermeeren, S. Wenmackers, M. Daenen, K. Haenen, O. A. Williams, M. Ameloot, M. Vandeven, P. Wagner, and L. Michiels, "Topographical and functional characterization of the ssDNA probe layer generated through EDC-mediated covalent attachment to nanocrystalline diamond using fluorescence microscopy," Langmuir **24**, 9125-9134 (2008).

3. P. Christiaens, V. Vermeeren, S. Wenmackers, M. Daenen, K. Haenen, M. Nesládek, M. vandeVen, M. Ameloot, L. Michiels, and P. Wagner, "EDC-mediated DNA attachment to nanocrystalline CVD diamond films," Biosensors & Bioelectronics **22**, 170-177 (2006).

4. W. S. Yang, O. Auciello, J. E. Butler, W. Cai, J. A. Carlisle, J. Gerbi, D. M. Gruen, T. Knickerbocker, T. L. Lasseter, J. N. Russell, L. M. Smith,

and R. J. Hamers, "DNA-modified nanocrystalline diamond thin-films as stable, biologically active substrates," Nature Materials **1**, 253-257 (2002).

5. O. A. Williams, and M. Nesládek, "Growth and properties of nanocrystalline diamond films," Physica Status Solidi A - Applications and Materials Science **203**, 3375-3386 (2006).

6. M. Krátká, A. Kromka, E. Ukraintsev, M. Ledinský, A. Brož, M. Kalbacova, and B. Rezek, "Function of thin film nanocrystalline diamond-protein SGFET independent of grain size," Sensors and Actuators B-Chemical **166**, 239-245 (2012).

7. S. Ingebrandt, Y. Han, F. Nakamura, A. Poghossian, M. J. Schöning, and A. Offenhäusser, "Label-free detection of single nucleotide polymorphisms utilizing the differential transfer function of field-effect transistors," Biosensors & Bioelectronics **22**, 2834-2840 (2007).

8. A. Poghossian, M. H. Abouzar, F. Amberger, D. Mayer, Y. Han, S. Ingebrandt, A. Offenhäusser, and M. J. Schöning, "Field-effect sensors with charged macromolecules: Characterisation by capacitance-voltage, constant-capacitance, impedance spectroscopy and atomic-force microscopy methods," Biosensors & Bioelectronics **22**, 2100-2107 (2007).

9. M. Y. Vagin, A. A. Karyakin, and T. Hianik, "Surfactant bilayers for the direct electrochemical detection of affinity interactions," Bioelectrochemistry **56**, 91-93 (2002).

10. A. Poghossian, M. H. Abouzar, M. Sakkari, T. Kassab, Y. Han, S. Ingebrandt, A. Offenhäusser, and M. J. Schöning, "Field-effect sensors for monitoring the layer-by-layer adsorption of charged macromolecules," Sensors and Actuators B-Chemical **118**, 163-170 (2006).

11. L. Grieten, S. D. Janssens, A. Ethirajan, N. Vanden Bon, M. Ameloot, L. Michiels, K. Haenen, and P. Wagner, "Real-time study of protein adsorption on thin nanocrystalline diamond," Physica Status Solidi A - Applications and Materials Science **208**, 2093-2098 (2011).

12. W. S. Yeap, Y. Y. Tan, and K. P. Loh, "Using detonation nanodiamond for the specific capture of glycoproteins," Analytical Chemistry **80**, 4659-4665 (2008).

13. X. F. Wang, Y. Ishii, A. R. Ruslinda, M. Hasegawa, and H. Kawarada, "Effective surface functionalization of nanocrystalline diamond films by direct carboxylation for pdgf detection via aptasensor," ACS Applied Materials & Interfaces **4**, 3526-3534 (2012).

14. B. van Grinsven, N. V. Bon, L. Grieten, M. Murib, S. D. Janssens, K. Haenen, E. Schneider, S. Ingebrandt, M. J. Schöning, V. Vermeeren, M. Ameloot, L. Michiels, R. Thoelen, W. De Ceuninck, and P. Wagner, "Rapid assessment of the stability of DNA duplexes by impedimetric real-time monitoring of chemically induced denaturation," Lab on a Chip **11**, 1656-1663 (2011).

15. B. van Grinsven, N. Vanden Bon, H. Strauven, L. Grieten, M. Murib, K. L. J. Monroy, S. D. Janssens, K. Haenen, M. J. Schöning, V. Vermeeren, M. Ameloot, L. Michiels, R. Thoelen, W. De Ceuninck, and P. Wagner, "Heat-Transfer Resistance at Solid-Liquid Interfaces: A Tool for the Detection of Single-Nucleotide Polymorphisms in DNA," ACS Nano **6**, 2712-2721 (2012).

16. O. A. Williams, M. Nesládek, M. Daenen, S. Michaelson, A. Hoffman, E. Osawa, K. Haenen, and R. B. Jackman, "Growth, electronic properties and applications of nanodiamond," Diamond and Related Materials **17**, 1080-1088 (2008).

17. V. Mortet, J. D'Haen, J. Potmesil, R. Kravets, I. Drbohlav, V. Vorlicek, J. Rosa, and M. Vanecek, "Thin nanodiamond membranes and their micro structural, optical and photoelectrical properties," Diamond and Related Materials **14**, 393-397 (2005).

18. S. Wenmackers, S. D. Pop, K. Roodenko, V. Vermeeren, O. A. Williams, M. Daenen, O. Douhéret, J. D'Haen, A. Hardy, M. K. Van Bael, K. Hinrichs, C. Cobet, M. vandeVen, M. Ameloot, K. Haenen, L. Michiels, N. Esser, and P. Wagner, "Structural and optical properties of DNA layers covalently attached to diamond surfaces," Langmuir **24**, 7269-7277 (2008).

19. B. van Grinsven, T. Vandenryt, S. Duchateau, A. Gaulke, L. Grieten, R. Thoelen, S. Ingebrandt, W. De Ceuninck, and P. Wagner, "Customized impedance spectroscopy device as possible sensor platform for biosensor applications," Physica Status Solidi A - Applications and Materials Science **207**, 919-923 (2010).

20. W. S. Yang, J. E. Butler, J. N. Russell, and R. J. Hamers, "Interfacial electrical properties of DNA-modified diamond thin films: Intrinsic response and hybridization-induced field effects," Langmuir **20**, 6778-6787 (2004).

21. J. Poté, P. Rossé, W. Rosselli, V. T. Van, and W. Wildi, "Kinetics of mass and DNA decomposition in tomato leaves," Chemosphere **61**, 677-684 (2005).

Chapter 3

Adding biosensing functionalities to implant materials: heat-transfer based characterization of DNA on synthetic sapphire chips

Submitted to *ACS Applied Materials and Interface,* January 2014

M. S. Murib [1], W. S. Yeap [1], Y. Eurlings [1], B. van Grinsven [1], H. G. Boyen [1], L. Michiels [2], M. Ameloot [2], R. Carleer [1,3], J. Warmer [4], P. Kaul [4], K. Haenen[1,3], W. De Ceuninck [1,3], M. J. Schöning [5], and P. Wagner [1,3]

1. Hasselt University, IMO, Wetenschapspark 1, B-3590 Diepenbeek, Belgium
2. Hasselt University, BIOMED, Agoralaan, B-3590 Diepenbeek, Belgium
3. IMEC vzw, IMOMEC, Wetenschapspark 1, B-3590 Diepenbeek, Belgium
4. Bonn-Rhein-Sieg University of Applied Sciences, von Liebig Str. 20, D-53359 Rheinbach, Germany
5. Aachen University of Applied Sciences, INB, H. Mussmann Str. 1, D-52428 Jülich, Germany

3.1 Abstract

In this study we show that synthetic sapphire (Al_2O_3), an established implant material, can also serve as a platform material for biosensors comparable to nanocrystalline diamond. Sapphire chips, beads, and powder were first modified with (3-Aminopropyl) triethoxysilane (APTES), followed by succinic anhydride (SA), and, finally, single-stranded deoxyribonucleic acid (ss-DNA) probe was EDC coupled to the functionalized layer. The presence of ATPES-succinic anhydride layer on sapphire powder was confirmed by Thermogravimetric analyis (TGA) and Fourier-transform infrared (FT-IR) spectroscopy. The areal DNA density was quantified using the Alexa-488 label in X-ray photoelectron spectroscopy (XPS). Fluorescence microscopy was performed to demonstrate the successful coupling of fluorescently tagged target DNA to the pre-immobilized probe DNA. Synthetic sapphire is especially suitable for the heat-transfer method (HTM) due to its high thermal conductivity and chemical inertness. The heat-transfer method was performed for the characterization of DNA on synthetic sapphire chips. These results bring forward the first step towards thermotronic detection schemes of biological compounds using synthetic sapphire as a platform material.

Keywords: Synthetic sapphire, nanocrystalline diamond, heat-transfer resistance, Fourier-transform infrared spectroscopy, thermogravimetric analysis, X-ray photoelectron spectroscopy, confocal fluorescence micrsocopy, single-nucleotide polymorphisms in DNA.

3.2 Introduction

Molecular electronics and biological sensing have placed increased emphasis on understanding the electrical properties of molecules and molecular layers on surfaces [1]. In recent years biological detection has been revolutionized by surface-based methods for detection of biological molecules such as cells [2], DNA [3] and proteins [3]. In modern biomedical sciences, the detection of DNA hybridization and / or protein binding at surfaces is made through a variety of "biochip" devices, lending particular importance to biologically modified surfaces [4]. In the field of substrate materials for biosensors, extensive work has been carried out on gold [5-11], silicon [12-14], glass [15], and carbon based materials [16-19]. Gold seems ideal for electronic sensing principles but it is not the most economic choice. The degradation of silicon and glass interfaces in aqueous solutions limits their use to that of disposable biosensors [20, 21]. Carbon-based materials like diamond or graphene are often used in electrochemical biosensors due to their inertness, low electrical resistivity and beneficial mechanical properties [16-19]. Different graphene-based materials were used as an electrochemical platform for the detection of various biomolecules and chemicals [22]. However, the surface modification of graphene is rather difficult because of its surface inertness due to the π orbitals [23]. Chemical vapour deposition (CVD) diamond has proven to be an excellent transducer material due to its chemical inertness, stability at elevated temperatures, biocompatibility, and excellent thermal conductivity [24]. Moreover, diamond can be doped up to metallic conductivity [25]. So far, diamond has been employed for sensing with chemical and thermal denaturation of DNA [16-18], aptamers [26], enzymes [27], and glucose [28, 29]. Recently, conducting diamond has been shaped into microelectrode arrays for eye retina implants [30].

In this paper, we will show that sapphire can also serve as a platform material for biosensors comparable to nanocrystalline diamond. Sapphire shows outstanding chemical inertness, wear resistance, and biocompatibility [31]. Hence, it is widely used for implant materials such as hip implants [31], dental implants [32], and endosseous implants [33]. Moreover, its wide optical transmission band from ultraviolet (UV) to near-infrared (near-IR) [34] suggests

application potential in optical biosensors. Due to the fact that sapphire has a good thermal conductivity [34] and low thermal expansion [35], it appears favorable for use in optical biosensors operating in a broader temperature regime. Table 3.1 shows the physical properties of several materials, i.e. sapphire, diamond, silicon, quartz, and copper such as their thermal expansion, thermal conductivity, and hardness. A previous theoretical study based on elastic light scattering showed that sapphire and diamond have comparable optical detection ability for the binding of proteins [36]. Sapphire has so far not been used as a platform material for biosensors with electronic readout due to its electrically insulating behavior [37]. However, thanks to the biosensoric heat transfer method [17] the immobilization platform does not need to be electrically conducting. Based on these results, and due to the fact that single-crystalline synthetic sapphire is cheap (10 €/1 cm^2) compared to nanocrystalline diamond (25 €/1 cm^2), we now report on the surface modification of sapphire materials (single crystalline chips, polycrystalline microbeads, and amorphous powder) with carboxylic groups and double-stranded DNA. We also report in this article on the heat-transfer resistance at sapphire surface-liquid interface to detect single-nucleotide polymorphisms in DNA.

Table 3.1: Thermal, mechanical and chemical properties of selected sensor materials. All data refer to ambient conditions (273-300 K).

	Sapphire	Diamond	Silicon	Quartz	Copper
Thermal conductivity [W / m . K]	27.21 (a)	2600 (a)	163.3 (a)	1.114 (a)	398 (e)
Linear thermal expansion coefficient [K^{-1}]	5.6×10^{-6} // c-axis (a) 5.0×10^{-6} ⊥ c-axis (a)	0.003×10^{-6} (a)	2.6×10^{-6} (a)	7.1×10^{-6} (a)	16.5×10^{-6} (e)
Specific heat capacity [J / Kg . K]	763 (a)	502 (a)	703 (a)	858 (a)	384.56 (e)
Knoop hardness	1800 // c-axis 2200 ⊥ c-axis (a)	5700 to 10400 (a)	1150 (a)	610 (a)	163 (f)
Chemical inertness	Inert (b)	Inert (c)	Degradable in aqueous solutions (d)	Degradable in aqueous solutions but less than silicon (d)	Not reactive in water, slow oxidation in moist air (g)

(a) reference 35, (b) reference 31, (c) reference 24, (d) references 20, 21, (e) reference 38, (f) reference 39, and (g) reference 40.

3.3 Experimental

3.3.1 Surface functionalization

3.3.1.1 Hydroxylation

The sapphire powder and beads were used for optimizing the DNA coupling protocol. The surface composition after each functionalization step can be easily followed by TGA and FT-IR. The sapphire beads were bought from Treibacher Schleifmittel GmbH under the name of ALODUR and the powder was bought from Nablatec under the name Granalox NM 9622. Detailed synthesis can be found from the company website. Prior to any functionalization, the powder and the beads were annealed at 500 °C for 5 hours to remove any surface bound organic impurities. Single-side polished single crystal α-Al_2O_3 (0, 1, $\bar{1}$, 2) chips were purchased from Crystec (Berlin, Germany). The chips were 10 × 10 × 1 mm^3, and the root-mean-square roughness of the polished surfaces measured by atomic force microscopy (AFM) was 0.44 nm over 1x1 μm^2. All sapphire samples were ultrasonically cleaned in acetone, ultrapure water (Sartorius Stedim Biotech Ultra Pure Water System Type 1) and isopropanol for 20 minutes in each bath. Next, the sapphire samples were immersed in 10 mM HNO_3 solution (Figure 3.1.a) at room temperature for 30 minutes to create OH groups on the surface [41, 42]. Afterwards, the sapphire samples were rinsed with ultrapure water and dried with nitrogen gas.

3.3.1.2 Silanization

Silanization of the sapphire samples was carried out by liquid phase deposition of a solution of silane in an organic solvent (Figure 3.1b) [43]. The samples were placed in a 600 mM solution of (3-Aminopropyl)triethoxysilane (APTES, 99%; Sigma-Aldrich) in toluene (≥ 99.9%, Sigma-Aldrich) for 15 hours in a nitrogen gas filled glovebox. To wash off the unbound APTES, the samples were first rinsed with toluene, followed by tetrahydrofuran (THF, ≥ 99.9%, Sigma-Aldrich). After drying the samples in a nitrogen steam, they were cured for 2 hours at 150 °C. Curing at this high temperature will create a much stronger film of APTES on the surface [43]. This creates an amine-modified surface and

subsequent reaction with succinic anhydride (SA) yielding a carboxyl-modified surface (Figure 3.1) [44].

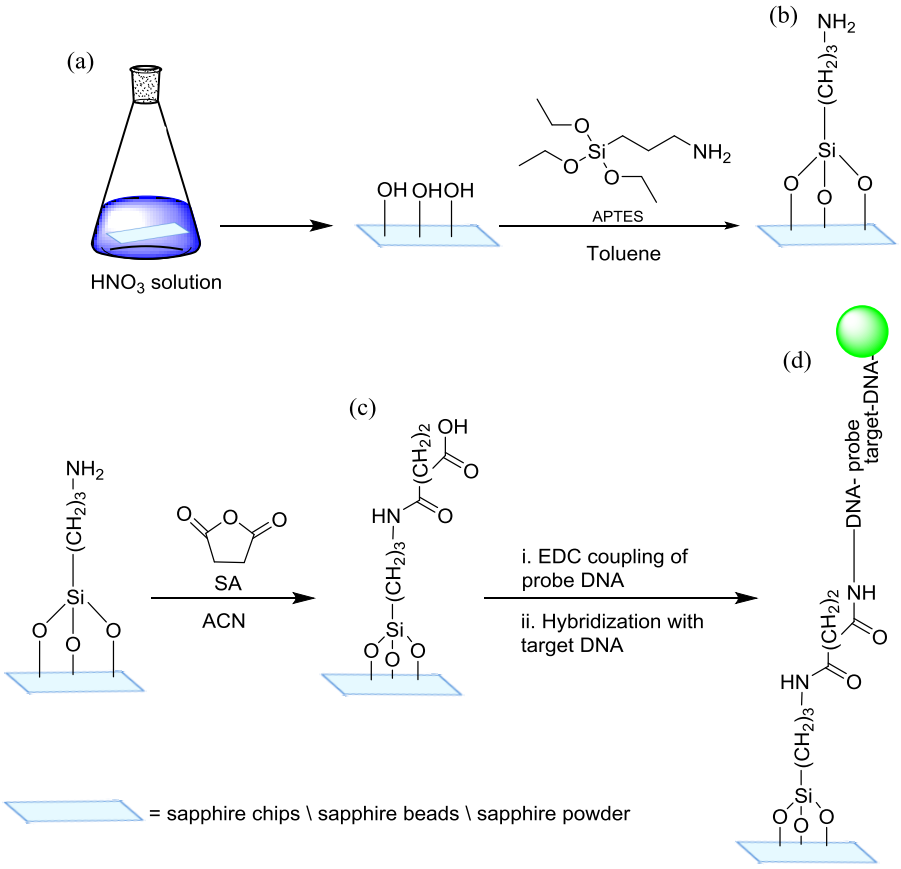

Figure 3.1: Chemical processes in the immobilization of DNA on sapphire surface. (a) Surface hydroxylation of sapphire with HNO_3 solution. (b) Amine terminated surface after functionalization with APTES in toluene. (c) Reaction with succinic anhydride in acetonitrile yielded carboxyl-modified surface. (d) Attachment of DNA probe and target DNA.

Succinic anhydride (SA, ≥ 99.9%, Sigma-Aldrich) was used as a cross-linker molecule to ensure the binding of the amino group of APTES to the 5'-NH_2 termination of the oligonucleotides by providing carboxylic groups at the surface. The samples were placed overnight in a solution 800 mM of SA in acetonitrile (ACN) (anhydrous, 99.8%, Sigma-Aldrich), after which they were rinsed with acetonitrile and dried with nitrogen gas. The amine terminated surface reacts

with one of the carbonyl groups of the SA causing the anhydride ring to open and to form a covalent bond with that carbonyl group. The other carbonyl group is released to form a free carboxylic acid terminated surface [45].

3.3.1.3 DNA grafting

Table 3.2 shows the base sequence of the probe DNA (36 bases), the corresponding full match target DNA (29 bases), mismatch target DNA at base pair 7, and mismatch target DNA at base pair 20. The position of the mismatches with respect to the probe DNA is underlined and indicated by bold letters. The first 7 adenine bases at the 5' terminus in the probe DNA served as a spacer to minimize steric hindering during hybridization due to the proximity of the solid surface. The amine (NH_2) modification at the 5' terminus in the probe DNA is used as a linker molecule of the DNA to the carboxylic terminated surface. The target DNA fragments carry a fluorescent Alexa-488 label at the 5' end to ensure the presence of the probe and target DNA on the surface. The Alexa-488 label will be also used to quantify the areal DNA density in XPS.

Table 3.2: Base sequences of the probe and the corresponding full match and mismatch target DNA and the corresponding theoretical melting temperatures.

Name	Sequence	T_m (°C)
Probe DNA	5´-NH_2-C_6H_{12}-AAAAAAACCCCTGCAGCCCATGTATACCCCCGAACC-3'	
Full Match	5'-Alexa 488-GGT TCG GGG GTA TAC ATG GGC TGC AGG GG-3'	79.5
Mismatch BP 7	5'-Alexa 488-GGT TCG GGG GTA TAC ATG GGC T**C**C AGG GG-3'	76.7
Mismatch BP 20	5'-Alexa 488- GGT TCG GGG **C**TA TAC ATG GGC TGC AGG GG-3'	75.0

Zero-length 1-ethyl-3-3-dimethylaminopropyl-carbodiimide (EDC) was used for the covalent coupling of the 5' side of an aminomodified 36 base pair ssDNA fragment to the carboxylic acid terminated surface in 2-[N-morpholino]-ethannesulphonic acid (MES) buffer at 4 °C. The carboxylic acid terminated sapphire samples (chip / bead / powder) were incubated for 2 hours in a solution made of 30 µL of probe DNA (10 pmol/µL) (Table 3.2, 36 bases,

Eurogentec) and 20 µL EDC (0.26 M) (Thermo Scientific) in MES-buffer (25 mM, pH 6). EDC will facilitate the forming of an amide bond between the carboxylic groups on the surface and the amine on the DNA strand. This reaction requires a pH 4.7 - 6.0, hence the pH of the MES-buffer [20]. After 2 hours of incubation at 4 °C the unbound probe DNA was rinsed off by stringency washes with 1 × Phosphate Buffered Saline (1 × PBS, homemade) and 2 × Saline-Sodium Citrate / 0.5% Sodium Dodecyl Sulfate (2 × SSC / 0.5% SDS, homemade) [20]. Reference samples were prepared by adding MES buffer instead of EDC to the probe DNA. Except for this, this EDC-negative sample underwent the same protocol as the EDC-positive sample.

3.3.1.4 DNA hybridization

Three different types of target DNA labeled with Alexa-488 (Eurogentec) have been used: a sequence, which was complementary to the probe ssDNA and two sequences with a 1-base mismatch at base pair 7 or at base pair 20 (Table 3.2). A solution of 6 µL DNA (100 pmol/µL) was added to 14 µL of 1 × Polymerase Chain Reaction buffer (PCR-buffer, diluted from 10 × PCR-buffer, Roche Diagnostics). This 20 µL of DNA/PCR solution was then added to the probe DNA functionalized sapphire samples and incubated at 35 °C for 2 hours [20]. After the hybridization, the samples were first washed with 2 x SSC / 0.5% SDS; then with 0.2 × SSC at 30 °C; thereafter with 0.2 × SSC at room temperature and finally with 1 × PBS at room temperature [20]. The calculated melting-temperatures (Table 3.2) were based on the online HyTher^{TM} algorithm [46, 47], taking into account the lengths of fragments, the identity and orientation of neighbouring bases, the ionic strength of the buffer, and the fact that all fragments are tethered at one end.

3.3.2 Characterisation of the surface functionalization

3.3.2.1 Quantification of carboxylic groups using Tuluidine Blue O

Toluidine Blue O (TBO, dye content 80%, Sigma-Aldrich) is a cationic compound that will bind with negatively charged groups, mostly deprotonated carboxylic groups on a surface. TBO can be detected by light absorption in the blue region. First, a calibration curve was made of a 5 x 10^{-4} M solution of TBO in 50% acetic

acid. From this solution a dilution series was made. The APTES-SA functionalized samples were soaked in a solution of 5 x 10^{-4} M of TBO in water (pH 10) for 5 hours at room temperature, during which the dye reacted with the ionized carboxylic groups. To wash away unbound dye molecules, the samples were rinsed thoroughly with 0.1 M NaOH. Thereafter, the samples were soaked in a 50% acetic acid solution for 10 minutes [48]. During this last step the bound TBO molecules were released into the solution, coloring it blue. By measuring the absorbance of these solutions with Varian Cary 500 UV-vis-NIR spectrophotometer (Leuven, Belgium) at 633 nm, the concentration of carboxylic groups on the surface could be determined.

3.3.2.2 Fourier-transform infrared spectroscopy (FT-IR)

Infrared spectroscopy was utilized to confirm the presence of APTES on sapphire powder surface. This technique tracks the functional groups on the functionalized sapphire surface. FT-IR spectra were collected using a Perkin Elmer Frontier FT-NIR/MIR spectrometer (Zaventem, Belgium) equipped with a heating cell (Harrick, USA) in the range of 2600-4000 cm^{-1} using KBr pellets technique. KBr powder was grinded with the functionalized sapphire powder and pressed into pellets. Prior to measurements, samples were heated at 120 °C for 2 hours under nitrogen gas in order to remove most of the absorbed water at the sapphire surface. Transmission spectra were acquired using 64 scans and an instrumental resolution of 4 cm^{-1}.

3.3.2.3 Thermogravimetric analysis

The thermal decomposition profile of the functionalized sapphire powder was studied under pyrolysis conditions using TGA (TA Instruments SDT Q600). All samples were heated at 10 °C / min in N_2 atmosphere from room temperature up to 700 °C.

3.3.2.4 X-ray photoelectron spectroscopy (XPS)

X-ray photoelectron spectroscopy (XPS) measurement was performed on a sapphire to estimate the DNA surface coverage. Preliminary results showed that there is one monolayer of APTES on the surface and that the number of DNA

molecules immobilized on the sapphire surface is about 2.8×10^{12} molecules cm^{-2}.

3.3.2.5 Confocal fluorescence microscopy

Fluorescence images were taken on a Zeiss LSM 510 META Axiovert 200 M laser scanning confocal fluorescence microscope. To excite the Alexa-488 fluorescence dye, a 488 nm argon-ion laser was used with a maximum intensity at the sample surface of 30 μW, in order to avoid bleaching during the image acquisition. The peak emission has a longer wavelength of 518 nm due to vibrational relaxation of the Alexa molecule after photon absorption. All images were collected with a 10 ×/0.3 Plan Neofluar air objective with a working distance of 5.6 mm. The image size was 225 by 225 μm². The pinhole size was 150 μm and the laser intensity was set at 10%. The detector gain, being a measure for the photomultiplier voltage in arbitrary units, was set to 950. The fluorescent intensity was analyzed using ImageJ software.

3.3.3 Heat-transfer measurements (HTM)

The denaturation and hybridization of the DNA on the sapphire samples were monitored with a thermal resistance measurement, which is based on the heat-transfer method (HTM) published recently [17]. A schematic layout of the sensors cell is displayed in Figure 3.2.

The device used has PID-controlled heat source, the DNA brush on sapphire, electrolyte, and thermocouples. The heat source is separated from the fluid compartment by the sample. A copper lid was mounted between the heating element and the sample. The internal temperature of the copper block, T_1, was measured by a thermocouple and steered via a PID controller with a power resistor. Heat transfer loss between the copper and the sample was eliminated by applying a thermally conductive silver paint. The fluid compartment was filled with 1 × PBS buffer, and the contact area sapphire-liquid is 28 mm^2. The heat is transferred from the heating element through the copper block and the sample. The temperature of the liquid, T_2, was measured by a second thermocouple. To regulate temperature, the thermocouple signal was mounted to a data acquisition unit (Picolog TC08, Picotech, United Kingdom) and from there

processed using a PID controller algorithm (parameters: P = 10, D = 5, I = 0.1).

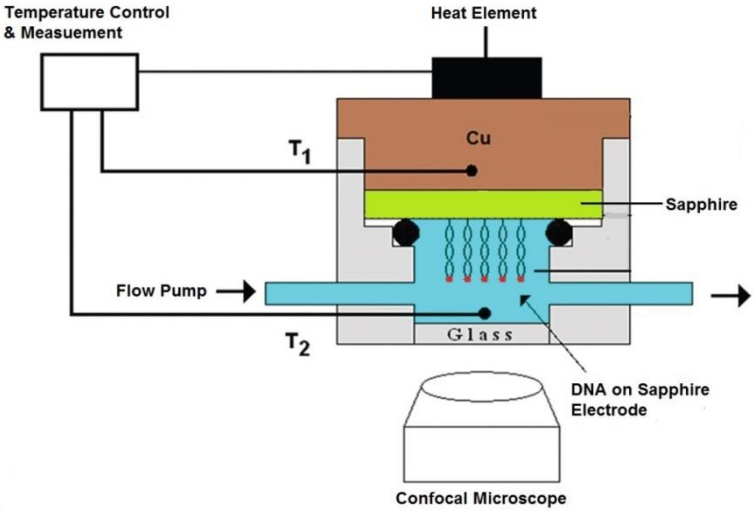

Figure 3.2: A schematic overview of the thermal resistance RTH measuring cell adapted from ref. [17]. The probe DNA is covalently immobilized on a sapphire electrode, while the cell is filled with PBS buffer. The temperature T_1 of the Cu backside contact is measured by a thermocouple and can be actively steered via a PID controller unit. The temperature T_2 inside the liquid is recorded by using a second thermocouple.

The calculated output voltage was sent via a second controller (NI USB 9263, National Instruments, USA) to a power operational amplifier (LM675, Farnell, Belgium) and fed into the power resistor [17]. The sample itself and any surface coverings determine the thermal resistance against the thermal current flowing from the heating element (T_1) to the fluid (T_2). Single stranded DNA on the surface curls up in irregular structures or hairpins and thus, increases the thermal resistance. Due to a higher persistence length, double stranded DNA will stand up on the surface and the spaces between the DNA duplexes allow for better thermal conductivity [17]. As T_1 increased with 1 °C/min from room temperature to 85 °C, the changes of T_2 were monitored. The thermal resistance is defined as the ratio of the temperature difference and the input power:

$$R_{th} = \frac{T_1 - T_2}{P} \quad (1).$$

3.4 Results and Discussion

3.4.1 Quantification of carboxylic groups using Tuluidine Blue O

The COOH densities of the functionalized samples are listed in Table 3.3. Besides sapphire samples, a diamond sample [49], which was also functionalized using the same chemical routes as sapphire, was used for comparison. The diamond surface counted $(1.83 \pm 0.4) \times 10^{14}$ carboxylic groups cm^{-2}, whereas the sapphire surface had $(5.33 \pm 0.4) \times 10^{14}$ carboxylic groups cm^{-2}. The COOH densities of functionalized samples are thus in the order of 10^{14} cm^{-2}, which is consistent with the formation of a dense monolayer [48, 50]. The number of carboxylic groups on both surfaces is of the same order of magnitude, indicating that sapphire is equally suitable as diamond for further functionalization with linker molecules. Moreover, the density of COOH group of our samples is comparable to the density of COOH groups on diamond surface ($4.8 \times 10^{14} \pm 0.5$ cm^{-2}) prepared using undecylenic acid (UA) [48], which was also determined by TBO. The treatment of the sapphire surface with HNO_3 has proven to be effective in creating an oxidized surface for further linking with APTES and carboxylation with SA.

Table 3.3: COOH areal densities of various samples.

Sample	COOH density [molecules cm^{-2}]
Sapphire-APTES-SA	$5.33 \pm (0.4) \times 10^{14}$
Diamond-APTES-SA	$1.83 \pm (0.4) \times 10^{14}$
Diamond-UA [48]	$4.8 \pm (0.5) \times 10^{14}$

3.4.2 Fourier-transform infrared spectroscopy (FT-IR) analysis

Figure 3.3 shows the FT-IR spectra of blank-and APTES-functionalized sapphire powder. Compared to the FT-IR spectrum of blank sapphire, the FT-IR spectrum of APTES-functionalized sapphire contains additional peaks at 2935, 3350, and 3450 cm^{-1}.

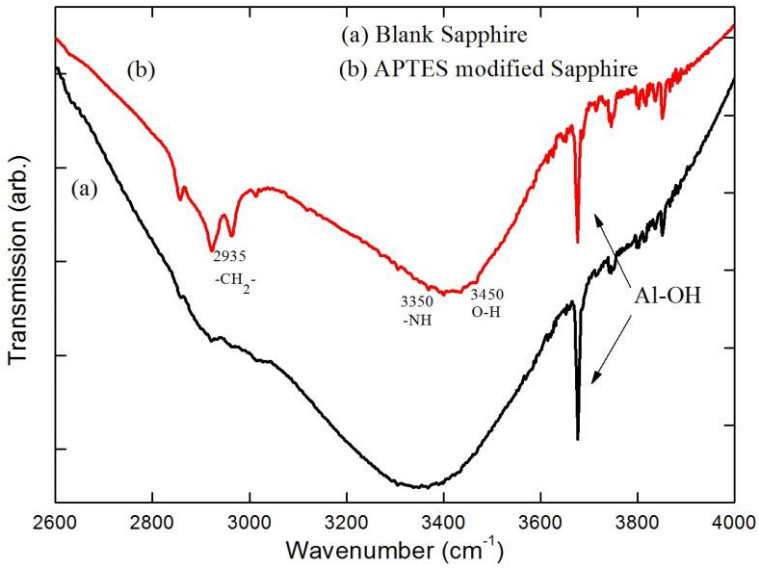

Figure 3.3: FT-IR analysis of functionalized sapphire powder. The peak at 2935 cm^{-1} points to the absorption of CH_2 groups. The peak at 3350 cm^{-1} points to the absorption of $–NH_2$ groups. The peak at 3450 cm^{-1} points to the absorption of OH groups. The peak at 3700 cm^{-1} points to the free Al-OH stretching bonds.

Blank sapphire powder shows a very broad peak centered at around 3350 cm^{-1}. This broad peak can be assigned to O-H stretching vibrations of hydroxyl groups of the non-modified sapphire powder. This peak became narrower and the peak center shifted to 3450 cm^{-1} after functionalization with APTES [51]. This indicates the decrease of surface OH groups after binding to APTES and an increase of $–NH_2$ groups. The absorption of CH_2 groups of APTES is observed at 2935 cm^{-1}, thus further confirms the presence of APTES layer on sapphire surfaces [51]. Unfortunately, the FT-IR data cannot directly indicate the presence of Si-O-Si or Al-O-Si bond linkages, as this region (1100 - 800 cm^{-1}) is obscured by significant absorbance of sapphire (Al-O-Al bonds). In spite of this, the presence of $–CH_2$ and -NH as well as the reduction of O-H at 3450 cm^{-1} after APTES modification confirms that APTES has been grafted on the surface of sapphire. The very sharp peak at 3700 cm^{-1} that appeared for both functionalized and non-functionalized sapphire samples can be assigned to free Al-OH stretching bonds [52].

3.4.3 Thermogravimetric analysis

Figure 3.4 shows the TGA curves of blank (black line), HNO_3 oxidized sapphire (red line), HNO_3-APTES-functionalized (green line) and HNO_3-APTES-SA-functionalized (blue line) sapphire powder. Mass loss was observed for all samples almost immediately after starting up the temperature program (from 86 °C to 436 °C). This mass loss might be due to desorption of surface water and contamination from the samples. A mass loss was observed (~1.2 w%) for both HNO_3-APTES-functionalized and HNO_3-APTES-SA-functionalized sapphire powder after heating up to 430 °C. At this temperature, this mass loss could be attributed to the burning off surface functional layer, i.e. APTES and APTES-SA [53]. On the other hand, there is no observable mass loss for blank and HNO_3 oxidized sapphire samples at this region confirming the absence of APTES and APTES-SA on both samples.

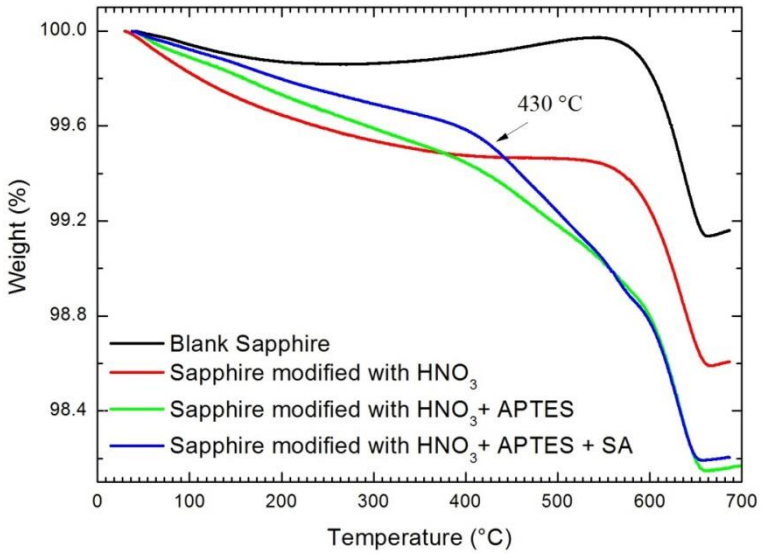

Figure 3.4: TGA analysis of sapphire powder with different functionalization steps. Samples were heated up at 10 °C / min in N_2 atmosphere from room temperature up to 700 °C.

3.4.4 Confocal microscopy

Single-strand probe DNA was first immobilized onto APTES-SA functionalized sapphire samples, i.e. chips and beads, followed by hybridization with fully complimentary DNA. This hybridization could be verified with confocal microscopy since the target DNA was labelled with Alexa-488. Figure 3.5 gives an overview of the images of the samples obtained by confocal microscopy.

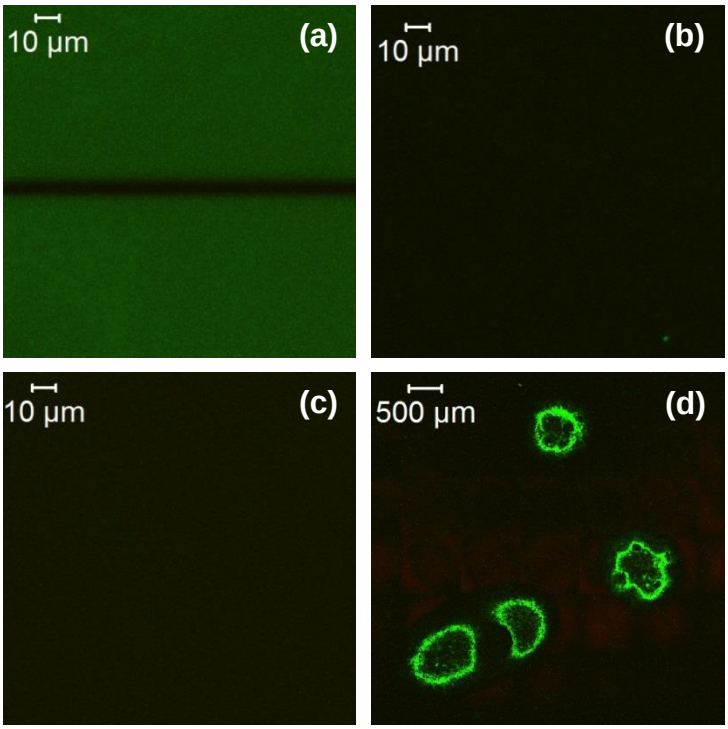

Figure 3.5: Confocal fluorescence images of sapphire sample. (a) Sapphire chip where the binding protocol was carried out as described in section 3.3.1.4. The black bar in the middle was induced by photobleaching of the Alexa-488 fluor. (b) Sapphire chip of (a) after denaturation with 0.1 M NaOH. (c) EDC-negative reference sapphire chip. (d) Sapphire beads where the binding protocol as described in section 2.1.4 was carried out.

Sapphire chips (Figure 3.5a) where the binding protocol was carried out as described in section 3.3.1.4. show intense fluorescence signals (66 confocal arbitrary units). This confirms the hybridization of target DNA to the probe DNA functionalized by the functionalization protocol. The black bar in the middle was induced by photobleaching of the Alexa-488 fluor. After denaturation with 0.1 M

NaOH, the fluorescence intensity drops down to 15 confocal arbitrary units background level due to reflected light (Figure 3.5b). In order to exclude the possibility of physical adsorption of the probe DNA on the APTES-SA functionalized sapphire samples, also an EDC-negative reference sapphire chip was prepared. As can be seen in Figure 3.5c, the EDC-negative reference sample shows no fluorescence signal excluding any physical adsorption of the probe DNA to the APTES-SA functionalized sapphire samples. Figure 3.5d shows the fluorescence signal of sapphire beads functionalized with the same binding protocol as described in section 3.3.1.4. As the beads are not spherical and the confocal volume is narrow, only the outer rim of the beads is apparent in the confocal image.

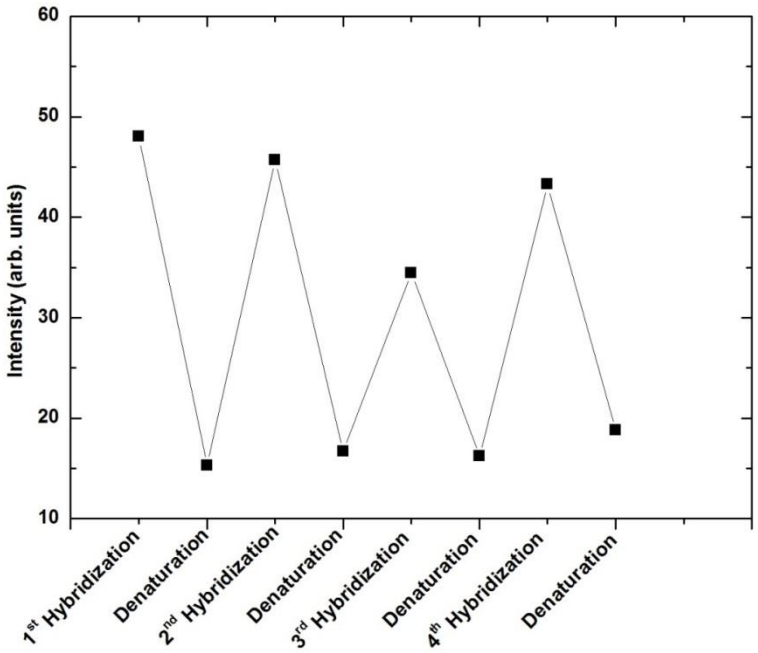

Figure 3.6: Fluorescence intensity after successive hybridization and denaturation steps for a sapphire chip. The intensity is averaged over an area of 225 x 225 μm^2.

Figure 3.6 shows the intensities for four successive hybridizations alternated by a chemical denaturation with 0.1 M NaOH on the sapphire chip. The increased intensity each after hybridization demonstrated the successful formation of DNA duplexes on the surface. These results show that the process of hybridization-

denaturation on the functionalized sapphire surface is reproducible and repeatable.

3.4.5 Sensor capabilities of sapphire chips in comparison to NCD electrodes

The first series of measurements described in this section refers to the stable, complementary DNA duplexes immobilized on a diamond thin film and a sapphire chip. The experiments were performed in a temperature stabilized environment of 19.1 °C. During the measurement, T_1 was increased with a heating rate of 1 °C/min from 35 °C to 85 °C. In addition, the same experiment condition was repeated using a sapphire chip functionalized only with single-stranded probe DNA. The temperature dependence of the heat-transfer resistance for these three experiments is shown in Figure 3.7. Clearly shown in Figure 3.7 the signal-to-noise ratio of the measurement obtained with sapphire chips is greatly improved in comparison to an analogous measurement on NCD thin film. The noise on the signal measured during the heating run on the sapphire sample was 0.03 °C/W, whereas the noise on the signal for the diamond sample was 0.09 °C/W. The contact area with water is always 28 mm^2, but sapphire is thicker than the NCD-on-silicon package (500 μm silicon, 150 nm NCD) and has lower heat conductivity (Table 3.1). Moreover, the sapphire chip has one interface less than diamond on silicon chip. To have one interface less should lower R_{th} value. The main effect here comes from the thickness difference between sapphire and diamond layer, and the different material. Thus, the baseline R_{th}-value appears to be higher for sapphire samples in comparison to diamond (9.3 ± 0.03 °C/W and 6.9 ± 0.09 °C/W, respectively) meaning that the used sapphire sample has a higher intrinsic thermal resistance.

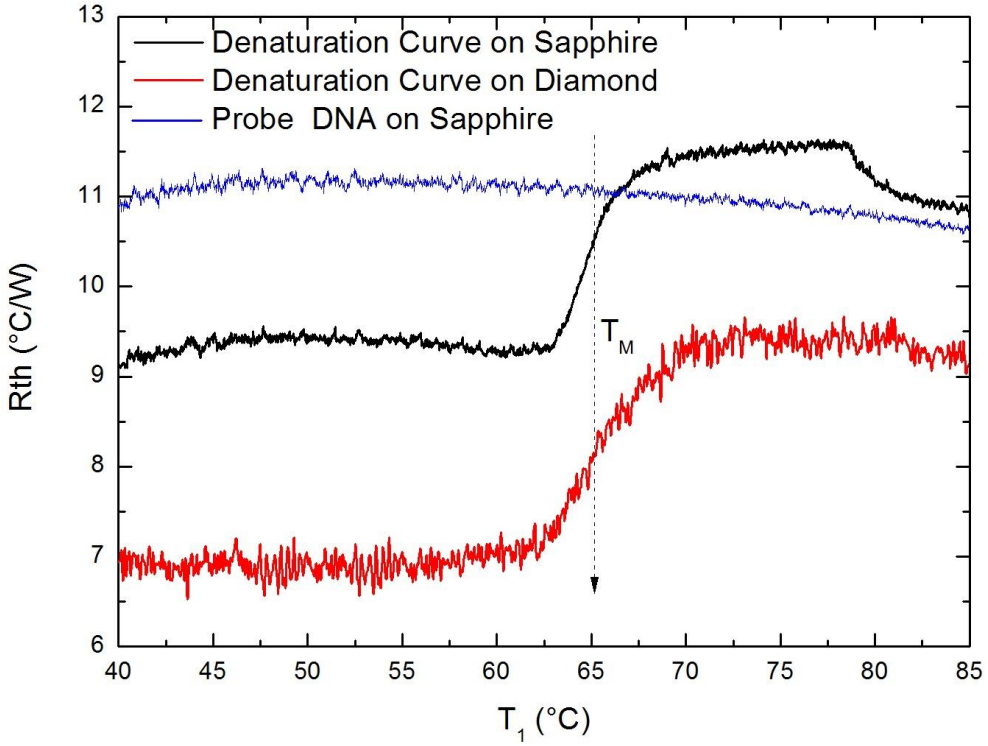

Figure 3.7: Thermal resistance as function of T_1, the temperature of the copper block. Data are shown for denaturation experiments with full matching DNA duplexes on sapphire chips (black curve) and NCD-coated silicon samples (red curve). In addition, the temperature dependence of the thermal resistance associated with a heating run on a sapphire chip containing single-stranded probe DNA is shown (blue curve).

The typical S-shape denaturation curve is apparent for both sapphire and diamond. The denaturation temperature or the melting temperature (T_m) is the temperature at which 50% of the dsDNA is changed to ssDNA. The denaturation temperature is identical for both substrates (65.2 ± 0.1 °C) and at first glance the denaturation-related increase in heat-transfer resistance also similar (2.3 ± 0.04 °C/W for sapphire and 2.5 ± 0.11 °C/W for NCD). However, in the denaturation curve for the sapphire chip, one can see that a decrease in thermal resistance occurs at 78.5 ± 0.1 °C. The overshoot in R_{th} can presumably be attributed to the non-specifically interactions of the denaturated, untethered ssDNA strand with the surface causing a higher insulation effect of the sapphire surface [54]. After a short time this interaction is broken, causing a drop in R_{th} of 0.6 °C/W. This effect is not clearly seen when the same experiment was

performed on an NCD thin film. This can be attributed to the higher surface coverage of probe DNA on sapphire chip than diamond chip, i.e. higher surface coverage of APTES-SA (Table 3.3), which requires more time to stabilize during denaturation. In addition, the diamond surface is rougher than the sapphire surface (RMS 17.96 nm and 0.44 nm, respectively, measured by AFM across an area of 1×1 μm^2) and this can possibly help to minimize the sterical hindering during denaturation.

3.4.6 DNA mutation analysis on sapphire chips

In the following, we will describe experiments performed with a sapphire chip in a temperature-stabilized environment of 19.1 °C, see Figure 3.8. First, the temperature-dependence of the thermal resistance was measured for a blank sapphire chip. The R_{th} value was about 9.0 °C/W and widely temperature-independent apart from a systematic drift down to 8.0 °C/W (black line). This is due to the fact that the viscosity of the liquid decreases which leads to better heat transfer. Attaching the APTES-SA crosslinker molecules (red line) resulted in a similar curve, shifted upward by 0.10 ± 0.07 °C/W, indicating that the increase in thermal resistance is not significant. In principle, this does not come as a surprise because APTES-SA has relatively short carbon chain not longer than 1 nm. Attaching the single-stranded probe DNA made the R_{th} rise to 11.0 °C/W at 40 °C and decrease to 10.6 °C/W at 85 °C (dark cyan line). This sample was subsequently hybridized with complementary target DNA (blue line), target DNA with a CC mismatch at base pair 7 (green line), and target DNA with the CC mismatch at base pair 20 (orange line). Note that the three hybridizations were performed with the original probe DNA on the same sapphire chip without any kind of surface regeneration. All curves exhibit the stepwise increase of R_{th} upon denaturation with midpoint temperatures of 64.5 °C ± 0.03 °C for the complement, 55.6 °C ± 0.03 °C for the mismatch at base pair 7, and 54.9 °C ± 0.03 °C for the mismatch at base pair 20. The relative order of stability agrees nicely with calculated melting-temperature values described in Table 3.2. We point out that our denaturation temperatures are lower than the predicted values; however, this effect was also observed by van Grinsven *et al.* measuring DNA mutations in a similar manner on NCD thin film electrodes [17].

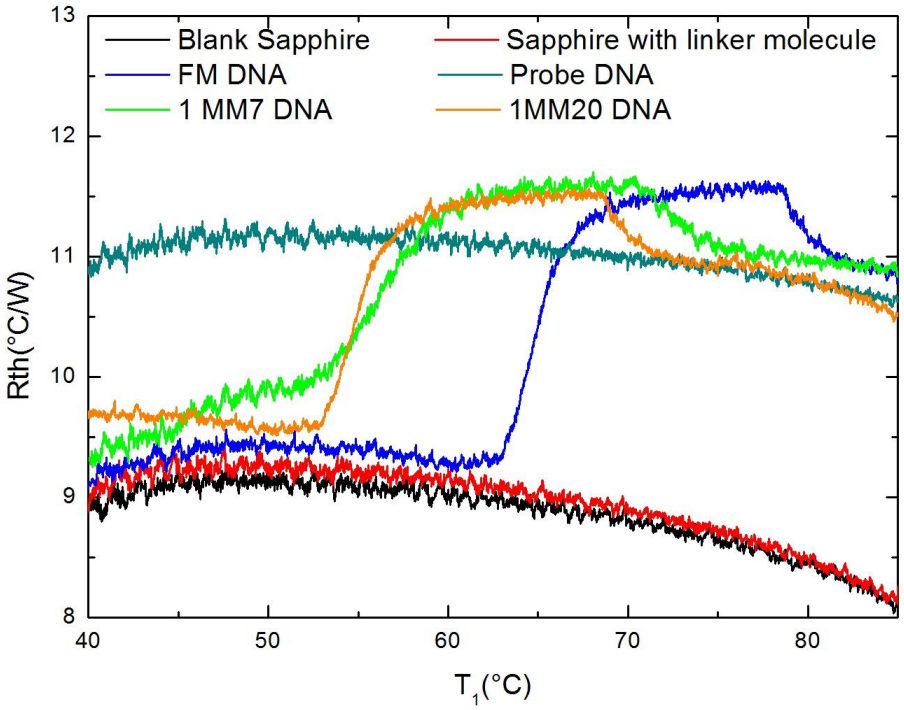

Figure 3.8: Heat-transfer resistance R_{th} as a function of temperature for a sapphire chip. Data are shown for denaturation experiments with full matching DNA duplexes on sapphire chips (dark blue curve), one mismatch at base pair 20 (brown curve), and one mismatch at base pair 7 (green curve). In addition, the temperature dependence of the thermal resistance associated with a heating run on a blank sapphire chip (black curve), sapphire chip containing single-stranded probe DNA (light blue curve), and linker molecule (red) are shown.

The unmodified chip (black line) and the chip with covalently attached APTES-SA linkers (red line) have a wide temperature independent R_{th} around 9 °C/W. In the configuration with attached probe DNA (dark cyan line) the heat-transfer resistance has notably increased to 11 °C/W, indicating an efficient thermal insulation by the highly flexible ss-DNA fragments. The R_{th} value of double-stranded DNA (blue line for the complementary duplexes) is comparable to the non-modified surface at low temperatures and switches to the ss-DNA behaviour upon denaturation with a midpoint temperature $T_{midpoint}$ = 64.5 °C ± 0.03 °C. Repeating the experiment with defective DNA duplexes results in a clear shift of $T_{midpoint}$ to lower temperatures: for the duplex with CC-mismatch at BP 7 (green line) we obtain $T_{midpoint}$ = 55.6 °C ± 0.1 °C and for the same mismatch at BP 20

(orange line) this is 54.9 °C ± 0.1 °C. The relative order of stability corresponds to the calculated data given in Table 2.

3.5 Conclusion

In this work, a successful surface functionalization of sapphire was achieved. After hydroxylating the surface, linker molecules were attached, so that later on probe DNA could be coupled covalently onto the surface. The surface coverage with carboxylic groups (COOH) was analyzed using toluidine blue O (TBO) and compared to the surface coverage of nanocrystalline diamond (NCD) with COOH. Sapphire- and NCD-surfaces show indeed the same order of surface coverage with COOH groups. Also TGA and FTIR confirmed the successful surface modification of the sapphire beads with APTES, suggesting a covalent binding of probe DNA to a synthetic sapphire material. Finally, hybridization with labeled target DNA was carried out. The results from the confocal microscopy demonstrated successful hybridization and denaturation cycles, indicating the reusability of this sensor. Quantification of the carboxylic groups on the surface showed comparable results to that of planar diamond surfaces. Finally, the RTH-measurement demonstrated the usefulness of a sapphire DNA sensor in the detection of SNP's or point mutations. Comparing the results obtained in this experiment to the results of van Grinsven *et al.* [17], sapphire is proven to be a perfect alternative for diamond in the creation of a DNA sensor.

To summarize, we have taken the first step towards utilizing a structural, electrically insulating implant material as a biosensor platform paving the way for future in-vivo biosensing devices.

3.6 Acknowledgements

This work is supported by the Life-Science Initiative Limburg and the Research Foundation Flanders (FWO) Projects G.0829.09, Synthetic diamond films as platform materials for novel DNA sensors based on electronic detection techniques and G.0B62.13N, Exploration of heat conductivity effects for applications in bio- and chemosensors, and Methusalem project NANO (Antwerp-Hasselt). The authors like to thank Guy Reggers for the TGA measurements, Huguette Penxten for the FT-IR measurements, Kathia L. Jiménez Monroy for

the AFM measurements, Matthias van Gompel for providing the Al_2O_3 chips and Bart Ruttens for the XRD measurements.

3.7 References

1. W. S. Yang, J. E. Butler, J. N. Russell, and R. J. Hamers, "Interfacial electrical properties of DNA-modified diamond thin films: Intrinsic response and hybridization-induced field effects," Langmuir **20**, 6778-6787 (2004).

2. K. Eersels, B. van Grinsven, A. Ethirajan, S. Timmermans, K. L. J. Monroy, J. F. J. Bogie, S. Punniyakoti, T. Vandenryt, J. J. A. Hendriks, T. J. Cleij, M. Daemen, V. Somers, W. De Ceuninck, and P. Wagner, "Selective identification of macrophages and cancer cells based on thermal transport through surface-imprinted polymer layers," ACS Applied Materials & Interfaces **5**, 7258-7267 (2013).

3. M. J. Heller, "DNA microarray technology: Devices, systems, and applications," Annual Review of Biomedical Engineering **4**, 129-153 (2002).

4. W. L. Xing, and J. Cheng, eds., "Biochips: Technology and Applications," (Springer-Verlag, 2003).

5. M. H. Abouzar, A. Poghossian, A. G. Cherstvy, A. M. Pedraza, S. Ingebrandt, and M. J. Schöning, "Label-free electrical detection of DNA by means of field-effect nanoplate capacitors: Experiments and modeling," Physica Status Solidi A - Applications and Materials Science **209**, 925-934 (2012).

6. U. Rant, K. Arinaga, S. Scherer, E. Pringsheim, S. Fujita, N. Yokoyama, M. Tornow, and G. Abstreiter, "Switchable DNA interfaces for the highly sensitive detection of label-free DNA targets," Proceedings of the National Academy of Sciences of the United States of America **104**, 17364-17369 (2007).

7. K. J. Cash, A. J. Heeger, K. W. Plaxco, and Y. Xiao, "Optimization of a reusable, DNA pseudoknot-based electrochemical sensor for sequence-specific DNA detection in blood serum," Analytical Chemistry **81**, 656-661 (2009).

8. S. O. Kelley, E. M. Boon, J. K. Barton, N. M. Jackson, and M. G. Hill, "Single-base mismatch detection based on charge transduction through DNA," Nucleic Acids Research **27**, 4830-4837 (1999).

9. L. Shi, Z. Y. Chu, Y. Liu, W. Q. Jin, and X. J. Chen, "Facile synthesis of hierarchically aloe-like gold micro/nanostructures for ultrasensitive DNA recognition," Biosensors & Bioelectronics **49**, 184-191 (2013).

10. W. Q. Su, M. Cho, J. D. Nam, W. S. Choe, and Y. Lee, "Highly sensitive electrochemical lead ion sensor harnessing peptide probe molecules on porous gold electrodes," Biosensors & Bioelectronics **48**, 263-269 (2013).

11. B. Peng, G. Y. Li, D. H. Li, S. Dodson, Q. Zhang, J. Zhang, Y. H. Lee, H. V. Demir, X. Y. Ling, and Q. H. Xiong, "Vertically aligned gold nanorod monolayer on arbitrary substrates: self-assembly and femtomolar detection of food contaminants," Acs Nano **7**, 5993-6000 (2013).

12. F. Wei, B. Sun, Y. Guo, and X. S. Zhao, "Monitoring DNA hybridization on alkyl modified silicon surface through capacitance measurement," Biosensors & Bioelectronics **18**, 1157-1163 (2003).

13. N. Lammerhardt, S. Merzsch, J. Ledig, A. Bora, A. Waag, M. Tornow, and P. Mischnick, "Toward three-dimensional microelectronic systems: directed self-assembly of silicon microcubes via DNA Surface functionalization," Langmuir **29**, 8410-8416 (2013).

14. J. A. Milton, S. Patole, H. B. Yin, Q. Xiao, T. Brown, and T. Melvin, "Efficient self-assembly of DNA-functionalized fluorophores and gold nanoparticles with DNA functionalized silicon surfaces: the effect of oligomer spacers," Nucleic Acids Research **41** (2013).

15. S. J. Oh, S. J. Cho, C. O. Kim, and J. W. Park, "Characteristics of DNA microarrays fabricated on various aminosilane layers," Langmuir **18**, 1764-1769 (2002).

16. M. S. Murib, B. van Grinsven, L. Grieten, S. D. Janssens, V. Vermeeren, K. Eersels, J. Broeders, M. Ameloot, L. Michiels, W. De Ceuninck, K. Haenen, M. J. Schöning, and P. Wagner, "Electronic monitoring of

chemical DNA denaturation on nanocrystalline diamond electrodes with different molarities and flow rates," Physica Status Solidi A - Applications and Materials Science **210**, 911-917 (2013).

17. B. van Grinsven, N. Vanden Bon, H. Strauven, L. Grieten, M. Murib, K. L. J. Monroy, S. D. Janssens, K. Haenen, M. J. Schöning, V. Vermeeren, M. Ameloot, L. Michiels, R. Thoelen, W. De Ceuninck, and P. Wagner, "Heat-transfer resistance at solid-liquid interfaces: A tool for the detection of single-nucleotide polymorphisms in DNA," ACS Nano **6**, 2712-2721 (2012).

18. B. van Grinsven, N. V. Bon, L. Grieten, M. Murib, S. D. Janssens, K. Haenen, E. Schneider, S. Ingebrandt, M. J. Schöning, V. Vermeeren, M. Ameloot, L. Michiels, R. Thoelen, W. De Ceuninck, and P. Wagner, "Rapid assessment of the stability of DNA duplexes by impedimetric real-time monitoring of chemically induced denaturation," Lab on a Chip **11**, 1656-1663 (2011).

19. Y. Zhang, H. Zhao, Z. J. Wu, Y. Xue, X. F. Zhang, Y. J. He, X. J. Li, and Z. B. Yuan, "A novel graphene-DNA biosensor for selective detection of mercury ions," Biosensors & Bioelectronics **48**, 180-187 (2013).

20. V. Vermeeren, S. Wenmackers, M. Daenen, K. Haenen, O. A. Williams, M. Ameloot, M. vandeVen, P. Wagner, and L. Michiels, "Topographical and functional characterization of the ssDNA probe layer generated through EDC-mediated covalent attachment to nanocrystalline diamond using fluorescence microscopy," Langmuir **24**, 9125-9134 (2008).

21. T. Strother, W. Cai, X. S. Zhao, R. J. Hamers, and L. M. Smith, "Synthesis and characterization of DNA-modified silicon (111) surfaces," Journal of the American Chemical Society **122**, 1205-1209 (2000).

22. S. X. Wu, Q. Y. He, C. L. Tan, Y. D. Wang, and H. Zhang, "Graphene-based electrochemical sensors," Small **9**, 1160-1172 (2013).

23. H. Kawarada, and A. R. Ruslinda, "Diamond electrolyte solution gate FETs for DNA and protein sensors using DNA/RNA aptamers," Physica Status Solidi A - Applications and Materials Science **208**, 2005-2016 (2011).

24. S. Wenmackers, V. Vermeeren, M. vandeVen, M. Ameloot, N. Bijnens, K. Haenen, L. Michiels, and P. Wagner, "Diamond-based DNA sensors: surface functionalization and read-out strategies," Physica Status Solidi A - Applications and Materials Science **206**, 391-408 (2009).

25. S. D. Janssens, P. Pobedinskas, J. Vacik, V. Petrakova, B. Ruttens, J. D'Haen, M. Nesládek, K. Haenen, and P. Wagner, "Separation of intra- and intergranular magnetotransport properties in nanocrystalline diamond films on the metallic side of the metal-insulator transition," New Journal of Physics **13**, 083008-083026 (2011).

26. D. T. Tran, V. Vermeeren, L. Grieten, S. Wenmackers, P. Wagner, J. Pollet, K. P. P. Janssen, L. Michiels, and J. Lammertyn, "Nanocrystalline diamond impedimetric aptasensor for the label-free detection of human IgE," Biosensors & Bioelectronics **26**, 2987-2993 (2011).

27. M. H. Abouzar, A. Poghossian, A. Razavi, A. Besmehn, N. Bijnens, O. A. Williams, K. Haenen, P. Wagner, and M. J. Schöning, "Penicillin detection with nanocrystalline-diamond field-effect sensor," Physica Status Solidi A - Applications and Materials Science **205**, 2141-2145 (2008).

28. K. P. Loh, S. L. Zhao, and W. De Zhang, "Diamond and carbon nanotube glucose sensors based on electropolymerization," Diamond and Related Materials **13**, 1075-1079 (2004).

29. J. Hernando, T. Pourrostami, J. A. Garrido, O. A. Williams, D. M. Gruen, A. Kromka, D. Steinmuller, and M. Stutzmann, "Immobilization of horseradish peroxidase via an amino silane on oxidized ultrananocrystalline diamond," Diamond and Related Materials **16**, 138-143 (2007).

30. P. Bergonzo, A. Bongrain, E. Scorsone, A. Bendali, L. Rousseau, G. Lissorgues, P. Mailley, Y. Li, T. Kauffmann, F. Goy, B. Yvert, J. A. Sahel, and S. Picaud, "3D shaped mechanically flexible diamond microelectrode arrays for eye implant applications: The MEDINAS project," IRBM **32**, 91-94 (2011).

31. A. G. Mamalis, J. J. Ramsden, A. I. Grabchenko, L. A. Lytvynov, V. A. Filipenko, and S. N. Lavrynenko, "A novel concept for the manufacture of individual sapphire-metallic hip joint endoprostheses," Journal of Biological Physics and Chemistry **6**, 113-117 (2006).

32. T. Takahashi, T. Sato, R. Hisanaga, O. Miho, Y. Suzuki, M. Tsunoda, and K. I. Nakagawa, "Long-term observation of porous sapphire dental implants," The Bulletin of Tokyo Dental College **49**, 23-27 (2008).

33. M. R. Rieger, W. K. Adams, G. L. Kinzel, and M. O. Brose, "Alternative Materials for three endosseous implants," The Journal of Prosthetic Dentistry **61**, 717-722 (1989).

34. G. Q. Zhou, Y. J. Dong, J. Xu, H. J. Li, J. L. Si, X. B. Qian, and X. Q. Li, "φ 140 mm sapphire crystal growth by temperature gradient techniques and its color centers," Materials Letters **60**, 901-904 (2006).

35. M. Keith, "The Crystran Handbook of Infra-Red and Ultra-Violet Optical Materials," (Crystran Ltd., 2008).

36. M. S. Murib, A. Q. Tran, W. De Ceuninck, M. J. Schöning, M. Nesládek, A. Serpengüzel, and P. Wagner, "Analysis of an optical biosensor based on elastic light scattering from diamond-, glass-, and sapphire microspheres," Physica Status Solidi A - Applications and Materials Science **209**, 1804-1810 (2012).

37. V. Osinsky, and O. Dyachenko, "Crystal lattice engineering the novel substrates for III-nitride-oxide heterostructures," Semiconductor Physics, Quantum Electronics & Optoelectronics **13**, 142-144 (2010).

38. J. F. Shackelford, and W. Alexander, eds., "CRC Materials Science and Engineering Handbook," (CRC Press LLC, 2001).

39. Website: http://www.tedpella.com/company_html/hardness.htm, January 26, 2014.

40. D. P. Goel, A. Ummat, and S. Menon, "New Radiant Science (Integrated Science), Book 7," (Allied Publishers, 2000).

41. J. P. Fitts, X. M. Shang, G. W. Flynn, T. F. Heinz, and K. B. Eisenthal, "Electrostatic surface charge at aqueous/alpha-Al_2O_3 single-crystal interfaces as probed by optical second-harmonic generation," Journal of Physical Chemistry B **109**, 7981-7986 (2005).

42. J. H. Sung, L. N. Zhang, C. S. Tian, G. A. Waychunas, and Y. R. Shen, "Surface structure of protonated R-sapphire $(1\bar{1}02)$ studied by sum-frequency vibrational spectroscopy," Journal of the American Chemical Society **133**, 3846-3853 (2011).

43. E. T. Vandenberg, L. Bertilsson, B. Liedberg, K. Uvdal, R. Erlandsson, H. Elwing, and I. Lundström, "Structure of 3-aminopropyl triethoxy silane on silicon-oxide," Journal of Colloid and Interface Science **147**, 103-118 (1991).

44. K. van der Maaden, K. Sliedregt, A. Kros, W. Jiskoot, and J. Bouwstra, "Fluorescent nanoparticle adhesion assay: A novel method for surface pK(a) determination of self-assembled monolayers on silicon surfaces," Langmuir **28**, 3403-3411 (2012).

45. I. M. Klotz, "Succinylation," in *Methods in Enzymology*, C. H. W. Hirs, ed. (Academic Press, 1967), p. 576.

46. Website: http://ozone3.chem.wayne.edu/, January 26, 2014.

47. J. SantaLucia, H. T. Allawi, and A. Seneviratne, "Improved nearest-neighbor parameters for predicting DNA duplex stability," Biochemistry **35**, 3555-3562 (1996).

48. Y. L. Zhong, K. F. Chong, P. W. May, Z. K. Chen, and K. P. Loh, "Optimizing biosensing properties on undecylenic acid-functionalized diamond," Langmuir **23**, 5824-5830 (2007).

49. O. A. Williams, M. Nesládek, M. Daenen, S. Michaelson, A. Hoffman, E. Osawa, K. Haenen, and R. B. Jackman, "Growth, electronic properties and applications of nanodiamond," Diamond and Related Materials **17**, 1080-1088 (2008).

50. W. S. Yang, O. Auciello, J. E. Butler, W. Cai, J. A. Carlisle, J. Gerbi, D. M. Gruen, T. Knickerbocker, T. L. Lasseter, J. N. Russell, L. M. Smith, and R. J. Hamers, "DNA-modified nanocrystalline diamond thin-films as stable, biologically active substrates," Nature Materials **1**, 253-257 (2002).

51. A. Huang, N. Wang, and J. Caro, "Seeding-free synthesis of dense zeolite FAU membranes on 3-aminopropyltriethixysilane-functionalized alumina supports," Journal of Membrane Science **389**, 272-279 (2012).

52. R. Chandrasekharan, L. Zhang, V. Ostroverkhov, S. Prakash, Y. Wu, Y. R. Shen, and M. A. Shannon, "High-temperature hydroxylation of alumina crystalline surfaces," Surface Science **602**, 1466-1474 (2008).

53. A. Krüger, J. Stegk, Y. J. Liang, L. Lu, and G. Jarre, "Biotinylated nanodiamond: Simple and efficient functionalization of detonation diamond," Langmuir **24**, 4200-4204 (2008).

54. K. Qamhieh, K. Y. Wong, G. C. Lynch, and B. M. Pettitt, "The melting mechanism of DNA tethered to a surface," International Journal of Numerical Analysis and Modeling **6**, 474-488 (2009).

Chapter 4

Analysis of an optical biosensor based on elastic light scattering from diamond-, glass-, and sapphire microspheres

Published in *Phys. Status Solidi A,* **209**, 1804–1810 (2012)

M. S. Murib[1], A. Q. Tran[1], W. De Ceuninck[1,2], M. J. Schöning[3], M. Nesládek[1,2], A. Serpengüzel[4], and P. Wagner[1,2]

1. Institute for Materials Research, Hasselt University, IMO, Wetenschapspark 1, 3590 Diepenbeek, Belgium
2. IMEC vzw, Division IMOMEC, Wetenschapspark 1, 3590 Diepenbeek, Belgium
3. Institute of Nano-and Biotechnologies, Aachen University of Applied Sciences, Heinrich-Mussmann-Strasse 1, 52428 Jülich, Germany
4. Microphotonics Research Laboratory, Department of Physics, Koç University, Rumelifeneri Yolu, Sarıyer, Istanbul 34450, Turkey

4.1 Abstract

Deoxyribonucleic acid (DNA) and protein recognition are now standard tools in biology. In addition, the special optical properties of microsphere resonators expressed by the high quality factor (Q-factor) of whispering gallery modes (WGMs) or morphology dependent resonances (MDRs) have attracted the attention of the biophotonic community. Microsphere based biosensors are considered as powerful candidates to achieve label-free recognition of single molecules due to the high sensitivity of their WGMs. When the microsphere surface is modified with biomolecules, the effective refractive index and the effective size of the microsphere change resulting in a resonant wavelength shift. The transverse electric (TE) and the transverse magnetic (TM) elastic light scattering intensity of electromagnetic waves at 600 and 1400 nm are numerically calculated for DNA and unspecific binding of proteins to the microsphere surface. The effect of changing the optical properties was studied for diamond (refractive index 2.34), glass (refractive index 1.50), and sapphire (refractive index 1.75) microspheres with a 50 μm radius. The mode spacing, the linewidth of WGMs, and the shift of resonant wavelength due to the change in radius and refractive index, were analyzed by numerical simulations. Preliminary results of unspecific binding of biomolecules are presented. The calculated shift in WGMs can be used for biomolecules detection.

Keywords: label-free biosensors, microcavity, microsphere, morphology dependent resonance, photonics, whispering gallery mode.

4.2 Introduction

The fundamental prerequisite for biological functions is the detection and specific interactions between proteins and other macromolecules within the cell [1]. Nucleic acids', e.g., DNA, modular structure enables the cell to generate a wide variety of molecules with very different binding specificities and thus, with a large variety of possible interactions [1]. Biomolecules recognition and DNA denaturation were studied by different types of measurement setups such as elastic measurements at the level of a single molecule [2], force-induced denaturation [3], and by monitoring the denaturation dynamics in real-time using impedance spectroscopy [4]. In addition, DNA hybridization can be detected optically using ring resonators [5], confocal microscopy [4], prism couplers [6], and spherical cavities [1].

A biosensor is composed of a modified solid surface (transducer), single-stranded DNA immobilized onto the surface (probe) for DNA sensing [or antibodies for protein sensing], and a complementary single-stranded DNA (target) hybridized to the probe DNA [or a target protein for the antibody] [7]. The target DNA is used to study the hybridization or denaturation physical properties of double stranded DNA. Confocal microscopy requires fluorescent labeling for detection, which is time-consuming, complex and expensive, and not suitable for rapid biophysical and routine characterization tasks [8]. In addition, real-time hybridization monitoring using confocal microscopy cannot be performed, because it is hard to distinguish between unbound targets in solution and those that have been hybridized to the probe on the surface, as both will fluoresce, when imaged [9]. The labeling for surface-enhanced Raman spectroscopy (SERS) [10] and total internal reflection fluorescence (TIRF) microscopy [11] behaves as an amplifier for an otherwise undetectable single-molecule signal, and also requires a prior knowledge of the target molecule that must be modified to be compatible with the label, which restricts an experiment's scope [10]. As a result, the demand for label-free biosensors has increased, and different technologies have been developed such as fiberoptic waveguides [12, 13]. Light is coupled through these waveguides and an evanescent field extends beyond the waveguide surface [5]. The analytes deposited onto the surfaces of these fiber-optic waveguides lie in the path of the

evanescent field, and as a result they change the effective refractive index of the guided mode [5]. Such waveguide sensors are size-effective. For example, in order to achieve a high signal and low detection limit, the waveguide must be of the order of a few centimeters long, since the sensing signal is accumulated along the waveguide [5]. Other non-optical label-free biosensors that were accomplished recently, are nanowires [14], nanoparticle probes [15], biochips [16], mechanical cantilevers [17], and field-effect sensors [18, 19].

Optical microcavities such as ring resonators or spherical resonators are promising optical label free detection setups [1, 20]. Recently, a silicon on insulator (SOI) microring resonator for sensitive label free biosensing was fabricated [21]. In addition, microring surface functionalization and a detection limit of 0.37 fg avidin mass (3260 molecules) were established [22, 23]. In an optical microcavity, the target molecules are sampled hundreds of times due to the recirculation of light within the microcavity by total internal reflection (TIR) [20]. The target molecule induces a change on the optical microcavity properties such as the size and refractive index, and as a result, a change in the whispering gallery mode (WGM) resonant wavelength is encountered [24].

In this article, a comparative theoretical study of an optical biosensor concept based on elastic light scattering from microspheres and the corresponding shift of WGMs, after an add-on layer to the sphere, is performed. Besides of the established photonic materials sapphire and glass, diamond is included in our study due to its excellent stability at elevated temperatures (commonly used in DNA-hybridization and denaturation studies), in a wide range of pH values, and for the well-known covalent coupling procedures [4, 7]. Consequently, diamond layers have been employed in DNA sensors based on electronic- and thermal readout principles [4, 25, 26], but its potential in photonic biosensing still needs to be explored.

Although diamond microspheres are not available commercially, planar diamond ring resonators were recently fabricated [27], and spherical diamond microshells can be synthesized by plasma coating [28]. Sapphire and glass spheres are readily available with diameters down to a few micron. The most common technique to fabricate silica microsphere resonators of several hundred microns diameter is melting a tip of an optical fiber by a hydrogen flame or an electric

arc [29]. Glass spheres usually exhibit a perfectly spherical geometry. Sapphire spheres are fabricated using spherical indentors and the end surface is polished down to a few nanometers of roughness [28]. Also sapphire spheres show a perfect spherical geometry. Diamond indentors can be fabricated as well, but the crystalline anisotropy is still a limiting factor when aiming at a spherical symmetry [30]. The Q-factors of glass- and sapphire spheres are limited by absorption [31, 32] while in case of diamond it would be limited by diffraction [32].

Table 4.1: Physical properties of the sphere materials.

Material	Glass	Sapphire	Diamond
Thermal expansion coefficient (K^{-1})	$7.1x10^{-6}$	$5.6x10^{-6}$	$0.003x10^{-6}$
Thermal conductivity ($Wm^{-1}K^{-1}$)	1.114	27.21	2600
Hardness scale [Mohs]	6	9	10

Table 4.1 shows the physical properties of each material including the thermal expansion [33], the thermal conductivity [33], and the scratch resistance [34]. Due to the fact that sapphire and diamond have a higher thermal conductivity and lower thermal expansion as compared to glass, both materials appear favorable for use in optical biosensors operating in a broader temperature regime. The theoretical calculation of the expected resonant wavelength shifts will be based on the Generalized Lorenz–Mie theory (GLMT) [35] and the detection mechanism will be analyzed. A biosensor, based on this wavelength shift, can be sufficiently sensitive to detect single molecules once properly designed and optimized [20].

4.3 Detection mechanism

A single-mode optical fiber (SMOF) half coupler can be used to couple an electromagnetic wave from a continuous wave (CW) laser source to the microsphere as illustrated in Figure 4.1a. The laser wavelength can be tuned to match the microsphere resonance, and as a result the light couples from the optical fiber to the microsphere. The electromagnetic wave is confined around

the inside surface of the microsphere by almost TIR [36], and it evanesces partially into the surrounding medium [20].

As a result, the light will interact with the molecules, once they are captured on the surface, on resonance [20]. The electromagnetic wave circumnavigates the sphere and returns back to its initial point in phase [36]. A periodic circumnavigating wave in the sphere produces a series of sharp peaks of morphology dependent resonances (MDRs) as a function of the size parameter $x = 2\pi a \times N/\lambda$, where a is the sphere radius, λ the wavelength of the laser in vacuum, and N the refractive index of the surrounding medium [36].

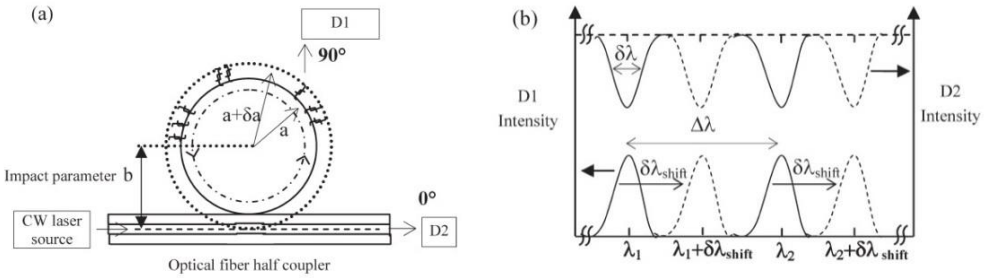

Figure 4.1: (a) Schematic geometry of the microsphere with a biologically modified surface coupled to a half coupler optical fiber. (b) Schematic of WGMs (λ_1 and λ_2) of same mode order and consecutive mode number, and their shift due to the sphere's surface modification.

The system was modeled using the GLMT, which describes the electromagnetic scattering of an arbitrary light beam by a spherical microparticle [31]. Elastic scattering intensity from the sphere and transmittance intensity at the output of the optical fiber for transverse electric (TE) and transverse magnetic (TM) polarization are calculated for diamond, sapphire, and glass spheres before and after surface modifications with biomolecules. Figure 4.1b shows the excited resonances manifested due to the circumnavigating light inside the sphere. Here, $\Delta\lambda$ represents the mode spacing of consecutive resonances having the same mode order (number of nodes or maxima of the intensity distribution in the radial direction) and consecutive mode number (the number of maxima between 0 and 180° in the angular intensity distribution of the mode; solid lines curve). $\Delta\lambda$ can be calculated using equation [31]:

$$\Delta\lambda = \frac{\lambda^2 arctan\sqrt{m^2-1}}{2\pi aN\sqrt{m^2-1}} \quad (4.1),$$

where m is the relative refractive index of the sphere (refractive index of the sphere/refractive index of the surrounding medium), λ the wavelength of the laser source in vacuum, N the refractive index of the surrounding medium, and a is the sphere's radius. A very important resonant property is the linewidth (δλ) and its respective quality factor (Q). Q is given by the equation [31]

$$Q = \frac{\lambda}{\delta\lambda} \quad (4.2).$$

The WGM resonant wavelength is given by the equation [5]

$$2\,\pi\,a\,N \leq n\lambda \leq 2\,\pi\,a\,N_1 \quad (4.3),$$

where *n* is the mode number, and N_1 the refractive index of the sphere. If the molecules are tethered onto the sphere's surface, these molecules will induce a change of the optical properties of the sphere such as its effective size and refractive index near the surface of the sphere. As a result, the resonance wavelength will change further and result in the phenomenon of resonant shift as shown by the dashed lines in Figure 4.1b [20]. The wavelength shift $\delta\lambda_{shift}$ can be calculated by the equation:

$$\frac{\delta\lambda_{shift}}{\delta\lambda} = \frac{\delta a}{a} + \frac{\delta m}{m} \quad (4.4),$$

where δ*a* is the change in sphere radius, and δ*m* is the change in the relative refractive index due to the interaction between the adsorbed molecules [24]. The quality factor is inversely proportional to the resonance linewidth, and so the narrower the linewidth, the higher the quality factor will be and lower concentrations can be detected. Relating Equations (4.2) and (4.4), the sensitivity to the size perturbation as a function of the quality factor and resonance shift can be calculated using the following equation:

$$\frac{\delta\lambda_{shift}}{\delta\lambda} \times \frac{1}{Q} = \frac{\delta a}{a} + \frac{\delta m}{m} \quad (4.5).$$

In addition, in order to determine low concentrations, it is advantageous to utilize narrow linewidth laser sources, which will result in high precision measurements.

4.4 Theoretical calculations

Elastic light scattering intensity and transmitted intensity calculations were performed as depicted schematically in Figure 4.1a. A transparent flow cell with the optical fiber half coupler (OFHC) fixed at its base can be used to host and to change the liquid medium surrounding the sphere. Initially, a phosphate buffer saline (PBS) solution (with a refractive index of 1.335 and pH of 7.2) is introduced in the flow cell. PBS is a typical electrolyte frequently used in biosensing experiments. A diamond sphere (with refractive index of 2.34, radius 50 μm) is placed on the OFHC inside the flow cell. The electromagnetic scattering of an arbitrary light beam by the spherical particle is described by the GLMT [35].

For the calculations, a Gaussian beam with an infinite skirt length and a beam waist (the point along the laser propagation direction where the beam radius is minimum) with a half-width of 5mm is assumed in the OFHC. The Gaussian beam propagates just at the edge of the microsphere [37]. The distance between the center of the sphere and the center of the OFHC (b) should satisfy the inequality ($a \leq b \leq ma$) in order to achieve the WGM resonances excitation [38], where b is the impact parameter.

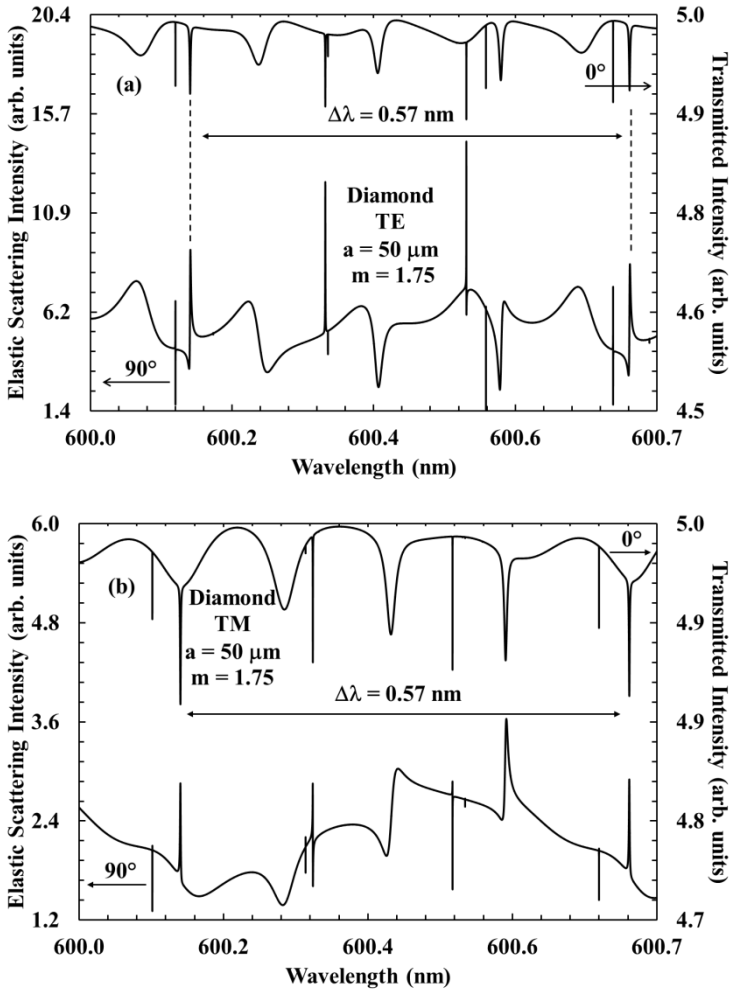

Figure 4.2: (a) Calculated TE polarized elastic scattering and transmitted spectra for a diamond sphere at 600 nm. (b) Calculated TM polarized elastic scattering and transmitted spectra for a diamond sphere at 600 nm.

Figures 4.2a and 4.2b represent the calculated TE and TM elastic scattering at 908 and the transmitted intensity from a diamond sphere of radius of 50 mm and relative index of refraction m = 1.75 (surface not modified with biomolecules) using the GLMT in the wavelength range from 600 to 600.7 nm and with a step size of 3.9 fm. The reason to choose a wavelength of 600 nm is that diamond, glass, and sapphire are completely transparent at this wavelength, while DNA molecules show only little light absorption.

For every maximum in the elastic scattering spectrum, there is a corresponding minimum in the transmittance spectrum. The minima in the transmittance spectrum correspond to the quantity of light coupled from the fiber into the sphere. The mode spacing ($\Delta\lambda$) was found to be 0.57 nm, which correlates well with the calculated value ($\Delta\lambda$ = 0.57 nm) obtained from Equation (4.1). The linewidth ($\delta\lambda$) of the resonances is about 8.16×10^{-5} nm, which corresponds to a quality factor Q of 7.35×10^{6} (using Equation (4.2)). A smaller step size will correspond to a narrower linewidth, and more resonances can be observed.

The case of add-on layers of biomolecules adsorbed or functionalized onto the surface of the sphere is also analyzed. The calculation is carried out for a diamond sphere (a = 50 μm, m = 1.75), a glass sphere (a = 50 μm, m = 1.12), and a sapphire sphere (a = 50 μm, m = 1.27). The covalent functionalization of diamond with probe DNA can be done photochemically using fatty-acids in combination with the zero-length crosslinker EDC (1-ethyl-3-[3-dimethylamino-propyl]-carbodiimide) or, in the case of glass, along the silane route [7, 25]. The covalent functionalization of sapphire with DNA has been developed in the meantime and is described in Chapter 3. For the diamond sphere, the add-on layer of biomolecules effect on the WGM resonances is analyzed at the transmitted region in the TE and TM polarization and in the wavelength range 600–600.7 nm. PBS absorbs less in the 650 nm wavelength range, and has a refractive index close to that of glass and sapphire. As a result, it is favorable to work in the visible wavelength range, as there will be less absorption of light by the medium, and a higher signal is expected from the interaction of biomolecules with the microsphere. In addition, since glass and sapphire are also transparent in the visible and infrared wavelength ranges, the calculation is repeated for a glass and sapphire microsphere with an add-on layer of biomolecules.

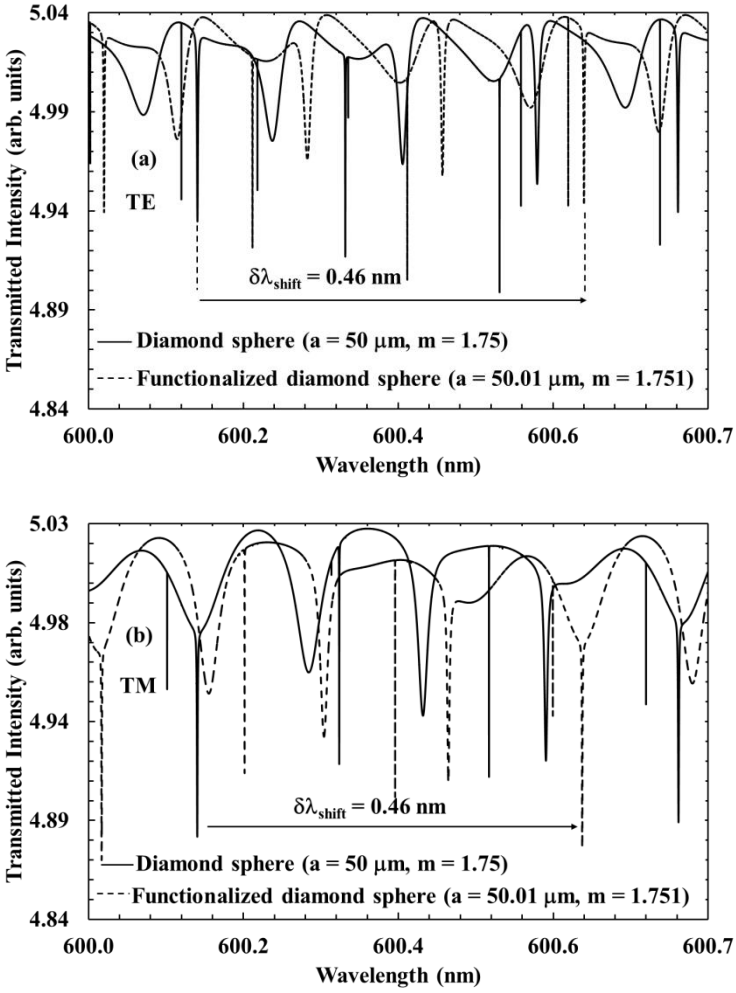

Figure 4.3: (a) Calculated TE transmitted spectra for diamond and functionalized diamond microsphere at 600.7 nm. (b) Calculated TM polarized transmitted spectra for diamond and functionalized diamond microsphere at 600 nm.

The effect of the add-on layer of biomolecules on glass spheres is analyzed for the scattering angle of 90° in the wavelength range of 600 – 600.7 nm, and for the TE and TM polarization of light. In order to broaden the analysis to the infrared wavelength range, the effect of the add-on biomolecular layer on sapphire spheres is analyzed for the transmitted intensity in the wavelength range of 1400 – 1403.1 nm, again for the TE and TM polarization of light. The radius of the diamond, glass, and sapphire sphere without the add-on layer is considered to be 50 and 50.01 μm with the add-on layer. For example, 1 base

pair (bp) DNA has a length of 0.33 nm. As a result, if a DNA strand of 30 bp is functionalized on the sphere, then approximately an increase of 0.01 mm (0.02%) in the sphere's radius will be encountered. An increase of 0.001 (0.05%) in the mean refractive index of the diamond, glass, and sapphire is assumed [6].

Figure 4.3a represents the calculated TE-polarized transmitted spectra and Figure 4.3b represents the calculated TM-polarized elastic scattering spectra for diamond and functionalized diamond sphere in the wavelength range from 600 to 600.7 nm. The diamond sphere has a radius of 50 μm and relative refractive index of 1.75, while the radius and relative refractive index of the functionalized diamond sphere is 50.01 μm and 1.751, respectively. The TE-polarized and the TM-polarized simulation spectra were calculated for a change of 0.01 μm in the radius and a change of 10^{-3} in the refractive index of the diamond sphere due to the surface modification with biomolecules. As a result, the resonances were red-shifted by 0.46 nm (0.077%), which correlates well with the size (0.02%) and index shift of the sphere (0.057%) calculated using Equation (4.4). The observed shift corresponds to more than 5600 times the resonance linewidth, which supports the possibility of identifying low concentrations of biomolecules.

The change in the radius and in the refractive index of a glass sphere due to surface modification is analyzed for the TE-polarized elastic scattering intensity (Figure 4.4a) and TM-polarized elastic scattering intensity (Figure 4.4b) in the wavelength range between 600 and 600.7 nm. As a result, the WGM resonance positions were red shifted by 0.64 nm (0.107%) in the TE-polarized elastic scattering intensity and 0.64 nm (0.107%) in the TM polarized light elastic scattering intensity. The shifted values correlate well with the size and refractive index change proposed due to sphere surface modifications (0.107%) calculated using Equation (4.4). The linewidth of the resonances is 5.19×10^{-5} nm, which corresponds to a quality factor of 1.16×10^{7}. The observed shift is about 12300 times the resonance linewidth.

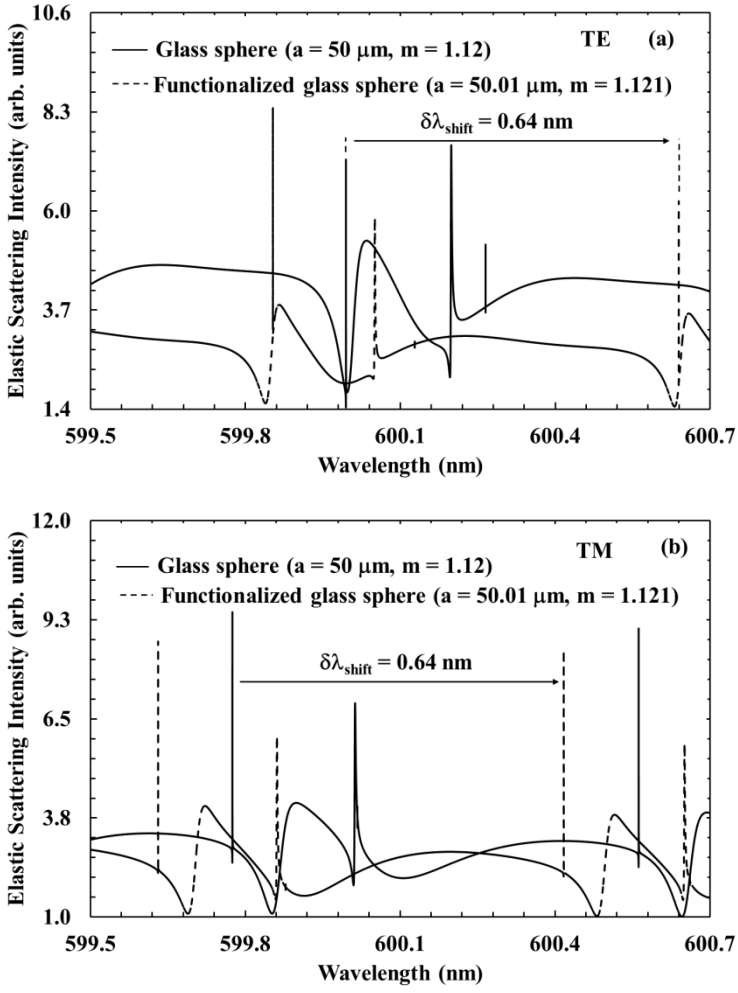

Figure 4.4: (a) Calculated TE polarized spectra for glass and functionalized glass microsphere at 600 nm. (b) Calculated TM polarized spectra for glass and functionalized glass microsphere at 600 nm.

Finally, we address sapphire, being the second hardest material next to diamond. Synthetic sapphire is used for implant materials such as hip implants, since it shows an outstanding chemical inertness, wear resistance, and biocompatibility [39]. Moreover, it has a wide optical transmission band from ultraviolet (UV) to near-infrared (near-IR) [40].

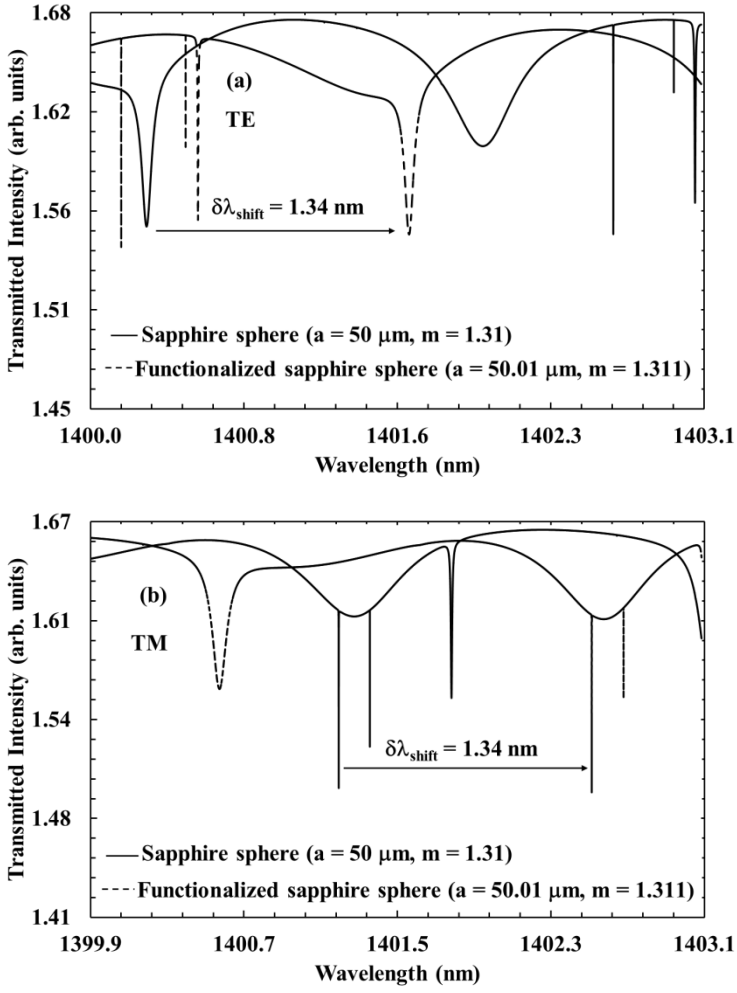

Figure 4.5 (a) Calculated TE polarized spectra for sapphire and functionalized sapphire microsphere at 1400 nm. (b) Calculated TM polarized spectra for sapphire and functionalized sapphire microsphere at 1400 nm.

Figure 4.5a represents the calculated TE-polarized transmitted spectra and Figure 4.5b represents the calculated TM polarized elastic scattering spectra for sapphire and functionalized sapphire sphere in the wavelength range 1400 to 1403.1 nm. The sapphire sphere has a radius of 50 μm and relative refractive index of 1.31, while the radius and relative refractive index of the functionalized sapphire sphere are 50.01 μm and 1.311, respectively. As a result, the resonances were red-shifted by 1.34 nm (0.096%), which correlates well with the size and index shift of the sphere (0.096%) calculated using Equation (4.4).

The linewidth of the resonances is 2.14×10^{-4} nm, which corresponds to a quality factor of 6.54×10^{6}. The observed spectral shift is around 6300 times the resonance linewidth, which is also in favor of the possibility of identifying low concentrations of biomolecules.

Table 4.2: Summary of the calculated results for glass-, sapphire-, and diamond spheres.

Material	**Glass**	**Sapphire**		**Diamond**
m	1.12	1.31		1.75
λ (nm)	600	600	1400	600
δλ (nm)	5.19×10^{-5}	5.56×10^{-5}	2.14×10^{-4}	8.16×10^{-5}
Q-factor	1.16×10^{7}	1.08×10^{7}	6.54×10^{6}	7.35×10^{6}
$\delta\lambda_{shift}$ (nm)	0.64	0.57	1.34	0.46
% $\delta\lambda_{shift}$ (TE)	0.107	0.095	0.096	0.077
% $\delta\lambda_{shift}$ (TM)	0.107	0.095	0.096	0.077
$\delta\lambda_{shift}/\delta\lambda$	12331	10251	6261	5637

Table 4.2 summarizes the calculated results for each sphere material in relation to sensitivity to size perturbation and refractive index perturbation. The shift in the resonant wavelength of glass due to the modification with DNA at 600 nm laser source wavelength corresponds to about 12300 times the linewidth of the resonance. This is more pronounced than in the case of diamond ($5637 \times \delta\lambda$) at the given wavelength of 600 nm. This is due to the fact that glass has a relative refractive index of 1.12 which is close to 1, while diamond has a relative refractive index of 1.75.

Sapphire is analyzed at 1400 nm, and the shift in resonant wavelength due to modification with DNA is about 0.096%. This small shift is due to the fact that the relative refractive index of sapphire is 1.31. The resonant shift for sapphire modified with DNA at 600 nm was also analyzed (data not shown) resulting in a resonant wavelength shift corresponding to about 10250 times the resonant linewidth. This wavelength shift is close to that of glass in agreement with the fact that the relative refractive index of sapphire (is 1.31) is only slightly higher than that of glass. As a result, glass and sapphire show a very similar resonant shift due to surface modification with DNA at 600 nm.

As for the surface perturbations, as long as the Q-factor of the WGMs is not sensitive to those perturbations, that mode can be used for the spectral measurements. Therefore choosing a low Q-factor (10^{6}) second order WGM

might be better than choosing a high Q-factor (10^9) first order mode for the spectral measurements [41].

In case of denaturation of DNA, it is expected that a blue shift in resonances will occur because single-stranded DNA has a smaller index of refraction than double-stranded DNA [6]. Naturally, if the sphere surface was initially modified with single stranded DNA followed by hybridization with its complementary DNA strand, then a red shift in the resonances wavelength is to be expected. Furthermore, the sensor concept may also serve for the specific recognition of proteins by immobilizing antibodies onto the spheres. Since antibodies are proteins as well the most important effect is an increase of the radius of the sphere upon binding of the target proteins and therefore a red shift in the WGM resonances should occur.

4.5 Conclusion

A concept for a label-free photonic biosensor was proposed with possible applications in the identification of biomolecules and in the observation of hybridization and denaturation of DNA. TE- and TM polarized elastic light scattering and transmitted light intensity from diamond-, glass-, and sapphire spheres were analyzed in the wavelength range 600 nm. In case of sapphire, the elastic light scattering intensities were also analyzed in the wavelength regime of 1400 nm. The resonance shift due to the sphere-surface modification was calculated and analyzed for several values of the size and relative refractive indices. The calculations showed that an optical biosensor based on spherical cavities is a good candidate for biomolecules identification and DNA hybridization and denaturation. The shift in resonances can be analyzed from the transmission signal of the optical fiber or from the elastic scattering intensity at 90° from the sphere. The chemical inertness, stability at elevated temperatures, biocompatibility, and excellent thermal conductivity of sapphire and diamond can be exploited in the development of biosensors. There is no technique for diamond spheres yet, but the microshells should be a good starting point. The anisotropy of sapphire is much weaker than diamond, and as a result sapphire can be shaped into a nearly perfect sphere. For a resonant linewidth of the order 10^{-5} nm at 600 nm, the modified glass and sapphire spheres had a spectral shift of 10^4 times the resonant linewidth, and the modified diamond sphere has

spectral shift of 5×10^3 times the resonant linewidth. Since sapphire and glass have shown close spectral shift with respect to resonant linewidth, sapphire can be considered an interesting alternative to glass biophotonic sensors. In summary, the diamond, sapphire, and glass microcavity based sensor can be used to study the kinetics and other physical properties of DNA and protein molecules.

4.6 Acknowledgments

Financial support by the Life-Science Initiative of the Province of Limburg and the Research Foundation Flanders FWO (Projects G.0829.09 and G.0997.11N) is greatly appreciated. Anh Quang Tran was supported by a grant of the Federal Belgian Development Cooperation.

4.7 References

1. M. Baaske, and F. Vollmer, "Optical resonator biosensors: molecular diagnostic and nanoparticle detection on an integrated platform," Chemphyschem **13**, 427-436 (2012).

2. T. Strick, J. F. Allemand, V. Croquette, and D. Bensimon, "Twisting and stretching single DNA molecules," Progress in Biophysics & Molecular Biology **74**, 115-140 (2000).

3. U. Bockelmann, P. Thomen, B. Essevaz-Roulet, V. Viasnoff, and F. Heslot, "Unzipping DNA with optical tweezers: high sequence sensitivity and force flips," Biophysical Journal **82**, 1537-1553 (2002).

4. B. van Grinsven, N. Vanden Bon, L. Grieten, M. Murib, S. D. Janssens, K. Haenen, E. Schneider, S. Ingebrandt, M. J. Schöning, V. Vermeeren, M. Ameloot, L. Michiels, R. Thoelen, W. De Ceuninck, and P. Wagner, "Rapid assessment of the stability of DNA duplexes by impedimetric real-time monitoring of chemically induced denaturation," Lab on a Chip **11**, 1656-1663 (2011).

5. J. D. Suter, I. M. White, H. Y. Zhu, H. D. Shi, C. W. Caldwell, and X. D. Fan, "Label-free quantitative DNA detection using the liquid core optical ring resonator," Biosensors & Bioelectronics **23**, 1003-1009 (2008).

6. Z. B. Bahsi, A. Buyukaksoy, S. M. Olmezcan, F. Simsek, M. H. Aslan, and A. Y. Oral, "A novel label-free optical biosensor using synthetic oligonucleotides from E. coli O157:H7: elementary sensitivity tests," Sensors **9**, 4890-4900 (2009).

7. S. Wenmackers, V. Vermeeren, M. vandeVen, M. Ameloot, N. Bijnens, K. Haenen, L. Michiels, and P. Wagner, "Diamond-based DNA sensors: surface functionalization and read-out strategies," Physica Status Solidi A - Applications and Materials Science **206**, 391-408 (2009).

8. A. Q. Liu, H. J. Huang, L. K. Chin, Y. F. Yu, and X. C. Li, "Label-free detection with micro optical fluidic systems (MOFS): a review," Analytical and Bioanalytical Chemistry **391**, 2443-2452 (2008).

9. P. M. Levine, P. Gong, R. Levicky, and K. L. Shepard, "Real-time, multiplexed electrochemical DNA detection using an active complementary metal-oxide-semiconductor biosensor array with integrated sensor electronics," Biosensors & Bioelectronics **24**, 1995-2001 (2009).

10. B. D. Moore, L. Stevenson, A. Watt, S. Flitsch, N. J. Turner, C. Cassidy, and D. Graham, "Rapid and ultra-sensitive determination of enzyme activities using surface-enhanced resonance Raman scattering," Nature Biotechnology **22**, 1133-1138 (2004).

11. T. Funatsu, Y. Harada, M. Tokunaga, K. Saito, and T. Yanagida, "Imaging of single fluorescent molecules and individual atp turnovers by single myosin molecules in aqueous-solution," Nature **374**, 555-559 (1995).

12. V. M. N. Passaro, F. Dell'Olio, B. Casamassima, and F. De Leonardis, "Guided-wave optical biosensors," Sensors **7**, 508-536 (2007).

13. J. P. Golden, G. P. Anderson, S. Y. Rabbany, and F. S. Ligler, "An evanescent-wave biosensor .ll. fluorescent signal acquisition from tapered fiber optic probes," IEEE Transactions on Biomedical Engineering **41**, 585-591 (1994).

14. Z. H. Zhong, D. L. Wang, Y. Cui, M. W. Bockrath, and C. M. Lieber, "Nanowire crossbar arrays as address decoders for integrated nanosystems," Science **302**, 1377-1379 (2003).

15. J. M. Nam, C. S. Thaxton, and C. A. Mirkin, "Nanoparticle-based bio-bar codes for the ultrasensitive detection of proteins," Science **301**, 1884-1886 (2003).

16. W. S. Yeo, D. H. Min, R. W. Hsieh, G. L. Greene, and M. Mrksich, "Label-free detection of protein-protein interactions on biochips," Angewandte Chemie-International Edition **44**, 5480-5483 (2005).

17. T. P. Burg, M. Godin, S. M. Knudsen, W. Shen, G. Carlson, J. S. Foster, K. Babcock, and S. R. Manalis, "Weighing of biomolecules, single cells and single nanoparticles in fluid," Nature **446**, 1066-1069 (2007).

18. S. Ingebrandt, Y. Han, F. Nakamura, A. Poghossian, M. J. Schöning, and A. Offenhäusser, "Label-free detection of single nucleotide polymorphisms utilizing the differential transfer function of field-effect transistors," Biosensors & Bioelectronics **22**, 2834-2840 (2007).

19. A. Poghossian, M. H. Abouzar, F. Amberger, D. Mayer, Y. Han, S. Ingebrandt, A. Offenhäusser, and M. J. Schöning, "Field-effect sensors with charged macromolecules: Characterisation by capacitance-voltage, constant-capacitance, impedance spectroscopy and atomic-force microscopy methods," Biosensors & Bioelectronics **22**, 2100-2107 (2007).

20. A. M. Armani, R. P. Kulkarni, S. E. Fraser, R. C. Flagan, and K. J. Vahala, "Label-free, single-molecule detection with optical microcavities," Science **317**, 783-787 (2007).

21. K. De Vos, I. Bartolozzi, E. Schacht, P. Bienstman, and R. Baets, "Silicon-on-Insulator microring resonator for sensitive and label-free biosensing," Optics Express **15**, 7610-7615 (2007).

22. R. Kirchner, M. K. Kaiser, B. Adolphi, R. Landgraf, and W. J. Fischer, "Chemical functional polymers for direct UV assisted nanoimprinting of

polymeric photonic microring resonators," Physica Status Solidi A-Applications and Materials Science **208**, 1308-1314 (2011).

23. K. De Vos, J. Girones, S. Popelka, E. Schacht, R. Baets, and P. Bienstman, "SOI optical microring resonator with poly(ethylene glycol) polymer brush for label-free biosensor applications," Biosensors & Bioelectronics **24**, 2528-2533 (2009).

24. F. Vollmer, and S. Arnold, "Whispering-gallery-mode biosensing: label-free detection down to single molecules," Nature Methods **5**, 591-596 (2008).

25. H. Kawarada, and A. R. Ruslinda, "Diamond electrolyte solution gate FETs for DNA and protein sensors using DNA/RNA aptamers," Physica Status Solidi A - Applications and Materials Science **208**, 2005-2016 (2011).

26. B. van Grinsven, N. Vanden Bon, H. Strauven, L. Grieten, M. Murib, K. L. J. Monroy, S. D. Janssens, K. Haenen, M. J. Schöning, V. Vermeeren, M. Ameloot, L. Michiels, R. Thoelen, W. De Ceuninck, and P. Wagner, "Heat-transfer resistance at solid-liquid interfaces: A Tool for the Detection of Single-Nucleotide Polymorphisms in DNA," Acs Nano **6**, 2712-2721 (2012).

27. B. J. M. Hausmann, B. Shields, Q. M. Quan, P. Maletinsky, M. McCutcheon, J. T. Choy, T. M. Babinec, A. Kubanek, A. Yacoby, M. D. Lukin, and M. Loncar, "Integrated diamond networks for quantum nanophotonics," Nano Letters **12**, 1578-1582 (2012).

28. J. K. Lee, M. W. Anderson, F. A. Gray, and P. John, "Fabrication of spherical diamond microshells," Diamond and Related Materials **16**, 701-704 (2007).

29. J. P. Laine, C. Tapalian, B. Little, and H. Haus, "Acceleration sensor based on high-Q optical microsphere resonator and pedestal antiresonant reflecting waveguide coupler," Sensors and Actuators a-Physical **93**, 1-7 (2001).

30. Website: Micro Star Technologies, Nano Indentors from Micro Star Technologies www.microstartech.com, January 26, 2014.

31. M. L. Gorodetsky, A. A. Savchenkov, and V. S. Ilchenko, "Ultimate Q of optical microsphere resonators," Optics Letters **21**, 453-455 (1996).

32. T. Yoshie, L. L. Tang, and S. Y. Su, "Optical microcavity: sensing down to single molecules and atoms," Sensors **11**, 1972-1991 (2011).

33. M. Keith, "The Crystran Handbook of Infra-Red and Ultra-Violet Optical Materials," (Crystran Ltd., 2008).

34. P. Chris, "DK Handbook to Rocks and Minerals," (Dorling Kindersley, 1992).

35. J. A. Lock, and G. Gouesbet, "Rigorous justification of the localized approximation to the beam-shape coefficients in generalized Lorenz-Mie theory .I. on-axis beams," Journal of the Optical Society of America A - Optics Image Science and Vision **11**, 2503-2515 (1994).

36. B. R. Johnson, "Theory of morphology-dependent resonances - shape resonances and width formulas," Journal of the Optical Society of America A - Optics Image Science and Vision **10**, 343-352 (1993).

37. A. Demir, and A. Serpengüzel, "Silica microspheres for biomolecular detection applications," IEE Proceedings Nanobiotechnology **152**, 105-108 (2005).

38. A. Serpengüzel, S. Arnold, G. Griffel, and J. A. Lock, "Enhanced coupling to microsphere resonances with optical fibers," Journal of the Optical Society of America B-Optical Physics **14**, 790-795 (1997).

39. A. G. Mamalis, J. J. Ramsden, A. I. Grabchenko, L. A. Lytvynov, V. A. Filipenko, and S. N. Lavrynenko, "A novel concept for the manufacture of individual sapphire-metallic hip joint endoprostheses," Journal of Biological Physics and Chemistry **6**, 113-117 (2006).

40. G. Q. Zhou, Y. J. Dong, J. Xu, H. J. Li, J. L. Si, X. B. Qian, and X. Q. Li, "Ø 140 mm sapphire crystal growth by temperature gradient techniques and its color centers," Materials Letters **60**, 901-904 (2006).

41. J. P. Barton, "Effects of surface perturbations on the quality and the focused-beam excitation of microsphere resonance," Journal of the Optical Society of America A - Optics Image Science and Vision **16**, 1974-1980 (1999).

Chapter 5

Photonic studies on polymer-coated sapphire-sphere: a model system for biological ligands

Under preparation for submission to ACS Photonics Journal (February 2014)

5.1 Abstract

Transmitted and elastic scattering intensity at 1510 nm are analyzed from a sapphire microsphere (radius 500 μm, refractive index 1.77) on an optical fiber half coupler for the first time. The 0.43 nm angular mode spacing of the resonances correlates well with the optical size of the sapphire sphere. The spectral linewidths of the resonances are on the order of 0.01 nm, which corresponds to quality factors on the order of 10^5. A polydopamine (PDA) layer has been used as a functionalizing agent on sapphire microspherical resonators in view of the implementation of biosensors. The various PDA layer thicknesses on the sapphire microsphere were characterized as a function of the resonance wavelength shift. It is shown that the polymeric functionalization does not affect the quality factor ($Q \approx 10^4$) of the sapphire microspheres. This functionalizing process of the microresonator constitutes a promising step towards the achievement of an ultra-sensitive biosensor.

Keywords: Label-free biosensor, microcavity, photonics, polydopamine, quality factor, sapphire microsphere, whispering gallery modes.

5.2 Introduction

Development of biological, biochemical and chemical sensors is the current need of the society. Biomolecule recognition and DNA denaturation were studied by different types of measurement setups such as elastic measurements at the level of a single molecule [1], force-induced denaturation [2], and by monitoring the denaturation dynamics in real-time using impedance spectroscopy [3], and heat-transfer method [4]. Other label-free biosensors that were shown recently are nanowires [5], nanoparticle probes [6], biochips [7], mechanical cantilevers [8], and field-effect sensors [9, 10]. Optical measurement techniques can provide high sensitivity, compactness, fast response and real-time measurements [11]. Optical biosensors are non-destructive to the sample, and the transduction processes generally take place on a surface and can be tailored to sense almost any kind of molecule, chemical and prebiotic as well as biological [12].

Optical sensing can be performed using ring resonators [13], confocal microscopy [3], prism couplers [14], and spherical cavities [15]. Optical microcavities such as ring resonators or spherical resonators, where optical rays are confined by total internal reflection, are promising optical label-free detection setups and play a common role in modern optics [11, 15 - 16].

Recently, a silicon-on-insulator (SOI) microring resonator for sensitive label-free biosensing was fabricated [17]. In addition, microring surface functionalization and a detection limit of 0.37 fg avidin mass (3260 molecules) were achieved [18, 19]. In an optical microcavity, the target molecules are sampled hundreds of times due to the recirculation of light within the microcavity by total internal reflection (TIR) [16]. The target molecule induces a change in the optical microcavity properties such as its size and as a result, a change in the whispering gallery mode (WGM) resonant wavelength is encountered [20]. In order to preserve the high quality of the transducer and the interaction with the sensing layer and the WGM [12, 21 - 22], a good control of surface functionalization of the transducer surface is a crucial step for producing reliable biosensors for the binding of the biological recognition element to it. The functional layer has to be very thin, i.e., 10 to 100 nm and homogeneous.

So far, silicon-on-insulator ring resonators [19] and glass microspheres [15] have been used as microcavity-based biosensors. The degradation of silicon and glass interfaces in aqueous solutions limits their use to that of biosensors [23, 24]. More recently, diamond ring resonators [25] and nearly spherical diamond resonators were fabricated [26]. However, their fabrication is expensive and diamond surface modification with proteins or DNA requires tedious functionalization steps [23, 27].

In this article, an experimental study of an optical biosensor concept based on elastic light scattering from sapphire microspheres and the corresponding shift of WGMs, after an add-on polydopamine (PDA) layer to the sphere, is performed. Mussel-inspired polydopamine coatings have been intensely studied in recent years [28 - 30]. Surface functionalization using this biopolymer is especially robust. Simply dipping any substrate into an aqueous solution of dopamine, a surface-adherent polydopamine thin film is formed within hours through oxidative self-polymerization [28]. The thickness of the formed polymer can be tuned with the concentration of the dopamine used or with the immersion time of the substrates. Using AFM, Lee at el. found that the thickness of the polymers formed on gold surfaces increase linearly with time at the beginning of the reaction and get saturated after 20 hours [28]. Polymers with the similar thickness were also obtained by Pop-Georgievski *et al.* on hydrogen and oxygenated diamond surfaces measured by spectroscopic ellipsometry [31]. Various post-modification reactions are possible to create a variety of ad-layers on this polymer coating to fulfil various purposes [29, 32 - 35]. WGMs have been used in polymeric microresonators [36, 37]. A PDA-coated sapphire microspheres have been proposed as an alternative to polymeric microresonators. Surface functionalization of this biopolymer on a sapphire microsphere could be used as a platform for future bio-optical biosensing applications. PDA can serve as a linker molecule. In this paper, we address sapphire, being the second hardest material next to diamond. Sapphire shows outstanding chemical inertness, wear resistance, and biocompatibility [38]. Hence, it is widely used for implants such as hip implants [38], dental implants [39], and endosseous implants [40]. Moreover, its wide optical transmission band from the ultraviolet (UV) to the near-infrared (near-IR) [41] suggests application potential in optical biosensors. Sapphire spheres are fabricated using

spherical indentors and the end surface is polished down to a few nanometers of roughness and show a perfect spherical geometry [42].

5.3 Experimental method

5.3.1 Surface functionalization

TRIS hydrochloride (reagent grade, minimum 99%) and dopamine hydrochloride (98.5%) were purchased from Sigma and used as received. The formation of a polydopamine film was carried out by immersing the sapphire microsphere into a solution of dopamine hydrochloride (2 mg/mL) in 10 mM TRIS-HCl buffer that was adjusted to pH 8.5 by adding 0.5 M NaOH. Immersion times were varied (2 h, 5 h, 10 h and 20 h) to create polydopamine films with different thicknesses [28]. To prevent the formation of microparticles in the dopamine solution, the solution together with the sapphire microsphere was stirred with a shaker during the reaction. After the reaction, the coated sapphire microsphere was thoroughly rinsed with copious quantities of deionized water and dried under a stream of nitrogen (Figure 5.1a).

Figure 5.1b presents a brief explanation of the polymerization mechanisms of dopamine adapted from Lee H. *et al.* [28]. Briefly, under an oxidative condition, e.g. alkaline buffer, dihydroxyl group protons in dopamine are deprotonated, becoming dopamine-quinone. Dopamine-quinone is then rearranged via intramolecular cyclization to leukodopaminechrome. Further oxidation and rearrangement leads to 5,6 dihydroxyindole, whose oxidation causes inter-molecular cross-linking to yield a polymer that is structurally similar to the bio-pigment melanin [28].

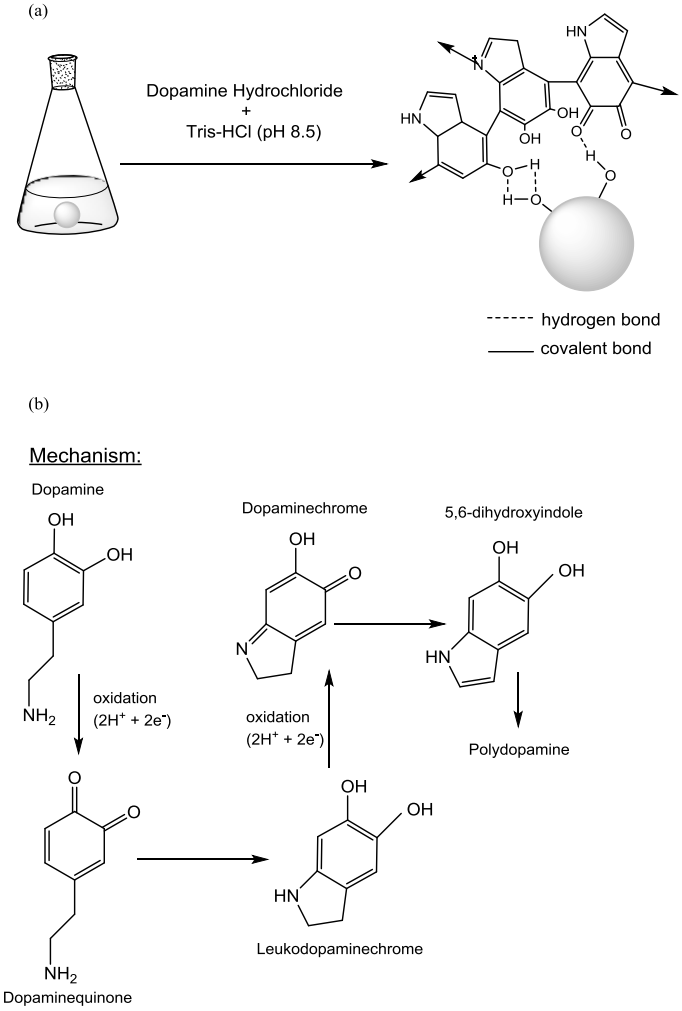

Figure 5.1: (a) Sapphire surface functionalization with PDA. (b) Polymerization mechanisms of dopamine adapted from Lee *et al.* [28].

5.3.2 X-ray photoelectron spectroscopy (XPS)

X-ray photoelectron spectroscopy (XPS) measurements were performed on a sapphire chip (1 cm × 1 cm) in order to confirm the presence of the PDA layer after polymerization. The sapphire chip used for XPS measurements was functionalized with PDA (5 h immersion), just as described in chapter 3 section 3.1. Photoemission experiments were carried out using a Scienta ESCA 200 spectrometer in ultrahigh vacuum with a base pressure of $1x10^{-10}$ mbar

(Linköping University, Sweden). The measurement chamber is equipped with a monochromatic Al K_α X-ray source (1486.6 eV). The XPS experimental conditions were set so that the full-width-at-half-maximum of the clean Au $4f_{7/2}$ line was 0.65 eV. All spectra were measured at a photoelectron take-off angle of 0°, i.e. normal emission.

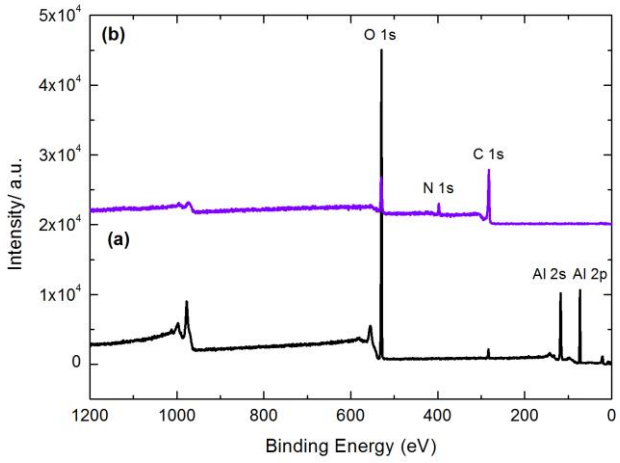

Figure 5.2: XPS spectra of a sapphire chip before (a) and after (b) 5 h functionalization with PDA layer.

Simple immersion of substrates in a dilute aqueous solution of dopamine, buffered to a slightly basic pH (2 mg of dopamine per milliliter of 10 mM TRIS buffer, pH 8.5), resulted in spontaneous deposition of a thin adherent polymer film. X-ray photoelectron spectroscopy (XPS) analysis of the sapphire chip coated during 5 hours (Figure 5.2 b) shows two additional peaks (N 1s and C 1s) as compared to (Figure 5.2 a), which can attributed to the nitrogen (N) and carbon (C) atoms in the PDA layer. Moreover, XPS analysis also revealed the absence of signals specific to the sapphire chip (Al 2p and Al 2s peaks), indicating the formation of a polymer coating of 10 nm or more in thickness [28].

5.3.3 Detection mechanism

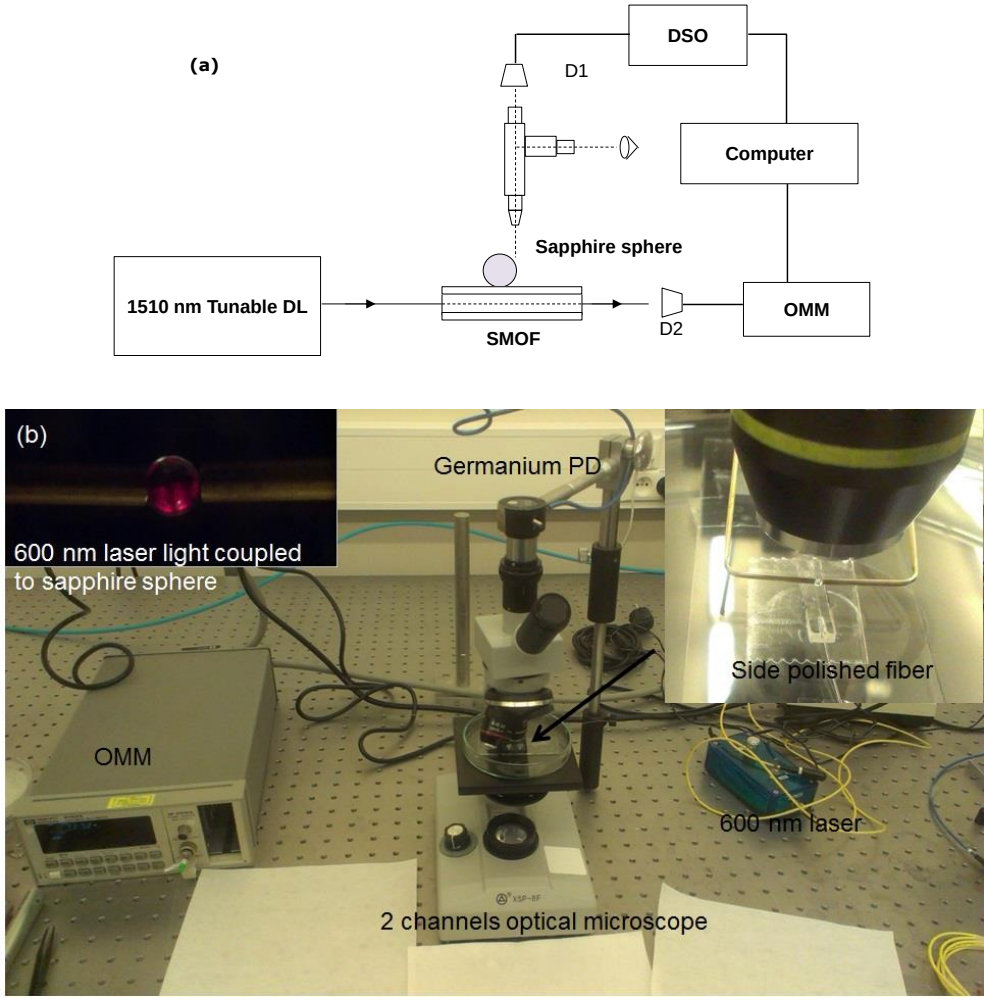

Figure 5.3: (a) Schematic geometry of the microsphere with a biologically modified surface coupled to a single mode half coupler optical fiber. (b) Photo of the optical setup used for the experiments. The optical setup was implemented at INTEC, Ghent University.

The system was modeled using the Generalized Lorenz-Mie Theory (GLMT), which describes the electromagnetic scattering of an arbitrary light beam by a spherical microparticle [43]. Elastic scattering intensity from the sphere and transmittance intensity at the output of the optical fiber for transverse electric (TE) and transverse magnetic (TM) polarization were calculated for sapphire spheres before and after surface modifications with biomolecules [44]. The mode spacing of consecutive resonances $\Delta\lambda$ having the same mode order

(number of nodes or maxima of the intensity distribution in the radial direction) and consecutive mode number (the number of maxima between 0 and 180°) in the angular intensity distribution of the mode; solid lines curve). $\Delta\lambda$ can be calculated using equation [43]:

$$\Delta\lambda = \frac{\lambda^2 arctan\sqrt{m^2-1}}{2\pi a\sqrt{m^2-1}} \quad (5.1),$$

where *m* is the relative refractive index of the sphere (refractive index of the sphere/refractive index of the surrounding medium), λ the wavelength of the laser source in vacuum, and a is the sphere's radius. If the molecules are tethered onto the sphere's surface, these molecules will induce a change of the optical properties of the sphere such as its effective size. As a result, the resonance wavelength will change further and result in the phenomenon of resonant shift [16]. The wavelength shift $\delta\lambda_{shift}$ can be calculated by the equation:

$$\frac{\delta\lambda_{shift}}{\lambda} = \frac{\delta a}{a} \quad (5.2).$$

Here, δa is the change in sphere radius due to the interaction between the adsorbed molecules [20].

5.4 Experimental results

The diode laser was tuned from 1510 nm to 1512 nm with a step size of 5 pm (Figure 5.3 a). The elastically scattered light from the sapphire microsphere at 90° is collected by a two-channel optical microscope and detected by a germanium (Ge) photodiode (PD). The elastically scattered light is separated by a beam splitter placed at an angle of 45° with respect to the collected beam. The Ge PD signal is sent to a digital storage oscilloscope (DSO) for signal monitoring and data acquisition (DAQ). The transmitted power through the optical fiber is detected by optical multimeter (OMM). All the optoelectronic equipment is controlled using the general purpose interface bus (GPIB) standard.

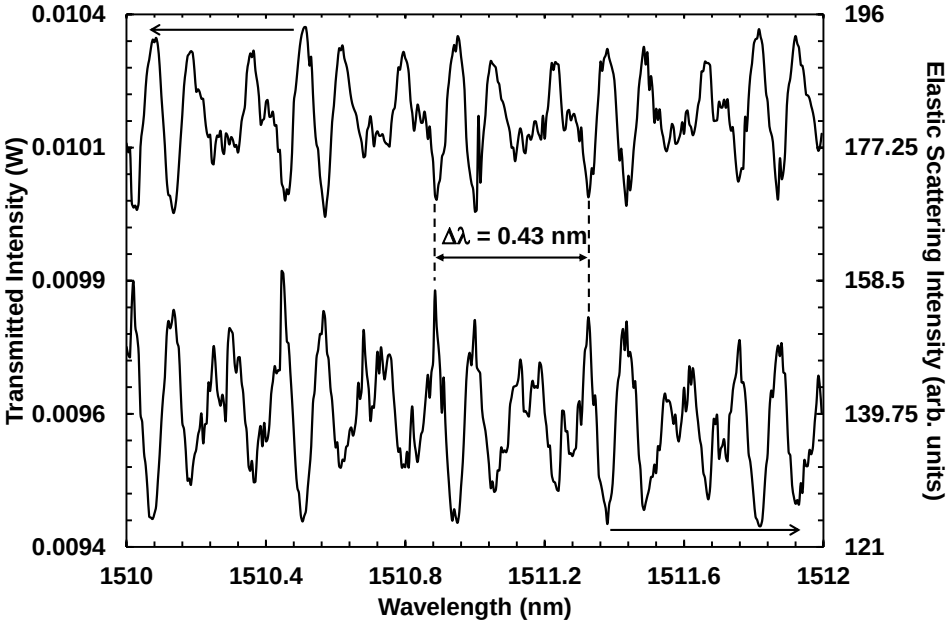

Figure 5.4: Measured elastic scattering intensity and the corresponding transmitted intensity spectra from sapphire sphere of radius 500 μm and refractive index 1.77.

Figure 5.4 shows the measured spectrum of the elastically scattered light from the sapphire microsphere. The $\Delta\lambda$ of the WGMs is observed to be 0.43 nm, which agrees well with the $\Delta\lambda$ estimated using Equation (5.1) for a 1 mm diameter sapphire microsphere with refractive index of 1.77. For each maximum in the elastic scattering spectrum, there is a corresponding minimum in the transmittance spectrum. The minima in the transmittance spectrum correspond to a fraction of the light coupled from the fiber into the sphere. The linewidth ($\delta\lambda$) of the resonances is about 0.01 nm, which corresponds to a quality factor Q on the order 10^5 (using $Q = \lambda / \delta\lambda$).

When adding layers of PDA to the surface of the sphere, we obtain the results in figure 5.5 (a & b). Figure 5.5a represents the transmitted intensity spectra and Figure 5.5b represents the elastic scattering intensity spectra for the non-modified and the modified sapphire sphere in the wavelength range from 1510 - 1512 nm.

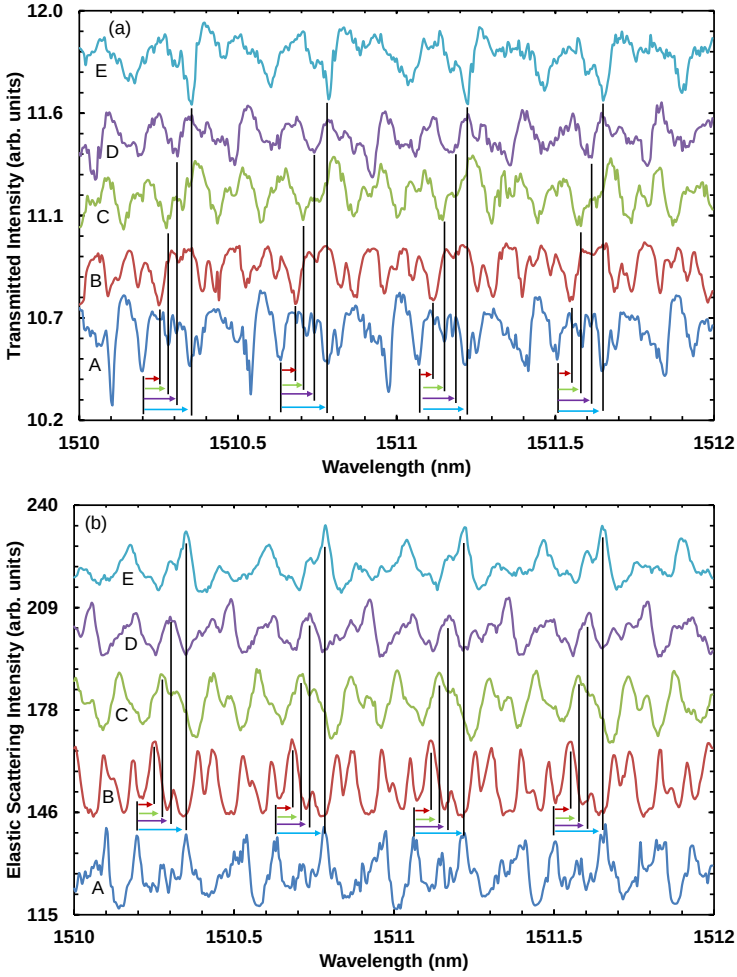

Figure 5.5: Transmitted intensity (a) and elastic scattering intensity spectra (b) from sapphire sphere with different polymerization time and the corresponding wavelength shift. A) non-modified sphere. B) 2 hrs. C) 5 hrs. D) 10 hrs. E) 20 hrs of polymerization.

Spectrum A represents the resonances from the non-modified sapphire sphere. Then, the sapphire sphere was polymer-coated during 2 hours and afterwards spectrum B was collected. As a result, the resonances were red-shifted by 0.05 nm. Using equation 5.2, this wavelength shift corresponds to a thickness of 16.55 nm, which is in the range of the thickness reported in Lee H. *et al.* [28]. The spectra were collected again for 5 hours, 10 hours, and 20 hours polymerization time, which corresponded to a shift of 0.075 nm (spectrum C), 0.11 nm (spectrum D), and 0.155 nm (spectrum E), respectively.

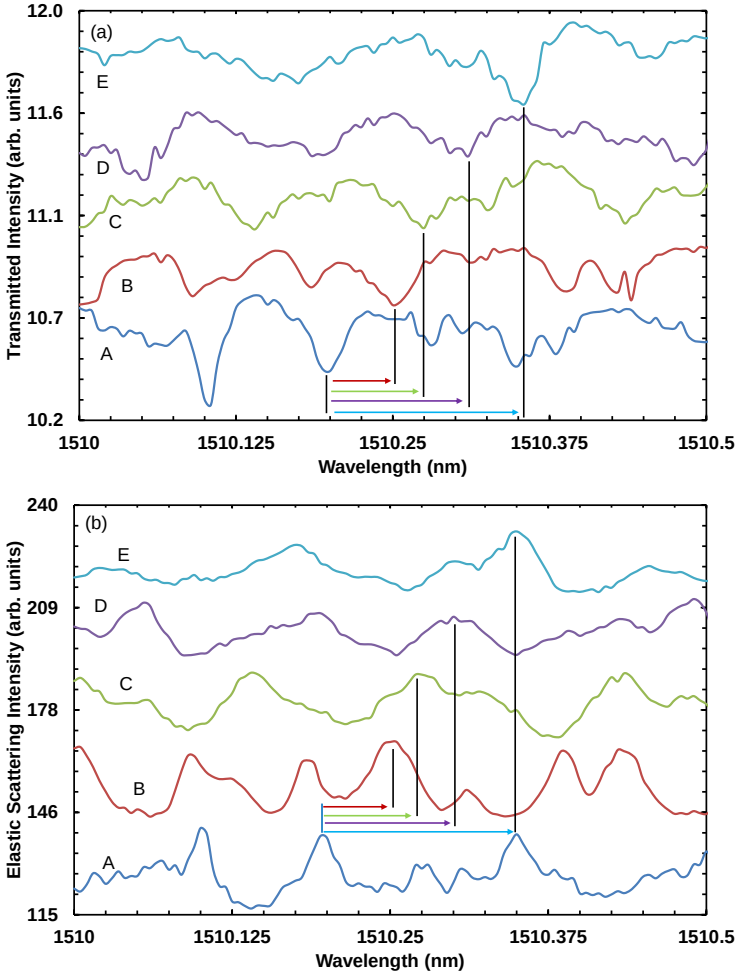

Figure 5.6: Zoom of figure 5.5. Single resonance of the transmitted intensity (a) and elastic scattering intensity spectra (b) from sapphire sphere with different polymerization time and the corresponding wavelength shift. A) non-modified sphere. B) 2 hrs. C) 5 hrs. D) 10 hrs. E) 20 hrs of polymerization.

The resulting shifts correspond to a polymer layer thickness of 24.8 nm, 36.4 nm, and 51 nm, respectively. This correlates well with the thickness data found in (Lee H. *et al.*) table 5.1 [28]. The spectrum of the non-modified sphere showed resonances with quality factor of 1.5 $\times 10^5$ while the spectra of the modified sphere showed resonances with maximum quality factor of 6.04 $\times$ 10^4. This is due to the fact that higher polymer concentrations lead to the formation

of an inhomogeneous coating, with the presence of clusters [11]. This scatters the photons out of the WGM and decreases the Q as shown in table 5.1 [45].

Figures 5.5a and 5.5b were zoomed into one resonance to study the relationship between the PDA layer thickness and the resonance quality factor. It can be seen from figures 5.6a and 5.6b that, as the PDA layer thickness increases, the resonance linewidth increases. As shown in table 5.1 the quality factors of the analyzed resonances were on the same order ($Q = 10^4$) and this verifies that the PDA layers are homogeneous.

Table 5.1: Resonance wavelength shift and the corresponding resulting polymer film thickness as a function to polymerization time.

Polymerization Time (hrs)	Resonance Wavelength Shift (nm)	Polymer film thickness (nm)	Quality factor (Q)
0	NA	NA	7.5×10^4
2	0.05	16.6	6.04×10^4
5	0.075	24.8	5.03×10^4
10	0.11	36.4	3.35×10^4
20	0.155	51.2	4.3×10^4

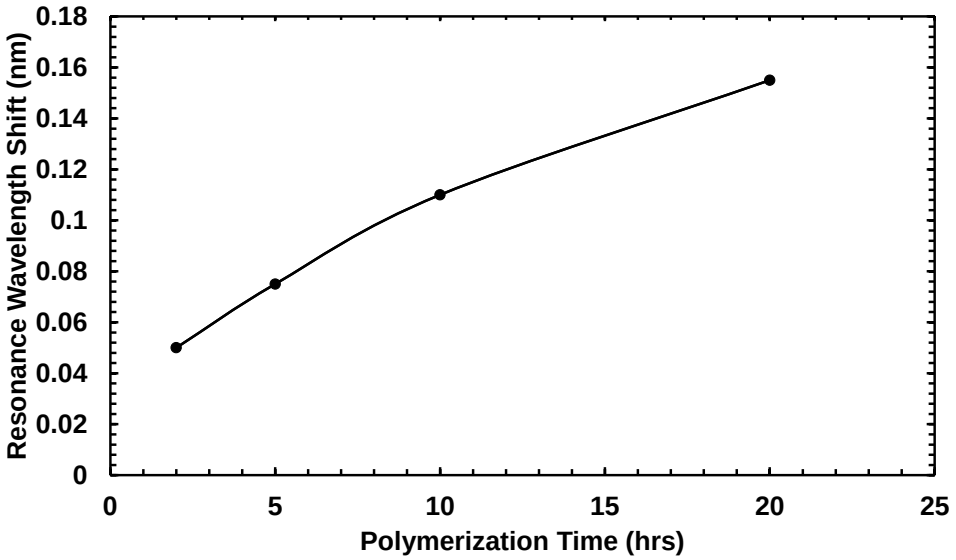

Figure 5.7: Resonance wavelength shift corresponding to the sapphire surface polymerization time. The solid line is a guide to the eye.

Figure 5.7 represents the resulting shift in resonance wavelengths as a function of the polymer film growth time. The polymer thicknesses corresponding to the resonance wavelength shifts were calculated using equation 5.2 as shown in table 5.1. As the polymerization time increases, the resonance wavelength shift, which corresponds to a thicker PDA layer on the sapphire surface, increases.

5.5 Conclusion

We have studied the transmitted intensity and the elastic scattering intensity from a sapphire sphere of radius 500 μm and 1.77 refractive index in the wavelength range of 1510 - 1512 nm. The highest quality factor on the order 10^5 was demonstrated for the first time in a spherical resonator fabricated out of this material. We have studied the shift in resonance wavelength arising from coating the sphere with different thicknesses of PDA layers. The quality factor of the resonances was studied as a function of the change in the PDA polymer thickness, and we found that it is almost preserved. We also verified that PDA layers are homogeneous as well and this allowed us to obtain high Q factors, comparable with the values achieved with silica spheres coated with polylactic acid (PLLA) [11], showing that PDA coating is a valid alternative method to silanization.

5.6 References

1. T. Strick, J. F. Allemand, V. Croquette, and D. Bensimon, "Twisting and stretching single DNA molecules," Progress in Biophysics & Molecular Biology **74**, 115-140 (2000).

2. U. Bockelmann, P. Thomen, B. Essevaz-Roulet, V. Viasnoff, and F. Heslot, "Unzipping DNA with optical tweezers: high sequence sensitivity and force flips," Biophysical Journal **82**, 1537-1553 (2002).

3. B. van Grinsven, N. V. Bon, L. Grieten, M. Murib, S. D. Janssens, K. Haenen, E. Schneider, S. Ingebrandt, M. J. Schöning, V. Vermeeren, M. Ameloot, L. Michiels, R. Thoelen, W. De Ceuninck, and P. Wagner, "Rapid assessment of the stability of DNA duplexes by impedimetric real-time monitoring of chemically induced denaturation," Lab on a Chip **11**, 1656-1663 (2011).

4. B. van Grinsven, N. Vanden Bon, H. Strauven, L. Grieten, M. Murib, K. L. J. Monroy, S. D. Janssens, K. Haenen, M. J. Schöning, V. Vermeeren, M. Ameloot, L. Michiels, R. Thoelen, W. De Ceuninck, and P. Wagner, "Heat-transfer resistance at solid-liquid interfaces: a tool for the detection of single-nucleotide polymorphisms in DNA," ACS Nano **6**, 2712-2721 (2012).

5. Z. H. Zhong, D. L. Wang, Y. Cui, M. W. Bockrath, and C. M. Lieber, "Nanowire crossbar arrays as address decoders for integrated nanosystems," Science **302**, 1377-1379 (2003).

6. J. M. Nam, C. S. Thaxton, and C. A. Mirkin, "Nanoparticle-based bio-bar codes for the ultrasensitive detection of proteins," Science **301**, 1884-1886 (2003).

7. W. S. Yeo, D. H. Min, R. W. Hsieh, G. L. Greene, and M. Mrksich, "Label-free detection of protein-protein interactions on biochips," Angewandte Chemie-International Edition **44**, 5480-5483 (2005).

8. T. P. Burg, M. Godin, S. M. Knudsen, W. Shen, G. Carlson, J. S. Foster, K. Babcock, and S. R. Manalis, "Weighing of biomolecules, single cells and single nanoparticles in fluid," Nature **446**, 1066-1069 (2007).

9. S. Ingebrandt, Y. Han, F. Nakamura, A. Poghossian, M. J. Schöning, and A. Offenhäusser, "Label-free detection of single nucleotide polymorphisms utilizing the differential transfer function of field-effect transistors," Biosensors & Bioelectronics **22**, 2834-2840 (2007).

10. A. Poghossian, M. H. Abouzar, F. Amberger, D. Mayer, Y. Han, S. Ingebrandt, A. Offenhäusser, and M. J. Schöning, "Field-effect sensors with charged macromolecules: Characterisation by capacitance-voltage, constant-capacitance, impedance spectroscopy and atomic-force microscopy methods," Biosensors & Bioelectronics **22**, 2100-2107 (2007).

11. S. Soria, S. Berneschi, M. Brenci, F. Cosi, G. N. Conti, S. Pelli, and G. C. Righini, "Optical microspherical resonators for biomedical sensing," Sensors **11**, 785-805 (2011).

12. J. L. Nadeau, V. S. Iltchenko, D. Kossakovski, G. H. Bearman, and L. Maleki, "High-Q whispering-gallery mode sensor in liquids," in Conference on Laser Resonators and Beam Control V (San Jose, California, 2002), pp. 172-180.

13. J. D. Suter, I. M. White, H. Y. Zhu, H. D. Shi, C. W. Caldwell, and X. D. Fan, "Label-free quantitative DNA detection using the liquid core optical ring resonator," Biosensors & Bioelectronics **23**, 1003-1009 (2008).

14. Z. B. Bahsi, A. Buyukaksoy, S. M. Olmezcan, F. Simsek, M. H. Aslan, and A. Y. Oral, "A novel label-free optical biosensor using synthetic oligonucleotides from E. coli O157:H7: elementary sensitivity tests," Sensors **9**, 4890-4900 (2009).

15. M. Baaske, and F. Vollmer, "Optical resonator biosensors: molecular diagnostic and nanoparticle detection on an integrated platform," ChemPhysChem **13**, 427-436 (2012).

16. A. M. Armani, R. P. Kulkarni, S. E. Fraser, R. C. Flagan, and K. J. Vahala, "Label-free, single-molecule detection with optical microcavities," Science **317**, 783-787 (2007).

17. K. De Vos, I. Bartolozzi, E. Schacht, P. Bienstman, and R. Baets, "Silicon-on-Insulator microring resonator for sensitive and label-free biosensing," Optics Express **15**, 7610-7615 (2007).

18. R. Kirchner, M. K. Kaiser, B. Adolphi, R. Landgraf, and W. J. Fischer, "Chemical functional polymers for direct UV assisted nanoimprinting of polymeric photonic microring resonators," Physica Status Solidi A - Applications and Materials Science **208**, 1308-1314 (2011).

19. K. De Vos, J. Girones, S. Popelka, E. Schacht, R. Baets, and P. Bienstman, "SOI optical microring resonator with poly(ethylene glycol) polymer brush for label-free biosensor applications," Biosensors & Bioelectronics **24**, 2528-2533 (2009).

20. F. Vollmer, and S. Arnold, "Whispering-gallery-mode biosensing: label-free detection down to single molecules," Nature Methods **5**, 591-596 (2008).

21. F. Vollmer, D. Braun, A. Libchaber, M. Khoshsima, I. Teraoka, and S. Arnold, "Protein detection by optical shift of a resonant microcavity," Applied Physics Letters **80**, 4057-4059 (2002).

22. V. S. Ilchenko, and A. B. Matsko, "Optical resonators with whispering-gallery modes - Part II: Applications," IEEE Journal of Selected Topics in Quantum Electronics **12**, 15-32 (2006).

23. V. Vermeeren, S. Wenmackers, M. Daenen, K. Haenen, O. A. Williams, M. Ameloot, M. Vandeven, P. Wagner, and L. Michiels, "Topographical and functional characterization of the ssDNA probe layer generated through EDC-mediated covalent attachment to nanocrystalline diamond using fluorescence microscopy," Langmuir **24**, 9125-9134 (2008).

24. T. Strother, W. Cai, X. S. Zhao, R. J. Hamers, and L. M. Smith, "Synthesis and characterization of DNA-modified silicon (111) surfaces," Journal of the American Chemical Society **122**, 1205-1209 (2000).

25. B. J. M. Hausmann, B. Shields, Q. M. Quan, P. Maletinsky, M. McCutcheon, J. T. Choy, T. M. Babinec, A. Kubanek, A. Yacoby, M. D. Lukin, and M.

Loncar, "Integrated diamond networks for quantum nanophotonics," Nano Letters **12**, 1578-1582 (2012).

26. V. S. Ilchenko, A. M. Bennett, P. Santini, A. A. Savchenkov, A. B. Matsko, and L. Maleki, "Whispering gallery mode diamond resonator," Optics Letters **38**, 4320-4323 (2013).

27. H. Kawarada, and A. R. Ruslinda, "Diamond electrolyte solution gate FETs for DNA and protein sensors using DNA/RNA aptamers," Physica Status Solidi A - Applications and Materials Science **208**, 2005-2016 (2011).

28. H. Lee, S. M. Dellatore, W. M. Miller, and P. B. Messersmith, "Mussel-inspired surface chemistry for multifunctional coatings," Science **318**, 426-430 (2007).

29. M. E. Lynge, R. van der Westen, A. Postma, and B. Stadler, "Polydopamine-a nature-inspired polymer coating for biomedical science," Nanoscale **3**, 4916-4928 (2011).

30. S. M. Kang, N. S. Hwang, J. Yeom, S. Y. Park, P. B. Messersmith, I. S. Choi, R. Langer, D. G. Anderson, and H. Lee, "One-step multipurpose surface functionalization by adhesive catecholamine," Advanced Functional Materials **22**, 2949-2955 (2012).

31. O. Pop-Georgievski, N. Neykova, V. Proks, J. Houdkova, E. Ukraintsev, J. Zemek, A. Kromka, and F. Rypacek, "Polydopamine-modified nanocrystalline diamond thin films as a platform for bio-sensing applications," Thin Solid Films **543**, 180-186 (2013).

32. K. Kang, I. S. Choi, and Y. Nam, "A biofunctionalization scheme for neural interfaces using polydopamine polymer," Biomaterials **32**, 6374-6380 (2011).

33. Y. Wan, D. Zhang, Y. Wang, P. Qi, and B. R. Hou, "Direct immobilisation of antibodies on a bioinspired architecture as a sensing platform," Biosensors & Bioelectronics **26**, 2595-2600 (2011).

34. H. Lee, J. Rho, and P. B. Messersmith, "Facile conjugation of biomolecules onto surfaces via mussel adhesive protein inspired coatings," Advanced Materials **21**, 431-434 (2009).

35. K. Sun, Y. Y. Xie, D. K. Ye, Y. Y. Zhao, Y. Cui, F. Long, W. Zhang, and X. Y. Jiang, "Mussel-inspired anchoring for patterning cells using polydopamine," Langmuir **28**, 2131-2136 (2012).

36. J. R. Schwesyg, T. Beckmann, A. S. Zimmermann, K. Buse, and D. Haertle, "Fabrication and characterization of whispering-gallery-mode resonators made of polymers," Optics Express **17**, 2573-2578 (2009).

37. J. Lutti, W. Langbein, and P. Borri, "High Q optical resonances of polystyrene microspheres in water controlled by optical tweezers," Applied Physics Letters **91** (2007).

38. A. G. Mamalis, J. J. Ramsden, A. I. Grabchenko, L. A. Lytvynov, V. A. Filipenko, and S. N. Lavrynenko, "A novel concept for the manufacture of individual sapphire-metallic hip joint endoprostheses," Journal of Biological Physics and Chemistry **6**, 113-117 (2006).

39. T. Takahashi, T. Sato, R. Hisanaga, O. Miho, Y. Suzuki, M. Tsunoda, and K. I. Nakagawa, "Long-term observation of porous sapphire dental implants," The Bulletin of Tokyo Dental College **49**, 23-27 (2008).

40. M. R. Rieger, W. K. Adams, G. L. Kinzel, and M. O. Brose, "Alternative materials for three endosseous implants," The Journal of Prosthetic Dentistry **61**, 717-722 (1989).

41. G. Q. Zhou, Y. J. Dong, J. Xu, H. J. Li, J. L. Si, X. B. Qian, and X. Q. Li, "φ 140 mm sapphire crystal growth by temperature gradient techniques and its color centers," Materials Letters **60**, 901-904 (2006).

42. Website: Micro Star Technologies, Nano Indentors from Micro Star, www.microstartech.com, January 26, 2014.

43. M. L. Gorodetsky, A. A. Savchenkov, and V. S. Ilchenko, "Ultimate Q of optical microsphere resonators," Optics Letters **21**, 453-455 (1996).

44. M. S. Murib, A. Q. Tran, W. De Ceuninck, M. J. Schöning, M. Nesládek, A. Serpengüzel, and P. Wagner, "Analysis of an optical biosensor based on elastic light scattering from diamond-, glass-, and sapphire microspheres," Physica Status Solidi A - Applications and Materials Science **209**, 1804-1810 (2012).

45. D. W. Vernooy, V. S. Ilchenko, H. Mabuchi, E. W. Streed, and H. J. Kimble, "High-Q measurements of fused-silica microspheres in the near infrared," Optics Letters **23**, 247-249 (1998).

Chapter 6

Photonic detection and characterization of DNA using sapphire spheres

Under preparation for submission to SPIE Biomedical Optics (February 2014)

6.1 Abstract

A microcavity-based deoxyribonucleic acid (DNA) optical biosensor is demonstrated for the first time using an insulating implant material for the optical cavity. Transmitted and elastic scattering intensity at 1510 nm are analyzed from a sapphire microsphere (radius 500 μm, refractive index 1.77) on an optical fiber half coupler. The 0.43 nm angular mode spacing of the resonances correlates well with the optical size of the sapphire sphere. The spectral linewidths of the resonances are on the order of 0.01 nm, which corresponds to quality factors on the order of 10^5. Probe DNA, consisting of a 36-mer fragment was covalently immobilized on a sapphire microsphere and hybridized with a 29-mer target DNA. Whispering gallery modes (WGM) resonances were monitored before the sapphire being functionalized with DNA and after it was functionalized with single-stranded DNA (ssDNA) and double-stranded DNA (dsDNA). The shift in resonances due to the surface modification with DNA was measured and correlated well with the estimated add-on DNA layer. It is shown that ssDNA is more uniformly oriented on the sapphire surface than the dsDNA. In addition, it is shown that functionalization of the sapphire spherical surface with DNA does not affect the quality factor ($Q \approx 10^4$) of the sapphire microspheres.

Keywords: Deoxyribonucleic acid, Label-free biosensor, microcavity, photonics, quality factor sapphire microsphere, whispering gallery modes.

6.2 Introduction

There is a growing effort for sensors to detect nanoparticles and biomolecules due to the advances in nanotechnology and biology [1]. Clinical diagnoses demand sensitive real-time label-free detection techniques [2]. Biomolecules recognition and DNA denaturation were studied by different types of measurement setups such as elastic measurements at the level of a single molecule [3], force-induced denaturation [4], and by monitoring the denaturation dynamics in real time using impedance spectroscopy [5]. Other label-free biosensors that have been shown recently, are nanowires [6], nanoparticle probes [7], biochips [8], mechanical cantilevers [9], and field-effect sensors [10, 11]. Label-free optical biosensors offer great advantages over conventional analytical techniques [12]. Optical biosensors are highly sensitive, fast, reproducible, and circumvent the need to modify target molecules [2, 12].

Optical biosensors are powerful transducers that detect the presence of molecules at a surface [13]. They are immune to electromagnetic interference, capable of performing remote sensing, and can provide multiplexed detection within a single device [14]. They can be extremely sensitive (nanomoles or less), non-destructive to the sample, and the transduction processes in optical biosensors generally take place on a surface and can be tailored to sense almost any kind of molecule, chemical and prebiotic as well as biological [15].

Optical sensing can be performed using ring resonators [16], confocal microscopy [5], prism couplers [17], spherical cavities [18], and fiber-optic waveguides [19, 20]. In ring resonators, spherical cavities, and fiber-optics waveguides, the light is coupled through the waveguides and an evanescent field extends beyond the waveguide surface by ≈ 100 nm [16]. The analytes bound to the surfaces of these waveguides will lie in the path of the evanescent field, and as a result they change the effective size and refractive index of the guided mode [16]. Optical sensing using confocal microscopy and fiber-optic waveguides have certain disadvantages. For example, fiber-optics waveguide sensors are typically quite long. In order to achieve a high signal and low detection limit, the waveguide must be on the order of a few centimeters long, since the sensing signal is accumulated along the waveguide [16]. Meanwhile, confocal microscopy requires fluorescent labeling for detection, which is time-

consuming, complex, and may not be suitable for rapid biophysical and routine characterization tasks [21]. In addition, real-time hybridization monitoring using confocal microscopy cannot be performed, because it is hard to distinguish between unbound targets in solution and those that have been hybridized to the probe on the surface, as both will fluoresce when imaged [22].

Optical microcavities such as ring resonators or spherical resonators are promising optical label-free detection setups [18, 23]. In an optical microcavity, the target molecules are sampled hundreds of times due to the recirculation of light within the microcavity by total internal reflection (TIR) [23]. The target molecule induces a change in the optical microcavity properties such as the size and refractive index, and as a result, a change in the whispering gallery mode (WGM) resonant wavelength is encountered [24]. Recently, a silicon-on-insulator (SOI) microring resonator for sensitive label-free biosensing was fabricated [25]. After coating with biotin receptor molecules, a detection limit of 0.37 fg avidin mass (3260 molecules) was shown [26, 27]. The first nearly spherical diamond was demonstrated quite recently [28]. Compared to sapphire, the anisotropy of sapphire is much weaker than diamond, and as a result sapphire can be shaped into a nearly perfect sphere. Moreover, a diamond sphere is still considered expensive to fabricate and requires more functionalization steps compared to sapphire sphere [29, 30].

In this article, an experimental study of an optical biosensor concept based on elastic light scattering from sapphire microspheres (radius 500 μm, refractive index 1.77) is performed. The sapphire microsphere surface was functionalized with DNA layers, and the corresponding shift of WGMs was monitored and analysed. We address sapphire, being the second hardest material after diamond. Sapphire shows outstanding chemical inertness, wear resistance, and biocompatibility [31]. Hence, it is widely used for implants such as hip implants [31], dental implants [32], and endosseous implants [33]. Moreover, its wide optical transmission band from the ultraviolet (UV) to the near-infrared (near-IR) [34] suggests application potential in optical biosensors. So far, silicon-on-insulator ring resonators [25] and glass microspheres [18] have been used as microcavity based biosensors. The degradation of silicon and glass interfaces in aqueous solutions limits their use to that of biosensors [30, 35].

6.3 Sapphire sphere modification with dsDNA

Probe DNA, consisting of a 36-mer fragment was covalently immobilized on the sapphire sphere and hybridized with 29-mer target DNA. The sapphire sphere was ultrasonically cleaned in acetone, ultrapure water (Sartorius Stedim Biotech Ultra Pure Water System Type 1) and isopropanol for 20 minutes in each bath. Next, it was immersed in 10 mM HNO_3 solution at room temperature for 30 minutes to create OH groups on the surface [36, 37]. Afterwards, the sapphire sphere was rinsed with ultrapure water and dried with nitrogen gas.

Silanisation of the sapphire samples was carried out by liquid phase deposition of a solution of silane in an organic solvent [38]. The samples were placed in a 600 mM solution of (3-Aminopropyl)triethoxysilane (APTES, 99%; Sigma-Aldrich) in toluene (≥ 99.9%, Sigma-Aldrich) for 15 hours in a nitrogen-filled glovebox. To wash off the unbound APTES, the samples were first rinsed with toluene, followed by tetrahydrofuran (THF, ≥ 99.9%, Sigma-Aldrich). After drying the samples in a nitrogen steam, they were cured for 2 hours at 150 °C. Curing at this high temperature will create a much stronger film of APTES on the surface [38]. This creates an amine-modified surface [39]. Zero-length 1-ethyl-3-[3-dimethylaminopropyl]-carbodiimide (EDC) was used for the covalent coupling of the 5' side of a carboxyl-modified 36-mer ssDNA fragment to the amine-modified surface in 2-[N-morpholino]-ethannesulphonic acid (MES) buffer at 4 °C. In a following step, 6 µl FAM-488-modified DNA was mixed with 14 µl 1× PCR buffer and added to the ssDNA-modified sapphire sphere (Table 6.1). The sphere was then incubated at 35 °C for 2 hours. Non-specifically bound DNA was removed using a double washing step. In a first step, the sphere was washed with 2 × saline sodium citrate (SSC) + 0.5% sodium dodecyl sulphate (SDS) for 30 minutes. Secondly, the sphere was washed twice with 0.2 × SSC at 30 °C for 5 minutes. Finally, the sphere was rinsed with phosphate buffered saline (PBS) of pH 7.2 and stored in PBS at 4 °C [30].

Table 6.1: Base sequences of the probe DNA and the corresponding full match DNA.

Name	Sequence
Probe DNA	5´-COOH-AAAAAAA CCC CTG CAG CCC ATG TAT ACC CCC GAA CC -3'
Full Match	5'-Alexa 488-GGT TCG GGG GTA TAC ATG GGC TGC AGG GG-3'

6.4 Confocal microscopy

A fluorescence image was taken on a Zeiss LSM 510 META Axiovert 200 M laser scanning confocal fluorescence microscope to confirm the dsDNA covalent binding to sapphire microsphere (Figure 6.1). To excite the Alexa-488 fluorescence dye, a 488 nm argon-ion laser was used with a maximum intensity at the sample surface of 30 μW, in order to avoid bleaching during the image acquisition. The peak emission has a longer wavelength of 518 nm due to vibrational relaxation of the Alexa molecule after photon absorption. The image was collected with a 10×/0.3 Plan Neofluar air objective with a working distance of 5.6 mm. The image size was 900 by 900 μm². The pinhole size was 150 μm and the laser intensity was set at 10%. The detector gain, being a measure for the photomultiplier voltage in arbitrary units, was set to 950. The fluorescent intensity was analyzed using ImageJ software. As the confocal volume is narrow only the outer rim of the microsphere is apparent in the confocal image.

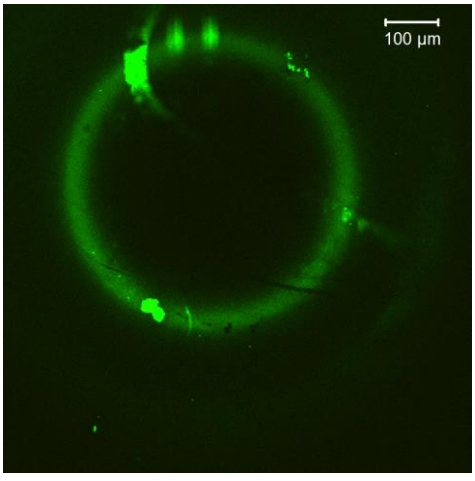

Figure 6.1: Confocal fluorescence image of a sapphire microsphere where the binding protocol was carried out as described in section 6.3.

6.5 Experimental results

The experimental setup and the detection mechanism are as explained in chapter 5 section 5.3.3. The same sapphire sphere was used in all the measurements.

In order to ensure the stability and repeatability of the resonances, the experiment was repeated at least three times with non-modified and modified sapphire spheres in air. Figure 6.2 represents the three repeated spectra for the transmitted intensity (a) and the elastic scattering intensity (b) from the non-modified sapphire sphere. The measurement was performed three times while keeping the sphere fixed in the same position. As a result, the resonances were proved to be repeatable and stable since they are quite overlapping. The $\Delta\lambda$ of the WGMs is observed to be 0.43 nm, which agrees well with the $\Delta\lambda$ estimated using equation 5.1 (see chapter 5) for a 1 mm diameter sapphire microsphere with a refractive index of 1.77. For every maximum in the elastic scattering spectrum, there is a corresponding minimum in the transmittance spectrum. The minima in the transmittance spectrum correlates to an amount of light coupled from the fiber into the sphere. The linewidth ($\delta\lambda$) of the resonances is about 0.01 nm, which corresponds to a quality factor Q on the order 10^5 (using $Q = \lambda / \delta\lambda$).

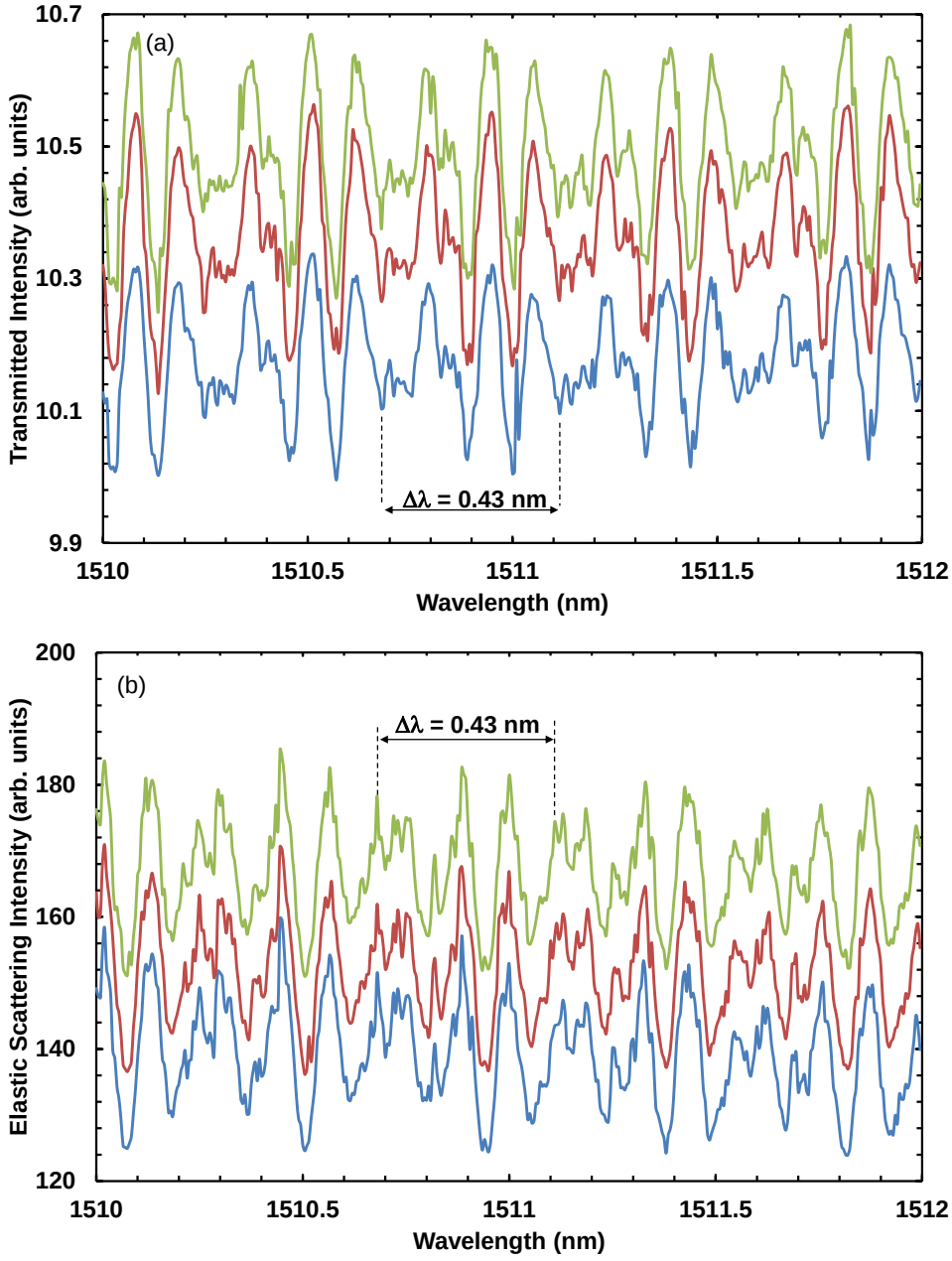

Figure 6.2: Transmitted intensity (a) and elastic scattering intensity (b) spectra from non-modified sapphire sphere repeated three times in order to demonstrate the reproducibility of the concept. Spectra were offset vertically in order to display them in one graph.

The next step was to investigate what would happen if the sphere was moved around the initial coupling point and then returned back to almost same position. As shown in figure 6.3, the resonance positions are overlapping but their intensities have changed due to the change in the coupling conditions.

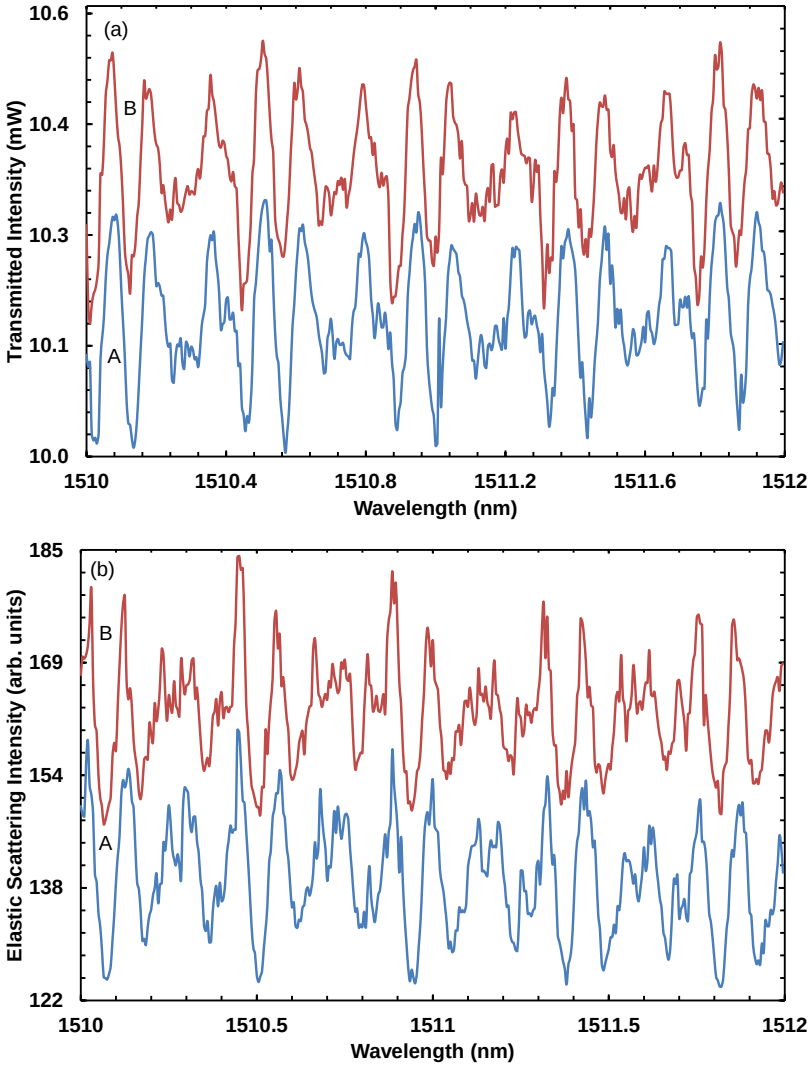

Figure 6.3: Transmitted intensity (a) and elastic scattering intensity (b) spectra from non-modified sapphire sphere repeated twice. A) Sphere initially on the coupler. B) Sphere was raised over the coupler and moved around the initial coupling point and then returned back to almost the same initial coupling point. Spectra were offset vertically in order to display them in one graph.

Then, the shift in WGMs of sapphire microsphere due to the surface functionalization with ssDNA was measured. The transmitted and the elastic scattering intensity spectra in the wavelength range from 1510 to 1512 nm are shown in figure 6.4a and Figure 6.4b, respectively.

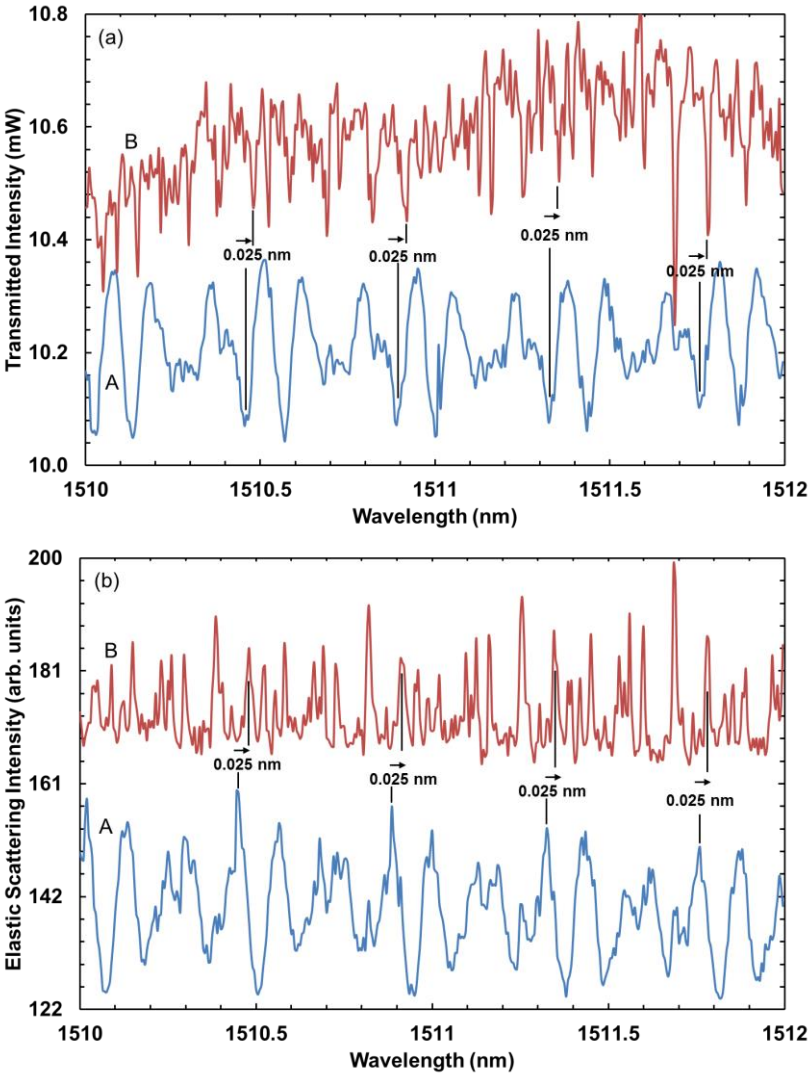

Figure 6.4: Transmitted intensity (a) and elastic scattering intensity (b) spectra from sapphire sphere modified with ssDNA and the corresponding shift. A) non-modified sphere. B) Same sphere modified with the ssDNA. Spectra were offset vertically in order to display them in one graph.

As can clearly be seen from Figures 6.4a and 6.4b, the resonances were red-shifted by 0.025 nm, which corresponds to a radius shift of 8.3 nm as calculated using equation 5.2 (see chapter 5). In our previous experiment, we found that the film thickness of the 36 base pairs ssDNA (with a stretched-out length of 22 nm) layer was about 7.6 nm with a surface roughness of 0.7 nm on nanocrystalline diamond, as measured by ellipsometry [40]. This correlates well with the 8.3 nm corresponding size shift measured in this setup.

After the hybridization with the target DNA (100 μM), the resonances were red-shifted further by 0.03 nm which corresponds to a size of shift of 10 nm, as calculated using equation 5.2. The transmitted and the elastic scattering intensity spectra are shown in figure 6.5a and figure 6.5b, respectively.

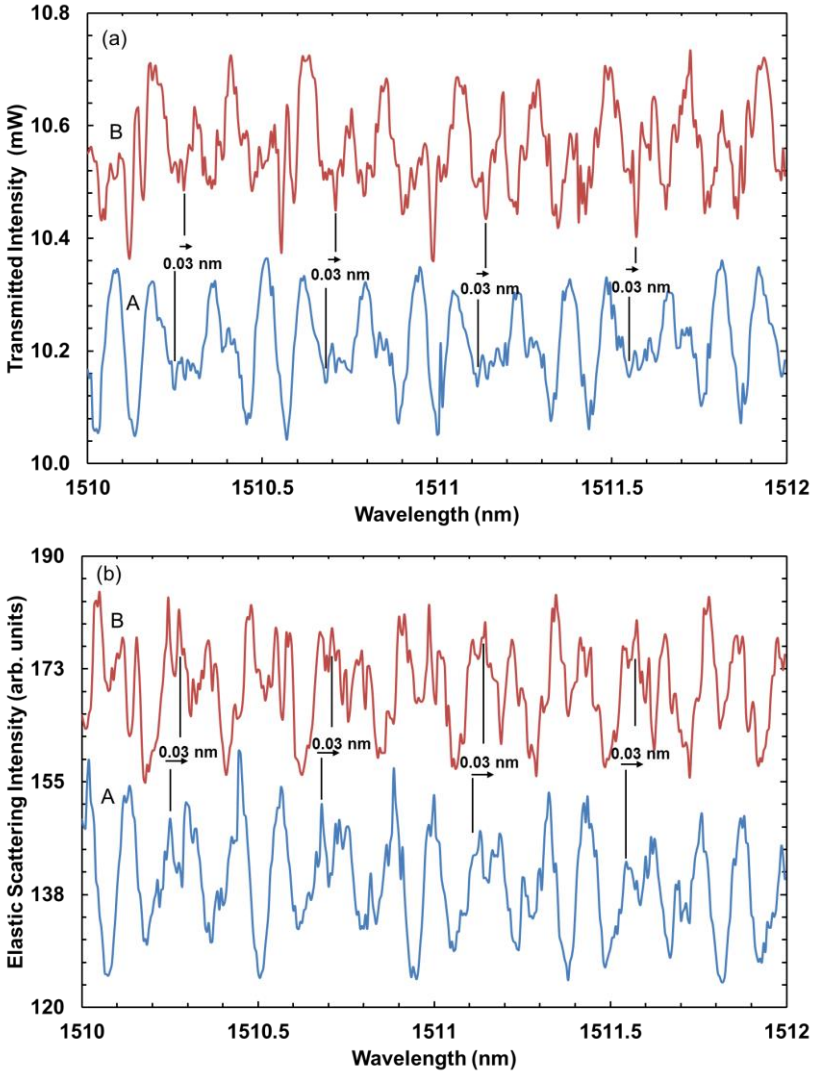

Figure 6.5: Transmitted intensity (a) and elastic scattering intensity (b) spectra from sapphire sphere modified with ssDNA and the corresponding shift. A) non-modified sphere. B) sphere modified with the dsDNA. Spectra were offset vertically in order to display them in one graph.

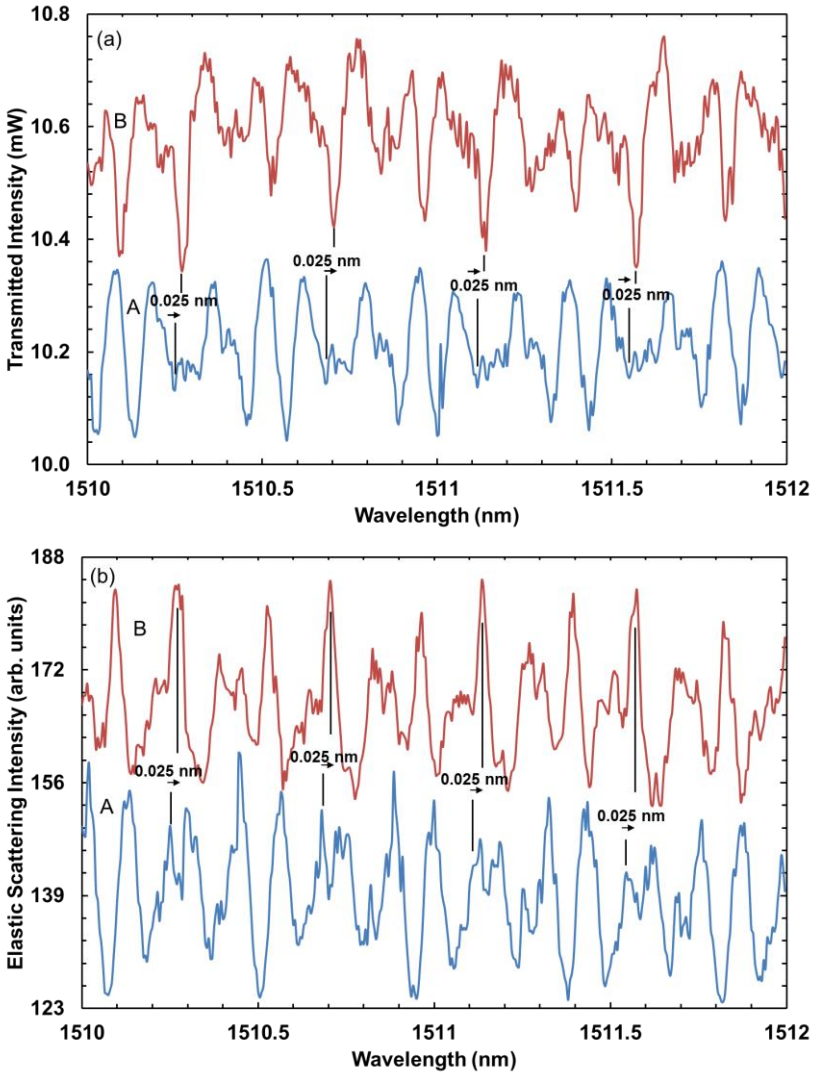

Figure 6.6: Transmitted intensity (a) and elastic scattering intensity (b) spectra from sapphire sphere after dsDNA is denatured and the corresponding shift. A) non-modified sphere. B) DNA modified sphere after denaturation of dsDNA to ssDNA. Spectra were offset vertically in order to display them in one graph.

The layer of 29 base pairs (bp) dsDNA (on top of an A7-ss-tail, giving a total stretchedout length of 14 nm) amounts to a film thickness of about 10.8 nm and a surface roughness of 1.7 nm on nanocrystalline diamond [40]. This again correlates well with the size shift value measured in this setup. The average mass density for the probe DNA onto the sphere surface was estimated to be

about 33 ng/mm^2. The mass of the probe DNA bound to the sphere surface was estimated to be about 0.1 μg, which corresponds to 5.4 × 10^{12} ssDNA molecules (Probe DNA molecular weight is 11060.3 g/mole). In addition, the observed shift corresponds to about 2.5 times the resonance linewidth in the ssDNA case and about three times in the dsDNA case, which supports the possibility of identifying about one third lower concentrations of biomolecules than what was detected in this experiment. In our case, there is a possibility of identifying about 0.05 μg probe DNA.

The dsDNA-functionalized sapphire sphere was denatured then by 0.1 M sodium hydroxide NaOH, rinsed with ultrapure water and dried in nitrogen gas. The transmitted intensity and the elastic scattering intensity spectra were collected again (Figure 6.6a and 6.6b). As expected, the resonances were blue-shifted back almost to the same position as in figure 6.4a and figure 6.4b.

The linewidths of the resonances for ssDNA, dsDNA, and denatured dsDNA are compared. The linewidths of the resonances for ssDNA spectra (Figure 6.4 a, b) were a little bit narrower, and more resonances showed up as compared to dsDNA spectra (Figure 6.5 a, b). This can be attributed to the fact that the surface is smoother and might be more homogeneous with ssDNA (surface roughness 0.7 nm) [40] than it is with dsDNA (surface roughness 1.7 nm) [40]. The smoother the microcavity surface, the higher the quality factor [41]. When the dsDNA was denatured, the linewidths remained broad (Figure 6.6 a, b). This can be attributed to the fact that there might be some denatured ssDNA strands still attached to the surface. This will result in a non-homogeneous surface that scatters the photons and decreases the resonances quality factor [41]. However, the quality factor was still preserved ($Q \approx 10^4$) in all the functionalization steps except for the ssDNA ($Q \approx 10^5$) functionalization step, when more resonances showed up due to surface smoothness.

6.7 Conclusion

A concept for a label-free photonic biosensor was proposed with possible applications in the identification of biomolecules and in the observation of hybridization and denaturation of DNA. Elastic light scattering and transmitted intensity from sapphire spheres were measured in the wavelength range of 1500

nm. The resonance shift due to the sphere-surface modification with ssDNA and dsDNA was measured and analyzed. The surface functionalization with ssDNA and dsDNA did not alter the quality factor ($Q \approx 10^4$). The surface modified with ssDNA was smoother and the ssDNA seemed to be aligned more homogenously than the dsDNA. This resulted in more resonances in the spectrum of ssDNA than in the dsDNA. The measurements showed that an optical biosensor based on spherical cavities is a good candidate for biomolecules identification and DNA hybridization and denaturation. The shift in resonances can be analyzed from the transmission signal of the optical fiber or from the elastic scattering intensity. Furthermore, for a resonant linewidth of 0.01 nm at 1500 nm, the modified sapphire sphere had a spectral shift of about 3 times the resonant linewidth, which supports the possibility of identifying about 0.05 μg probe DNA. In summary, this sapphire microcavity-based sensor can be used to study the kinetics and other physical properties of DNA and protein molecules. All in all, we have taken the first step towards utilizing a structural, electrically insulating implant material as a microcavity-based optical biosensor platform paving the way for future in vivo-biosensing devices.

6.8 References

1. N. Lagos, and M. M. Sigalas, "Single particle detection in a system of two microdisks," Sensors and Actuators B-Chemical **153**, 252-255 (2011).

2. S. Zlatanovic, L. W. Mirkarimi, M. M. Sigalas, M. A. Bynum, E. Chow, K. M. Robotti, G. W. Burr, S. Esener, and A. Grot, "Photonic crystal microcavity sensor for ultracompact monitoring of reaction kinetics and protein concentration," Sensors and Actuators B-Chemical **141**, 13-19 (2009).

3. T. Strick, J. F. Allemand, V. Croquette, and D. Bensimon, "Twisting and stretching single DNA molecules," Progress in Biophysics & Molecular Biology **74**, 115-140 (2000).

4. U. Bockelmann, P. Thomen, B. Essevaz-Roulet, V. Viasnoff, and F. Heslot, "Unzipping DNA with optical tweezers: high sequence sensitivity and force flips," Biophysical Journal **82**, 1537-1553 (2002).

5. B. van Grinsven, N. V. Bon, L. Grieten, M. Murib, S. D. Janssens, K. Haenen, E. Schneider, S. Ingebrandt, M. J. Schöning, V. Vermeeren, M. Ameloot, L. Michiels, R. Thoelen, W. De Ceuninck, and P. Wagner, "Rapid assessment of the stability of DNA duplexes by impedimetric real-time monitoring of chemically induced denaturation," Lab on a Chip **11**, 1656-1663 (2011).

6. Z. H. Zhong, D. L. Wang, Y. Cui, M. W. Bockrath, and C. M. Lieber, "Nanowire crossbar arrays as address decoders for integrated nanosystems," Science **302**, 1377-1379 (2003).

7. J. M. Nam, C. S. Thaxton, and C. A. Mirkin, "Nanoparticle-based bio-bar codes for the ultrasensitive detection of proteins," Science **301**, 1884-1886 (2003).

8. W. S. Yeo, D. H. Min, R. W. Hsieh, G. L. Greene, and M. Mrksich, "Label-free detection of protein-protein interactions on biochips," Angewandte Chemie-International Edition **44**, 5480-5483 (2005).

9. T. P. Burg, M. Godin, S. M. Knudsen, W. Shen, G. Carlson, J. S. Foster, K. Babcock, and S. R. Manalis, "Weighing of biomolecules, single cells and single nanoparticles in fluid," Nature **446**, 1066-1069 (2007).

10. A. Poghossian, M. H. Abouzar, F. Amberger, D. Mayer, Y. Han, S. Ingebrandt, A. Offenhäusser, and M. J. Schöning, "Field-effect sensors with charged macromolecules: Characterisation by capacitance-voltage, constant-capacitance, impedance spectroscopy and atomic-force microscopy methods," Biosensors & Bioelectronics **22**, 2100-2107 (2007).

11. S. Ingebrandt, Y. Han, F. Nakamura, A. Poghossian, M. J. Schöning, and A. Offenhäusser, "Label-free detection of single nucleotide polymorphisms utilizing the differential transfer function of field-effect transistors," Biosensors & Bioelectronics **22**, 2834-2840 (2007).

12. D. Dey, and T. Goswami, "Optical Biosensors: A revolution towards quantum nanoscale electronics device fabrication," Journal of Biomedicine and Biotechnology **2011,** (2011). doi:10.1155/2011/348218.

13. R. Narayanaswamy, and O. S. Wolfbeis (Eds.), "Optical Sensors, Industrial, Environmental, and Diagnostic Applications," (Springer, 2004), ISBN: 978-3-662-09111-1.

14. X. D. Fan, I. M. White, S. I. Shopova, H. Y. Zhu, J. D. Suter, and Y. Z. Sun, "Sensitive optical biosensors for unlabeled targets: A review," Analytica Chimica Acta **620**, 8-26 (2008).

15. J. L. Nadeau, V. S. Iltchenko, D. Kossakovski, G. H. Bearman, and L. Maleki, "High-Q whispering-gallery mode sensor in liquids," in Conference on Laser Resonators and Beam Control V(San Jose, Ca, 2002), pp. 172-180.

16. J. D. Suter, I. M. White, H. Y. Zhu, H. D. Shi, C. W. Caldwell, and X. D. Fan, "Label-free quantitative DNA detection using the liquid core optical ring resonator," Biosensors & Bioelectronics **23**, 1003-1009 (2008).

17. Z. B. Bahsi, A. Buyukaksoy, S. M. Olmezcan, F. Simsek, M. H. Aslan, and A. Y. Oral, "A novel label-free optical biosensor using synthetic oligonucleotides from E. coli O157:H7: elementary sensitivity tests," Sensors **9**, 4890-4900 (2009).

18. M. Baaske, and F. Vollmer, "Optical Resonator Biosensors: Molecular diagnostic and nanoparticle detection on an integrated platform," ChemPhysChem **13**, 427-436 (2012).

19. V. M. N. Passaro, F. Dell'Olio, B. Casamassima, and F. De Leonardis, "Guided-wave optical biosensors," Sensors **7**, 508-536 (2007).

20. J. P. Golden, G. P. Anderson, S. Y. Rabbany, and F. S. Ligler, "An evanescent-wave biosensor .ll. fluorescent signal acquisition from tapered fiber optic probes," IEEE Transactions on Biomedical Engineering **41**, 585-591 (1994).

21. A. Q. Liu, H. J. Huang, L. K. Chin, Y. F. Yu, and X. C. Li, "Label-free detection with micro optical fluidic systems (MOFS): a review," Analytical and Bioanalytical Chemistry **391**, 2443-2452 (2008).

22. P. M. Levine, P. Gong, R. Levicky, and K. L. Shepard, "Real-time, multiplexed electrochemical DNA detection using an active complementary metal-oxide-semiconductor biosensor array with integrated sensor electronics," Biosensors & Bioelectronics **24**, 1995-2001 (2009).

23. A. M. Armani, R. P. Kulkarni, S. E. Fraser, R. C. Flagan, and K. J. Vahala, "Label-free, single-molecule detection with optical microcavities," Science **317**, 783-787 (2007).

24. F. Vollmer, and S. Arnold, "Whispering-gallery-mode biosensing: label-free detection down to single molecules," Nature Methods **5**, 591-596 (2008).

25. K. De Vos, I. Bartolozzi, E. Schacht, P. Bienstman, and R. Baets, "Silicon-on-Insulator microring resonator for sensitive and label-free biosensing," Optics Express **15**, 7610-7615 (2007).

26. R. Kirchner, M. K. Kaiser, B. Adolphi, R. Landgraf, and W. J. Fischer, "Chemical functional polymers for direct UV assisted nanoimprinting of polymeric photonic microring resonators," Physica Status Solidi A - Applications and Materials Science **208**, 1308-1314 (2011).

27. K. De Vos, J. Girones, S. Popelka, E. Schacht, R. Baets, and P. Bienstman, "SOI optical microring resonator with poly(ethylene glycol) polymer brush for label-free biosensor applications," Biosensors & Bioelectronics **24**, 2528-2533 (2009).

28. V. S. Ilchenko, A. M. Bennett, P. Santini, A. A. Savchenkov, A. B. Matsko, and L. Maleki, "Whispering gallery mode diamond resonator," Optics Letters **38**, 4320-4323 (2013).

29. H. Kawarada, and A. R. Ruslinda, "Diamond electrolyte solution gate FETs for DNA and protein sensors using DNA/RNA aptamers," Physica Status Solidi A - Applications and Materials Science **208**, 2005-2016 (2011).

30. V. Vermeeren, S. Wenmackers, M. Daenen, K. Haenen, O. A. Williams, M. Ameloot, M. vandeVen, P. Wagner, and L. Michiels, "Topographical and functional characterization of the ssDNA probe layer generated through

EDC-mediated covalent attachment to nanocrystalline diamond using fluorescence microscopy," Langmuir **24**, 9125-9134 (2008).

31. A. G. Mamalis, J. J. Ramsden, A. I. Grabchenko, L. A. Lytvynov, V. A. Filipenko, and S. N. Lavrynenko, "A novel concept for the manufacture of individual sapphire-metallic hip joint endoprostheses," Journal of Biological Physics Chemistry **6**, 113-117 (2006).

32. T. Takahashi, T. Sato, R. Hisanaga, O. Miho, Y. Suzuki, M. Tsunoda, and K. I. Nakagawa, "Long-term observation of porous sapphire dental implants," The Bulletin of Tokyo Dental College **49**, 23-27 (2008).

33. M. R. Rieger, W. K. Adams, G. L. Kinzel, and M. O. Brose, "Alternative materials for three endosseous implants," The Journal of Prosthetic Dentistry **61**, 717-722 (**1989**).

34. G. Q. Zhou, Y. J. Dong, J. Xu, H. J. Li, J. L. Si, X. B. Qian, and X. Q. Li, "φ 140 mm sapphire crystal growth by temperature gradient techniques and its color centers," Materials Letters **60**, 901-904 (2006).

35. T. Strother, W. Cai, X. S. Zhao, R. J. Hamers, and L. M. Smith, "Synthesis and characterization of DNA-modified silicon (111) surfaces," Journal of the American Chemical Society **122**, 1205-1209 (2000).

36. J. P. Fitts, X. M. Shang, G. W. Flynn, T. F. Heinz, and K. B. Eisenthal, "Electrostatic surface charge at aqueous/alpha-Al_2O_3 single-crystal interfaces as probed by optical second-harmonic generation," Journal of Physical Chemistry B **109**, 7981-7986 (2005).

37. J. H. Sung, L. N. Zhang, C. S. Tian, G. A. Waychunas, and Y. R. Shen, "Surface structure of protonated r-sapphire $(1\bar{1}02)$ studied by sum-frequency vibrational spectroscopy," Journal of the American Chemical Society **133**, 3846-3853 (2011).

38. E. T. Vandenberg, L. Bertilsson, B. Liedberg, K. Uvdal, R. Erlandsson, H. Elwing, and I. Lundstrom, "Structure of 3-aminopropyl triethoxy silane

on silicon-oxide," Journal of Colloid and Interface Science **147**, 103-118 (1991).

39. K. van der Maaden, K. Sliedregt, A. Kros, W. Jiskoot, and J. Bouwstra, "Fluorescent nanoparticle adhesion assay: a novel method for surface pK(a) determination of self-assembled monolayers on silicon surfaces," Langmuir **28**, 3403-3411 (2012).

40. S. Wenmackers, S. D. Pop, K. Roodenko, V. Vermeeren, O. A. Williams, M. Daenen, O. Douheret, J. D'Haen, A. Hardy, M. K. Van Bael, K. Hinrichs, C. Cobet, M. vandeVen, M. Ameloot, K. Haenen, L. Michiels, N. Esser, and P. Wagner, "Structural and optical properties of DNA layers covalently attached to diamond surfaces," Langmuir **24**, 7269-7277 (2008).

41. D. W. Vernooy, V. S. Ilchenko, H. Mabuchi, E. W. Streed, and H. J. Kimble, "High-Q measurements of fused-silica microspheres in the near infrared," Optics Letters **23**, 247-249 (1998).

Chapter 7

General Conclusion

The main goal of this work was to optimize biosensors for the characterization of DNA molecules based on electronic and thermal sensing principles and to develop a DNA biosensor based on photonic sensing principle.

The results obtained in this thesis prove that the denaturation times provided by van Grinsven *et al.* can be decreased by increasing the flow rate or the concentration of NaOH solution used. Measurements performed using low concentrations of NaOH show that high flow rates are necessary to denature the DNA. The mechanical force exerted by the fluid motion contributes to the denaturation of the dsDNA and the removal of the denatured strands. Therefore the NaOH concentration should be at least 0.1 M to ensure full denaturation of the dsDNA at flow rates below 0.5 ml/min. Optimal conditions for industrial applications, requiring high throughput can be found in the high molarity and high flow rate range, where denaturation occurs faster. However, if the application requires more detail, lower flow rates at a NaOH concentration of 0.1 M should be used.

A successful surface functionalization of sapphire with carboxylic groups (COOH) was achieved. After hydroxylating the surface, linker molecules were attached, so that later on, probe DNA could be coupled onto the surface. The surface coverage with COOH was analyzed using toluidine blue O (TBO) and compared to the surface coverage of nanocrystalline diamond (NCD) with COOH. Sapphire- and NCD- surfaces show indeed an identical surface coverage with COOH groups. Also TGA and FTIR confirmed the successful surface modification of the sapphire beads with APTES, suggesting a covalent binding of probe DNA to a synthetic sapphire material. Finally, hybridization with labeled target DNA was carried out. The results from the confocal microscopy demonstrated successful hybridization and denaturation cycles, indicating the reusability of this sensor. Quantification of the carboxylic groups on the surface showed comparable

results to that of planar diamond surfaces. Finally, the RTH-measurement demonstrated the usefulness of a sapphire DNA sensor in the detection of SNPs or point mutations. Comparing the results obtained in this experiment to the results of van Grinsven *et al.*, sapphire is proven to be a perfect alternative for diamond in the creation of a DNA sensor.

A concept for a label-free photonic biosensor was proposed with possible applications in the identification of biomolecules and in the observation of hybridization and denaturation of DNA. TE- and TM-polarized elastic light scattering and transmitted intensity from diamond-, glass-, and sapphire spheres were analyzed in the wavelength range of 600 nm. In the case of sapphire, the elastic light scattering intensities were also analyzed in the wavelength regime of 1400 nm. The resonance shift due to the sphere-surface modification was calculated and analyzed for several values of the size and relative refractive indices. The calculations showed that an optical biosensor based on spherical cavities is a good candidate for biomolecules identification and DNA hybridization and denaturation. The shift in resonances can be analyzed from the transmission signal of the optical fiber or from the elastic scattering intensity at 90° from the sphere. The chemical inertness, stability at elevated temperatures, biocompatibility, and excellent thermal conductivity of sapphire and diamond can be exploited in the development of biosensors. The anisotropy of sapphire is much weaker than diamond, and as a result sapphire can be shaped into a nearly perfect sphere. For a resonant linewidth of the order 10^5 nm at 600 nm, the modified glass and sapphire spheres had a spectral shift of 10^4 times the resonant linewidth, and the modified diamond sphere has spectral shift of 5103 times the resonant linewidth. Since sapphire and glass have shown similar spectral shift with respect to resonant linewidth, sapphire can be considered an interesting alternative to glass biophotonic sensors.

The transmitted intensity and the elastic scattering intensity from a sapphire sphere of radius 500 μm and 1.77 refractive index in the range of 1510-1512 nm, were measured. The highest quality factor of the order 10^5 was demonstrated for the first time to our knowledge in a spherical resonator fabricated out of this material. We have studied the shift in resonance wavelength due to coating the sphere with different thicknesses of PDA layer.

The quality factor of the resonances was studied as a function of the change in the PDA polymer thickness on the sapphire surface, and we found that it is almost preserved despite a small decrease. We also verified that PDA layers are homogeneous as well and allowed us to obtain high Q factors showing that PDA coating is a valid alternative to silanization.

Elastic light scattering and transmitted intensity from DNA-functionalized sapphire spheres were measured in the wavelength range 1500 nm. The resonance shift due to the sphere-surface modification with ssDNA and dsDNA was measured and analyzed. The surface functionalization with ssDNA and dsDNA did not alter the quality factor ($Q \approx 10^4$). The surface modified with ssDNA was smoother and the ssDNA seemed to be aligned more homogenously than the dsDNA. This resulted in more resonances in the spectrum of ssDNA than in the dsDNA. The measurements showed that an optical biosensor based on spherical cavities is a good candidate for biomolecule identification and DNA hybridization and denaturation. The shift in resonances can be analyzed from the transmission signal of the optical fiber or from the elastic scattering intensity. Furthermore, for a resonant linewidth of 0.01 nm at 1500 nm, the modified sapphire sphere had a spectral shift of about 3 times the resonant linewidth, which supports the possibility of identifying lower concentrations of biomolecules.

In summary, the diamond- and sapphire-based sensors can be used to study the kinetics and other physical properties of DNA and protein molecules. Optimization of the flow rates and NaOH molarities for dsDNA denaturation using impedance can be a valuable asset in the field of mutation analysis.

All in all, these results bring forward the first step towards thermotronic and photonics microcavity-based optical detection schemes of biological compounds using synthetic sapphire as a platform material.

Appendix 1

Nomenclature

a	Sphere Radius
A	Adenine
AC	Alternating Current
ACN	Acetonitrile
AFM	Atomic Force Microscopy
Ag	Silver
Al_2O_3	Alumina / Sapphire
APTES	3-Aminopropyl Triethoxysilane
Au	Gold
b	Impact Parameter
$B(CH_3)_3$	Trimethyl Borane
bp	Base Pair
C	Cytosine
C_2	Molecular Layer Capacitance
C_3	Space Charge Layer Capacitance
CH_4	Methane molecule
COOH	Carboxyl
Cu	Cupper
CVD	Chemical Vapour Deposition
CW	Continuous Wave
D	Detector
DAQ	Data Acquisition
DL	Diode Laser
DNA	Deoxyribonucleic Acid
dsDNA	Double-Stranded Deoxyribonucleic Acid
DSO	Digital Storage Oscilloscope
EDC	1-Ethyl-3-[3-Dimethylaminopropyl]-Carbodiimide
FET	Field Effect Transistors
FT-IR	Fourier Transform-Infra Red
G	Guanine
Ge	Germanium

GLMT	Generalized Lorenz-Mie Theory
GPIB	General Purpose Interface Bus
H_2	Hydrogen molecule
HNO_3	Nitric Acid
HTM	Heat-Transfer-Method
KBr	Potassium Bromide
m	Relative Refractive Index
MDRs	Morphology Dependent Resonances
MES	2-[N-morpholino]-EthanneSulphonic Acid
MPECVD	Microwave Plasma-Enhanced Chemical Vapour Deposition
n	Mode Number
N	Refractive Index of Surrounding Medium
N_1	Sphere Refractive index
NaOH	Sodium Hydroxide
NCD	Nanocrystalline Diamond
NH_2	Amine
OFHC	Optical Fiber Half Coupler
OMM	Optical Multimeter
P	Phosphate
PBS	Phosphate Buffered Saline
PCR	Polymerase Chain Reaction
PD	Photodiode
PDA	Polydopamine
PLL	Polylactic Acid
Q	Quality Factor
R_1	Solution Resistance
R_2	Molecular Layer Resistance
R_3	Space Charge Layer Resistance
RMS	Root Mean Square
R_{th}	Thermal Resistance
RS	Raman Spectroscopy
SA	Succinic Anhydride
SDS	Sodium Dodecyl Sulphate
SERS	Surface-Enhanced Raman Spectroscopy

SMOF	Single Mode Optical Fiber
SNP	Single Nucleotide Polymorphisms
SOI	Silicon on Insulator
SSC	Saline Sodium Citrate
ss-DNA	Single-Stranded Deoxyribonucleic Acid
T	Thymine
TBO	Toluidine Blue O
TE	Transverse Electric
TGA	Thermo Gravimetric Analysis
THF	Tetrahydrofuran
TIR	Total Internal Reflection
TIRF	Total Internal Reflection Fluorescence
TM	Transverse Magnetic
UA	Undecyclenic Acid
UV	UltraViolet
WGM	Whispering Gallery Mode
XPS	X-Ray Photoelectron Spectroscopy
$Y_{imaginary}$	Imaginary Admittance
Y_{real}	Real Admittance
Z	Impedance
δa	Change in Sphere Radius
$\delta\lambda$	Resonant Linewidth
$\Delta\lambda$	Mode Spacing
δm	Change in Relative Refractive Index
$\delta\lambda_{shift}$	Wavelength Shift
λ	Laser Wavelength in Vacuum

Appendix 2

Publications and Conference contributions

Publications

1. B. van Grinsven, N. V. Bon, L. Grieten, **M. Murib**, S. D. Janssens, K. Haenen, E. Schneider, S. Ingebrandt, M. J. Schöning, V. Vermeeren, M. Ameloot, L. Michiels, R. Thoelen, W. De Ceuninck, and P. Wagner, "Rapid assessment of the stability of DNA duplexes by impedimetric real-time monitoring of chemically induced denaturation," Lab on a Chip **11**, 1656-1663 (2011).

2. **M. S. Murib**, A. Q. Tran, W. De Ceuninck, M. J. Schöning, M. Nesládek, A. Serpengüzel, and P. Wagner, "Analysis of an optical biosensor based on elastic light scattering from diamond-, glass-, and sapphire microspheres," Physica Status Solidi A - Applications and Materials Science **209**, 1804-1810 (2012).

3. B. van Grinsven, N. Vanden Bon, H. Strauven, L. Grieten, **M. Murib**, K. L. J. Monroy, S. D. Janssens, K. Haenen, M. J. Schöning, V. Vermeeren, M. Ameloot, L. Michiels, R. Thoelen, W. De Ceuninck, and P. Wagner, "Heat-transfer resistance at solid-liquid interfaces: A tool for the detection of single-nucleotide polymorphisms in DNA," ACS Nano **6**, 2712-2721 (2012).

4. M. Peeters, F. J. Troost, B. Van Grinsven, F. Horemans, J. Alenus, **M. S. Murib**, D. Keszthely, A. Ethirajan, R. Thoelen, T. J. Cleij, and P. Wagner, "MIP-based biomimetic sensor for the electronic detection of serotonin in human blood plasma," Sensors and Actuators B: Chemical, **171-172**, 602-610, 2012.

5. **M. S. Murib**, B. van Grinsven, L. Grieten, S. D. Janssens, V. Vermeeren, K. Eersels, J. Broeders, M. Ameloot, L. Michiels, W. De Ceuninck, K. Haenen, M. J. Schöning, and P. Wagner, "Electronic monitoring of chemical DNA denaturation on nanocrystalline diamond electrodes with different molarities and flow rates," Physica Status Solidi a-Applications and Materials Science **210**, 911-917 (2013).

6. K. Bers, B. van Grinsven, T. Vandenryt, **M. Murib**, W. Janssen, B. Geerets, M. Ameloot, K. Haenen, L. Michiels, W. De Ceuninck, and P. Wagner, "Implementing heat transfer resistivity as a key element in a nanocrystalline diamond based single nucleotide polymorphism detection array," Diamond and Related Materials **38**, 45-51 (2013).

7. N. V. Bon, B. van Grinsven, **M. S. Murib**, W. S. Yeap, K. Haenen, W. De Ceuninck, P. Wagner, M. Ameloot, V. Vermeeren, L. Michiels, "Heat-transfer-based detection of SNPs in the PAH gene of PKU patients," accepted in International Journal of Nanomedicine (January 2014).

8. **M. S. Murib**, W. S. Yeap, Y. Eurlings, B. van Grinsven, H. G. Boyen, L. Michiels, M. Ameloot, R. Carleer, J. Warmer, P. Kaul, K. Haenen, W. De Ceuninck, M. J. Schöning, and P. Wagner, "Adding biosensing functionalities to implant materials: heat-transfer based characterization of DNA on synthetic sapphire chips," submitted to ACS Applied Materials and Interface (January 2014).

9. **M. S. Murib**, W. S. Yeap, D. Martens, P. Bienstman, W. De Ceuninck, M. J. Schöning, L. Michiels, K. Haenen, M. Ameloot, A. Serpengüzel, and P. Wagner, "Photonic detection and characterization of DNA using sapphire spheres," in preparation for SPIE Biomedical Optics (February 2014).

10. **M. S. Murib**, W. S. Yeap, D. Martens, X. J. Liu, P. Bienstman, M. Fahlman, W. De Ceuninck, M. J. Schöning, L. Michiels, K. Haenen, M. Ameloot, A. Serpengüzel, and P. Wagner, "Photonic studies on polymer-coated sapphire-spheres: a model system for biological ligands," in preparation for ACS photonics (February 2014).

11. W.S. Yeap, **M.S. Murib**, W. Cuypers, X.J. Liu, B. van Grinsven, W. Maes, M. Fahlman, P. Wagner, and K. Haenen, "Copper (I) Catalyzed Click Reactions on Phenylazide Functionalized Boron-doped Diamond by Electrografting," in preparation for submission (February 2014).

Poster contributions at conferences

1. EnFI 2013, Hasselt, Belgium (08 - 09 / 07 / 2013)
   Synthetic sapphire as a platform material for DNA sensors.
   M.S. Murib, W.S. Yeap, L. Michiels, M. Ameloot, R. Carleer, J. Warmer, P. Kaul, K. Haenen, W. De Ceuninck, M.J. Schöning, and P. Wagner.

2. Diamond Workshop (SBDD XVIII), Hasselt, Belgium (27 / 02 – 01 / 03 - 2013)
   Electronic monitoring of chemical DNA denaturation on nanocrystalline diamond electrodes with different sodium hydroxide molarities and flow rates.
   M. S. Murib, B. van Grinsven, L. Grieten, S. D. Janssens, V. Vermeeren, K. Eersels, J. Broeders, M. Ameloot, L. Michiels, W. De Ceuninck, K. Haenen, M. J. Schöning, and P. Wagner.

3. EnFI 2012, Zweibrücken, Germany (16 – 17 / 07 / 2012)
   Real-time study of chemically induced DNA denaturation by impedance spectroscopy with NCD-based sensor electrodes.
   M. S. Murib, B. van Grinsven, L. Grieten, S. D. Janssens, L. Michiels, W. De Ceuninck, K. Haenen, M. J. Schöning, and P. Wagner.

4. EnFI 2012, Zweibrücken, Germany (16 – 17 / 07 / 2012)
   MIP-based biomimetic sensor for the electronic detection of serotonin in human blood plasma.
   M. Peeters, F. J. Troost, B. van Grinsven, F. Horemans, J. Alenus, **M. S. Murib**, D. Keszthelyi, A. Ethirajan, R. Thoelen, T. J. Cleij, and P. Wagner.

5. Biosensors 2012, Cancún, Mexico (15 – 18 / 05 - 2012)
   MIP-based biomimetic sensor for the detection of serotonin in plasma.
   M. Peeters, F. J. Troost, B. van Grinsven, F. Horemans, J. Alenus, **M. S. Murib**, D. Keszthelyi, A. Ethirajan, R. Thoelen, T. J. Cleij, and P. Wagner.

6. Belgian Physical Society, Brussels, Belgium (30 / 05 / 2012)
   Real-time study of chemically induced DNA denaturation by impedance spectroscopy with NCD-based sensor electrodes.
   M. S. Murib, B. van Grinsven, L. Grieten, S. D. Janssens, L. Michiels, W. De Ceuninck, K. Haenen, M. J. Schöning, and P. Wagner.

7. Nanosense Symposium, Hasselt, Belgium (25 / 04 / 2012)
   MIP-based biomimetic sensor for the detection of serotonin in plasma.
   M. Peeters, F. J. Troost, B. van Grinsven, F. Horemans, J. Alenus, **M. S. Murib**, D. Keszthelyi, A. Ethirajan, R. Thoelen, T. J. Cleij, and P. Wagner.

8. Nanosense Symposium, Hasselt, Belgium (25 / 04 / 2012)
   Real-time study of chemically induced DNA denaturation by impedance spectroscopy with NCD-based sensor electrodes.
   M. S. Murib, B. van Grinsven, L. Grieten, S. D. Janssens, L. Michiels, W. De Ceuninck, K. Haenen, M. J. Schöning, and P. Wagner.

9. Biomedica 2012, Liège, Belgium (18 / 04 / 2012)
   MIP-based biomimetic sensor for the detection of serotonin in human blood plasma.
   M. Peeters, F. J. Troost, B. van Grinsven, F. Horemans, J. Alenus, **M. S. Murib**, D. Keszthelyi, A. Ethirajan, R. Thoelen, T. J. Cleij, and P. Wagner.

10. Diamond Workshop (SBDD XVII), Hasselt, Belgium (14 – 16 / 03 - 2012)
    Real-time study of chemically induced DNA denaturation by impedance spectroscopy with NCD-based sensor electrodes.
    M. S. Murib, B. van Grinsven, L. Grieten, S. D. Janssens, L. Michiels, W. De Ceuninck, K. Haenen, M. J. Schöning, and P. Wagner.

11. EnFI 2011, Linz, Austria (18 – 19 / 06 / 2011)
    Analysis of an optical biosensor based on elastic light scattering intensity from a microcavity.
    M. S. Murib, A. T. Quan, W. De Ceuninck, M. Nesládek, and P. Wagner.

12. Belgian Physical Society, Namur, Belgium (25 / 05 / 2011)
    Design of an Optical Biosensor Based on Microphotonics.
    M. S. Murib, W. De Ceuninck, M. Nesládek, and P. Wagner.

13. Biomedica 2011, Eindhoven, The Netherlands (07 – 08 / 04 /2011)
    Design of an Optical Biosensor Based on Microphotonics.
    M. S. Murib, W. De Ceuninck, M. Nesládek, and P. Wagner.

14. Belgian Physical Society, Utrecht, The Netherlands (23 / 04 / 2010)
    Polarization Behavior of Elastic Scattering from a Silicon Microsphere on an Optical Fiber Coupler
    M. S. Murib, E. Yüce, O. Gürlü and A. Serpengüzel.

Appendix 3

List of Figures and Tables

Chapter 3:

Chapter 4:

Chapter 5:

Chapter 6: